





**Déterminer les effets des paramètres géométriques du massif rocheux sur l'érosion à l'aide d'un modèle réduit d'évacuateur de crues**

**Par**  
**Marie-Hélène Wisse**  
**Sous la direction de Ali Saeidi, ing., Ph.D et Marco Quirion, ing., Ph.D**

**Mémoire présenté à l'Université du Québec à Chicoutimi en vue de l'obtention du grade de Maître ès sciences appliquées (M.Sc.A) en géologie et génie géologique**

# TABLE DES MATIÈRES

<b>LISTE DES TABLEAUX</b> .....	<b>iv</b>
<b>LISTE DES FIGURES</b> .....	<b>v</b>
<b>LISTE DES SYMBOLES ET ABRÉVIATIONS</b> .....	<b>ix</b>
<b>REMERCIEMENTS</b> .....	<b>xi</b>
<b>RÉSUMÉ</b> .....	<b>xii</b>
<b>CHAPITRE 1 INTRODUCTION</b> .....	<b>1</b>
<b>1.1 MISE EN CONTEXTE</b> .....	<b>1</b>
<b>1.2 REVUE DE LITTÉRATURE</b> .....	<b>1</b>
1.2.1 INDICE DE KIRSTEN .....	2
1.2.2 MÉTHODES DE PELLIS .....	4
1.2.3 FORMULES SEMI-EMPIRIQUES PRÉDISANT LA PROFONDEUR DE L'ÉROSION .....	5
1.2.4 MÉTHODES SEMI-ANALYTIQUES .....	6
<b>1.3 PROBLÉMATIQUE</b> .....	<b>9</b>
<b>1.4 OBJECTIFS</b> .....	<b>10</b>
1.4.1 OBJECTIF GÉNÉRAL .....	10
1.4.2 OBJECTIFS SPÉCIFIQUES .....	10
<b>1.5 MÉTHODOLOGIE</b> .....	<b>11</b>
1.5.1 ÉTUDE APPROFONDIE DES MODÈLES PHYSIQUES EXISTANTS .....	11
1.5.2 ÉVALUATION DES PARAMÈTRES D'ORIENTATION DES JOINTS .....	12
1.5.3 RÉALISATION DES ESSAIS SUR LE MODÈLE RÉDUIT .....	12
<b>1.6 STRUCTURE DU MÉMOIRE</b> .....	<b>14</b>
<b>CHAPITRE 2 REVUE DE LITTÉRATURE TRAITANT DES MODÈLES PHYSIQUES EXISTANTS POUR ÉTUDIER L'ÉROSION DU MASSIF ROCHEUX DANS LES ÉVACUATEURS DE CRUES</b> .....	<b>16</b>
<b>ABSTRACT</b> .....	<b>18</b>
<b>2.1 INTRODUCTION</b> .....	<b>19</b>
<b>2.2 HYDRAULIC FLUME EXPERIMENTS</b> .....	<b>21</b>
2.2.1 MODELS USING PRESSURE MEASUREMENTS TO DESCRIBE FLOW .....	21
2.2.2 MODELS USING EROSION PATTERNS TO QUALIFY FLOW .....	29
2.2.3 ROBERTS' MODEL.....	33
2.2.4 SUMMARY.....	34
<b>2.3 MODELS THAT INCLUDE THE STUDY OF THE GEOMETRICAL PARAMETERS OF THE ROCK MASS ON EROSION</b> .....	<b>36</b>
2.3.1 PLUNGING JET MODELS.....	36
2.3.2 OPEN-CHANNEL FLOW MODELS.....	41
2.3.3 RONG ET AL.'S MODEL .....	48
2.3.4 SUMMARY.....	49
<b>2.4 DISCUSSION</b> .....	<b>51</b>

2.4.1	INFLUENCE OF JOINT ORIENTATION AND PROTRUSION .....	52
2.4.2	INFLUENCE OF JOINT OPENING .....	52
2.4.3	INFLUENCE OF BLOCK VOLUME .....	53
2.4.4	INFLUENCE OF JOINT CONDITION.....	53
2.4.5	NATURE OF POTENTIALLY ERODIBLE SURFACE.....	53
2.4.6	FLOW TYPES.....	54
<b>2.5</b>	<b>CONCLUSIONS AND FUTURE CHALLENGES.....</b>	<b>54</b>
<b>CHAPITRE 3 COMPARAISON DE PARAMÈTRES D'ORIENTATION DES</b>		
<b>JOINTS ET LEUR EFFET SUR L'ÉRODABILITÉ DU MASSIF ROCHEUX DANS</b>		
<b>LES ÉVACUATEURS DE CRUES.....</b>		
	<b>55</b>	
	<b>ABSTRACT .....</b>	<b>57</b>
<b>3.1</b>	<b>INTRODUCTION.....</b>	<b>58</b>
<b>3.2</b>	<b>MATERIALS AND METHODS .....</b>	<b>60</b>
3.2.1	STEP 1 – SELECTION OF A JOINT ORIENTATION PARAMETER.....	61
3.2.2	STEP 2 – CLASSIFY THE DATABASE ACCORDING TO GSI <sub>CHART</sub> .....	62
3.2.3	STEP 3 - CLASSIFY THE JOINT ORIENTATION PARAMETER CHOSEN FOR EACH GSI CLASS .....	62
3.2.4	STEP 4 – CLASSIFICATION OF DAMAGE LEVEL .....	64
3.2.5	STEP 5 – CLASSIFICATION OF THE STREAM POWER .....	64
3.2.6	STEP 6 – DRAW THE DAMAGE CLASS GRAPH AS A FUNCTION OF THE MEAN STREAM POWER CLASS FOR THE CHOSEN JOINT ORIENTATION PARAMETER.....	65
3.2.7	STEP 7 – INTERPRET THE RESULTS .....	65
<b>3.3</b>	<b>THEORY.....</b>	<b>65</b>
3.3.1	PRESENTATION OF THE $J_s$ PARAMETER .....	65
3.3.2	PRESENTATION OF THE $E_{DOA}$ PARAMETER .....	67
3.3.3	PRESENTATION OF THE $C_{UP}$ PARAMETER .....	68
<b>3.4</b>	<b>RESULTS.....</b>	<b>70</b>
3.4.1	CLASSIFICATION OF THE GSI <sub>CHART</sub> INDEX .....	70
3.4.2	CLASSIFICATION OF THE $J_s$ PARAMETER.....	70
3.4.3	CLASSIFICATION OF THE $E_{DOA}$ PARAMETER.....	71
3.4.4	CLASSIFICATION OF THE $C_{UP}$ PARAMETER.....	72
3.4.5	EFFECTS OF $J_s$ ON ROCK MASS EROSION .....	73
3.4.6	EFFECTS OF THE $E_{DOA}$ PARAMETER .....	74
3.4.7	EFFECTS OF THE $C_{UP}$ PARAMETER .....	76
3.4.8	COMPARISON OF RESULTS .....	77
<b>3.5</b>	<b>DISCUSSION .....</b>	<b>77</b>
<b>3.6</b>	<b>CONCLUSION.....</b>	<b>80</b>
<b>CHAPITRE 4 : ÉTUDE DE L'ÉROSION DU MASSIF ROCHEUX DANS LES</b>		
<b>ÉVACUATEURS DE CRUES NON RECOUVERTS À L'AIDE D'UN MODÈLE</b>		
<b>RÉDUIT EN LABORATOIRE.....</b>		
	<b>81</b>	
	<b>ABSTRACT .....</b>	<b>83</b>
<b>4.1</b>	<b>UNLINED SPILLWAY EROSION.....</b>	<b>84</b>
<b>4.2</b>	<b>DESIGN OF A SCALED PHYSICAL MODEL .....</b>	<b>85</b>
<b>4.3</b>	<b>PRELIMINARY TESTS RESULTS .....</b>	<b>87</b>
<b>4.4</b>	<b>FURTHER ONGOING TESTS .....</b>	<b>89</b>

4.5	DISCUSSION .....	89
4.6	CONCLUSION.....	89
<b>CHAPITRE 5 : EFFETS DE L'OUVERTURE DES JOINTS ET DE LA SAILLIE DES BLOCS SUR LES PARAMÈTRES HYDRAULIQUES DANS LE MASSIF ROCHEUX D'UN ÉVACUATEURS DE CRUES À L'AIDE D'UN MODÈLE PHYSIQUE EN LABORATOIRE.....</b>		
	ABSTRACT .....	92
5.1	INTRODUCTION.....	94
5.2	METHODOLOGY.....	97
5.2.1	PRESENTATION OF THE PHYSICAL MODEL.....	97
5.2.2	GOVERNING EQUATIONS.....	98
5.2.3	TESTING PROGRAM.....	101
5.2.4	INSTRUMENTATION AND CALIBRATION OF THE PHYSICAL MODEL.....	102
5.2.5	MODIFICATION OF THE PHYSICAL TO MEASURE HYDRAULIC PARAMETERS IN THE JOINTS AND IN THE CHANNEL .....	103
5.2.6	SELECTION OF JOINT OPENINGS, PROTRUSION TYPES AND BLOCK SIZES .....	104
5.3	RESULTS AND DISCUSSION .....	107
5.3.1	ANALYSIS OF THE PHYSICAL MODEL DATA.....	107
5.3.2	EVALUATION OF THE EFFECTS OF JOINT OPENING AND PROTRUSION CONFIGURATION ON SURFACE PRESSURE FLUCTUATIONS .....	110
5.3.3	MEAN FLOW VELOCITY ON TOP OF THE BLOCKS AND IN THE JOINTS .....	111
5.4	CONCLUSION.....	116
<b>CHAPITRE 6 : CONCLUSIONS .....</b>		
6.1	CONCLUSIONS SUR LES MODÈLES PHYSIQUES EXISTANTS D'ÉVACUATEURS DE CRUES.....	117
6.2	CONCLUSIONS LES PARAMÈTRES D'ORIENTATION DES JOINTS.....	117
6.3	CONCLUSIONS SUR LES EFFETS DE LA SAILLIE ET DE L'OUVERTURE DES JOINTS SUR L'ÉROSION.....	118
	RÉFÉRENCES.....	120

## LISTE DES TABLEAUX

TABLE 2.1 : SUMMARY OF THE TESTS PERFORMED IN THE MODEL OF MANSO AND SCHLEISS (2006) .....	23
TABLE 2.2 : SUMMARY OF METHODS STUDYING THE HYDRAULIC CHARACTERISTICS OF THE FLOW .....	35
TABLE 2.3 : SUMMARY OF TESTS CARRIED OUT FOR EACH JOINT IN THE BOLLAERT AND SCHLEISS MODEL (2002) .....	41
TABLE 2.4 : SUMMARY OF THE TEST PROGRAM OF REINIUS (1986).....	42
TABLE 2.5 : BLOCK DISPLACEMENT TESTS PERFORMED BY MONTGOMERY (1984).....	43
TABLE 2.6 : SUMMARY OF THE CHARACTERISTICS OF THE METHODS, INCLUDING ROCK MASS GEOMETRICAL CHARACTERISTICS.....	50
TABLE 2.7 : MODELS CHARACTERIZING THE EFFECTS OF THE GEOMETRICAL PARAMETERS OF THE ROCK.....	52
TABLE 3.1 : $J_s$ PROPOSED CLASSIFICATION (BOUMAIZA ET AL., 2019B) .....	63
TABLE 3.2 : EDOA PROPOSED CLASSIFICATION (BOUMAIZA ET AL., 2019B).....	63
TABLE 3.3 : $C_{UP}$ PROPOSED CLASSIFICATION .....	63
TABLE 3.4 : PROPOSED CLASSIFICATION OF DAMAGE LEVELS (PELLS, 2016) .....	64
TABLE 3.5 : PROPOSED STREAM POWER CLASSIFICATION. MODIFIED FROM BOUMAIZA ET AL (2019B).....	64
TABLE 3.6 : RELATIVE GROUND STRUCTURE NUMBER (JS) PROPOSED VALUES REBUILT FROM KIRSTEN (1982).....	67
TABLE 5.1 : SCALE HYDRAULIC DESIGN OF THE PHYSICAL MODEL BASED ON THE PROTOTYPE (KOULIBALY, 2021) .....	97
TABLE 5.2 : CONFIGURATION SETUP AND THE VARIATION OF PROTRUSION HEIGHT FOR EACH ROW OF BLOCKS WITH THE FLOW DIRECTION (BLUE ARROW). .....	106

## LISTE DES FIGURES

FIGURE 1.1 : LIMITES D'ÉRODABILITÉ DÉFINIES AVEC L'INDICE DE KIRSTEN SELON DIFFÉRENTS AUTEURS. TIRÉ DE PELLIS (2016).....	4
FIGURE 1.2: FORCES AGISSANT LORS DU PROCESSUS DE SOULÈVEMENT DE BLOCS (PELLIS, 2016).....	7
FIGURE 1.3: ILLUSTRATION DU MODULE QSI, TRADUIT DE (BOLLAERT, 2012).....	8
FIGURE 1.4: SOMMAIRE DE LA MÉTHODOLOGIE SUIVIE POUR LA RÉALISATION DES ESSAIS SUR LE MODÈLE RÉDUIT.....	13
FIGURE 1.5: A SCHÉMA DU MODÈLE RÉDUIT (KOULIBALY, 2021) B BLOC INSTRUMENTÉ AVEC DES ENTRÉES ET SORTIES D'EAU (© MARIE-HÉLÈNE WISSE) .....	14
FIGURE 2.1 : DIAGRAM OF WITHERS' PHYSICAL MODEL. REDRAWN FROM WITHERS (1991)..	22
FIGURE 2.2 : DIAGRAM OF THE JET'S CHARACTERISTICS PRODUCED BY THE MODEL OF ERVINE ET AL. REDRAWN FROM ERVINE ET AL. (1997).....	22
FIGURE 2.3 : DIAGRAM OF THE MANSO AND SCHLEISS MODEL. REDRAWN FROM MANSO AND SCHLEISS (2006).....	24
FIGURE 2.4 : CONDITION OF THE PARADISE DAM SPILLWAY FOLLOWING THE 2013 FLOOD. DASHED RED LINES OUTLINE THE ERODED AREA. MODIFIED FROM LESLEIGHTER ET AL. (2016).....	25
FIGURE 2.5 : A ARRANGEMENT OF PRESSURE TRANSDUCERS AND B LESLEIGHTER ET AL.'S PHYSICAL MODEL DURING TESTING. MODIFIED FROM LESLEIGHTER ET AL. (2016).....	26
FIGURE 2.6 : GU ET AL.'S PHYSICAL MODEL OF A STEPPED SPILLWAY. MODIFIED FROM GU ET AL. (2017).....	27
FIGURE 2.7 : KOTE AND NANGARE'S PHYSICAL MODEL FOR THE STEPPED PLAIN ROLLER BUCKET SPILLWAY. MODIFIED FROM KOTE AND NANGARE (KOTE ET NANGARE, 2019) .....	29
FIGURE 2.8 : A OVERVIEW OF SAWADOGO'S PHYSICAL MODEL B SIX LAYERS OF CUBES. MODIFIED FROM SAWADOGO (2010).....	30
FIGURE 2.9 : COMPARISON OF THE NUMERICAL MODEL OUTPUT AND FIELD MEASUREMENTS. MODIFIED FROM SAWADOGO (2010).....	31
FIGURE 2.10 : DIAGRAM OF WILKINSON'S PHYSICAL MODEL. REDRAWN FROM WILKINSON ET AL. (2018).....	32
FIGURE 2.11 : DIAGRAM OF THE FLUME SECTION USED FOR ROBERTS' STUDY. REDRAWN FROM ROBERTS (1943).....	34
FIGURE 2.12 : DIAGRAM OF ANNANDALE'S PHYSICAL MODEL. REDRAWN FROM ANNANDALE ET AL. (1998).....	37

FIGURE 2.13 : <b>A</b> DIAGRAM OF LIU ET AL.'S PHYSICAL MODEL <b>B</b> A LARGER VIEW OF THE TEST SECTION. TAKEN FROM LIU ET AL. (1998) .....	38
FIGURE 2.14 : BOLLAERT AND SCHLEISS' PHYSICAL MODEL, AS MODIFIED FROM BOLLAERT AND SCHLEISS (2002).....	40
FIGURE 2.15 : JOINT TYPES AND LOCATION OF PRESSURE SENSORS IN THE PHYSICAL MODEL OF BOLLAERT AND SCHLEISS. MODIFIED FROM BOLLAERT AND SCHLEISS (2002).....	40
FIGURE 2.16 : DIAGRAM OF THE PHYSICAL MODEL USED IN BOTH THE REINIUS AND MONTGOMERY STUDIES. REBUILT FROM REINIUS (1986) .....	43
FIGURE 2.17 : DIAGRAM OF THE PHYSICAL MODEL, MODIFIED FROM WANG AND JIANG (2010) .....	45
FIGURE 2.18 : <b>A</b> PHYSICAL MODEL USED IN GEORGE ET AL.'S EXPERIMENT <b>B</b> EXAMPLE OF AN INSTRUMENTED BLOCK. MODIFIED FROM GEORGE ET AL. (2015) .....	46
FIGURE 2.19 : <b>A</b> PELL'S FLOW CHANNEL <b>B</b> THE INSTRUMENTED BLOCK USED IN PELL'S MODEL. MODIFIED FROM PELL'S (2016).....	47
FIGURE 2.20 : <b>A</b> RONG ET AL.'S EXPERIMENTAL SETUP <b>B</b> EXAMPLE OF A MODELED JOINT. TAKEN FROM RONG ET AL. (2020) .....	48
FIGURE 3.1 : METHODOLOGY FOR COMPARING JOINT ORIENTATION PARAMETERS .....	61
FIGURE 3.2 : GSI DETERMINATION CHART AND CLASS SEPARATION MODIFIED FROM MARINOS AND HOEK (2000).....	62
FIGURE 3.3 : SKETCH OF A FRACTURED ROCK MASS. REBUILT FROM (KIRSTEN, 1982).....	66
FIGURE 3.4 : $E_{DOA}$ VALUES FOR A HORIZONTAL CHANNEL (PELLS, 2016) .....	68
FIGURE 3.5 : EXPERIMENTAL SETUP. REWORKED FROM REINIUS (1986) .....	68
FIGURE 3.6 : SIMULATED FRACTURE BETWEEN PIEZOMETERS 5 AND 8. DYNAMIC PRESSURES ARE ALSO SHOWN. REWORKED FROM REINIUS (1986).....	69
FIGURE 3.7 : DISTRIBUTION OF DATA BY $GSI_{CHART}$ CLASS .....	70
FIGURE 3.8 : DISTRIBUTION OF $J_s$ CLASSES OF PELL'S (2016) CASE STUDIES DATA .....	71
FIGURE 3.9 : DISTRIBUTION OF $E_{DOA}$ CLASSES OF PELL'S (2016) CASE STUDIES DATA .....	71
FIGURE 3.10 : DISTRIBUTION OF THE DATA ACCORDING TO REINIUS' STUDY (1986).....	72
FIGURE 3.11 : DISTRIBUTION OF PELL'S (2016) DATA BY $C_{UP}$ CLASSIFICATION.....	73
FIGURE 3.12 : RESULTS OF THE EFFECTS OF THE $J_s$ PARAMETER ON THE ROCK'S VULNERABILITY TO EROSION. LINES REPRESENT THE LINEAR APPROXIMATION OF THE DATA DISTRIBUTION <b>A</b> $GSI_{CHART}$ CLASS 1 <b>B</b> $GSI_{CHART}$ CLASS 2 <b>C</b> $GSI_{CHART}$ CLASS 3 <b>D</b> $GSI_{CHART}$ CLASS 4.....	74
FIGURE 3.13 : RESULTS OF THE EFFECTS OF THE $E_{DOA}$ PARAMETER ON THE ROCK'S VULNERABILITY TO EROSION. LINES REPRESENT THE LINEAR APPROXIMATION OF THE DATA DISTRIBUTION <b>A</b> $GSI_{CHART}$ CLASS 1 <b>B</b> $GSI_{CHART}$ CLASS 2 <b>C</b> $GSI_{CHART}$ CLASS 3 <b>D</b> $GSI_{CHART}$ CLASS 4.....	75



FIGURE 3.14 : RESULTS OF THE EFFECTS OF THE $C_{UP}$ PARAMETER ON THE ROCK'S VULNERABILITY TO EROSION. LINES REPRESENT THE LINEAR APPROXIMATION OF THE DATA DISTRIBUTION <b>A</b> $GSI_{CHART}$ CLASS 1 <b>B</b> $GSI_{CHART}$ CLASS 2 <b>C</b> $GSI_{CHART}$ CLASS 3 <b>D</b> $GSI_{CHART}$ CLASS 4.....	76
FIGURE 4.1 : PHOTOGRAPH OF ROMAINE-4 SPILLWAY OUTLINED IN RED (© HYDRO-QUÉBEC) .....	84
FIGURE 4.2 : SKETCH OF THE 1:40 SCALED PHYSICAL MODEL, MODIFIED FROM (KOULIBALY, 2021).....	86
FIGURE 4.3 : PHOTOGRAPH OF THE SCALED PHYSICAL MODEL (© MARIE-HÉLÈNE WISSE)...	86
FIGURE 4.4 : PRESSURE MEASURED ON SENSORS C1, C2, D1 AND D2. <b>A</b> ) TEST ONE. JOINT OPENING OF 2.5 CM, NO PROTRUSION; <b>B</b> ) TEST TWO. JOINT OPENING OF 0.5 MM, NO PROTRUSION; <b>C</b> ) TEST THREE. JOINT OPENING OF 0.5 MM, PROTRUSION OF THE MIDDLE ROW OF 2.8 CM UPWARDS .....	88
FIGURE 5.1 : LAYOUT AND DIMENSIONS OF THE PHYSICAL MODEL. MODIFIED FROM KOULIBALY ET AL. (2022) .....	98
FIGURE 5.2 : DISTRIBUTION OF FORCES AND WATER PRESSURE APPLIED AROUND A BLOCK (© MARIE-HÉLÈNE WISSE).....	99
FIGURE 5.3 : TESTING PROTOCOL APPLIED TO THE PHYSICAL MODEL OF HYDRO-QUÉBEC'S ROMAINE-4 DAM SPILLWAY .....	101
FIGURE 5.4 : <b>A</b> ) COPPER TUBES INSTALLED INSIDE THE MOULD; <b>B</b> ) INITIAL WATER ENTRIES (BLUE ARROWS) AND WATER EXITS (RED ARROWS) (© MARIE-HÉLÈNE WISSE).....	102
FIGURE 5.5 : <b>A</b> ) INSTRUMENTED 15 × 15 × 30 CM BLOCK WITHOUT ELBOWS; <b>B</b> ) INSTRUMENTED 15 × 15 × 30 CM BLOCK WITH CONNECTED ELBOWS; <b>C</b> ) THE PHYSICAL MODEL CHANNEL EQUIPPED WITH THE LVDT SENSOR AND THE TUBES CONNECTED TO THE WATER EXITS AT THE TOP OF THE INSTRUMENTED BLOCK (© MARIE-HÉLÈNE WISSE) .....	104
FIGURE 5.6 : EXAMPLES OF THE JOINT OPENINGS TESTED ON THE 15 × 15 × 30 CM BLOCKS; <b>A</b> ) 38 MM; <b>B</b> ) 20 MM; AND <b>C</b> ) 10 MM (© MARIE-HÉLÈNE WISSE).....	105
FIGURE 5.7 : EXAMPLE OF A PROTRUSION SETUP WITH THE CENTRE BLOCK HAVING A 20 MM PROTRUSION. A 7 MM JOINT OPENING WAS USED ALONG THE BOTTOM OF ALL BLOCKS (© MARIE-HÉLÈNE WISSE) .....	105
FIGURE 5.8 : TOTAL PRESSURE AND STATIC WATER HEIGHT FOR <b>A</b> ) FACE A; <b>B</b> ) FACE B; <b>C</b> ) FACE C; AND <b>D</b> ) FACE D.....	108
FIGURE 5.9 : STATIC PRESSURE ON <b>A</b> ) FACE A; <b>B</b> ) FACE B; <b>C</b> ) FACE C; AND <b>D</b> ) FACE D.....	109
FIGURE 5.10 : VELOCITY ON <b>A</b> ) FACE A; <b>B</b> ) FACE B; <b>C</b> ) FACE C; AND <b>D</b> ) FACE D .....	110
FIGURE 5.11 : FACE A PRESSURE COEFFICIENT OF VARIATION FOR FLOW RATES OF <b>A</b> ) 180 L/S; <b>B</b> ) 240 L/S; <b>C</b> ) 315 L/S; AND <b>D</b> ) 340 L/S .....	111

FIGURE 5.12 : MEAN FLOW VELOCITY ON TOP OF THE BLOCKS FOR DIFFERENT JOINT OPENINGS (JO) AND FLOW RATE IN THE CHANNEL IN THE CASE OF NO PROTRUSION (CONFIGURATION 0).....	112
FIGURE 5.13 : VARIATION OF $V_A/V_{CH}$ A) PROTRUSION CONFIGURATION 4; B) CONFIGURATION 6; C) CONFIGURATION 3; AND D) CONFIGURATION 8.....	113
FIGURE 5.14 : VARIATION OF $V_B/V_{CH}$ FOR A) PROTRUSION CONFIGURATION 4; B) CONFIGURATION 6; C) CONFIGURATION 3; AND D) CONFIGURATION 8.....	114
FIGURE 5.15 : THE VELOCITY DIFFERENTIAL BETWEEN THE UPSTREAM AND THE DOWNSTREAM FACE OF THE INSTRUMENTED BLOCK A) CONFIGURATION 4; B) CONFIGURATION 6; C) CONFIGURATION 3; AND D) CONFIGURATION 8.....	115

## LISTE DES SYMBOLES ET ABRÉVIATIONS

$c$ : Vitesse moyenne des vagues (m/s)	$J_s$ : Facteur de l'orientation des blocs, indice d'excavabilité
$C_{\text{joint}}$ : Coefficient de pression sous le bloc	$K$ : Indice de Kirsten
$C_{\text{surf}}$ : Coefficient de pression à la surface du bloc	$K_b$ : Facteur de la taille des blocs
$C_{\text{uplift}}$ : Coefficient de pression subi par le bloc	$K_d$ : Facteur de la résistance au cisaillement des joints
$C_r$ : Coefficient de densité	$K_h$ : Indice de résistance du massif rocheux
$d$ : Diamètres des grains (mm)	$KI$ : Pression appliquée dans le joint
$D_s$ : Profondeur de l'érosion atteinte selon le niveau d'eau (m)	$KIC$ : Résistance du joint
$E_{\text{doa}}$ : Paramètre d'ajustement des joints pour l'érodabilité	$L_{\text{bloc}}$ : Longueur d'un bloc (m)
$e_{\text{GSI}}$ : Indice de résistance du roc à l'érodabilité	$L_f$ : Longueur d'un joint (m)
$f$ : Facteur de correction dépendant de la géométrie et de la persistance du joint	$M_s$ : Facteur de résistance à la compression d'une roche intacte
$F_o$ : Forces agissant sur le dessus du bloc (kN)	$m_s$ : Masse du bloc (kg)
$F_{\text{QSL}}$ : Force de soulèvement quasi stable (kN)	$V_b$ : Volume des blocs
$F_{\text{sh}}$ : Résistance au cisaillement du joint (kN)	$\Pi_{\text{UD}}$ : Dissipation de puissance unitaire ( $\text{kW}\cdot\text{m}^{-2}$ )
$F_u$ : Forces agissant sous le bloc (kN)	$\Delta E$ : Perte d'énergie
$G_b$ : Poids d'un bloc (kg)	$\text{GSI}$ : Indice de résistance du massif rocheux
$g$ : Accélération gravitationnelle ( $\text{m}\cdot\text{s}^{-2}$ )	$\text{LF}$ : Facteur de probabilité
$H_n$ : Charge nette (m)	$\text{P1}$ : Facteur de l'isolation cinétique du système
$h_{\text{up}}$ : Hauteur de soulèvement du bloc (m)	$\text{P2}$ : Facteur de la nature de la surface potentiellement érodable
$J_a$ : Facteur du degré d'altération des joints	$\text{P3}$ : Facteur des caractéristiques des joints
$J_n$ : Facteur du nombre de joints	$\text{P4}$ : Facteur de l'espacement des joints
$J_o$ : Facteur de l'ouverture des joints	

P5 : Facteur de la forme des blocs

$P_{\max}$  : Pression maximale dynamique (kPa)

Q : Débit volumique ( $\text{m}^3.\text{s}^{-1}$ )

RF : Facteur d'importance

RMEI : Indice d'érodabilité du roc

RMR : Indice d'érodabilité du roc

RQD : Indice de qualité du roc

$\sigma_w$  : Contrainte exercée par l'eau (kPa)

q : Débit unitaire ( $\text{m}^2.\text{s}^{-1}$ )

$\gamma$  : Poids volumique ( $\text{kN}.\text{m}^{-3}$ )

$\gamma_r$  : Poids volumique du roc ( $\text{kN}.\text{m}^{-3}$ )

$\rho$  : Masse volumique ( $\text{kg}.\text{m}^{-3}$ )

$T_{\text{up}}$  : Coefficient de temps

$\Gamma$  : Coefficient pour les formules prédisant la profondeur de l'érosion

UCS : Résistance à la compression uniaxiale  
MPa

$Y_o$  : Hauteur d'eau à la surface du lit (m)

$Y_s$  : Profondeur de l'érosion selon le niveau initial  
(m)

$Z_b$  : Hauteur du bloc (M)

## REMERCIEMENTS

Je tiens à remercier mon directeur de maîtrise, professeur Ali Saeidi, pour son accompagnement et son soutien tout au long de mon parcours à la maîtrise. Merci de m'avoir donné l'opportunité de travailler sur un projet aussi innovant et stimulant.

Merci à mon co-directeur Marco Quirion pour ses précieux conseils et d'avoir allumé en moi l'intérêt pour la mécanique des roches lors des cours à Polytechnique.

Un énorme merci à Aboubacar Sidiki Koulibaly pour son magnifique travail de conception du modèle réduit, Luc Chatigny pour la construction du modèle et les nombreux ajustements nécessaires tout au long des essais, Carol Mercier pour l'aide importante qu'il a apportée pour l'instrumentation du modèle et David Noël pour son aide à la conception et à la construction des blocs de béton. Je remercie également le groupe de recherche R<sup>2</sup>eau et l'équipe d'ingénierie d'Hydro-Québec pour leur soutien et leurs conseils tout au long du projet.

Un merci supplémentaire au professeur Romain Chesnaux pour avoir pris du temps pour m'indiquer les plus belles randonnées du Saguenay.

Sur une note plus personnelle, je tiens à remercier mes parents qui m'ont soutenu tout au long de mon parcours scolaire. Au primaire, pour m'avoir donné l'opportunité d'aller à cette école d'où je tire les plus beaux souvenirs et qui m'influence encore certainement dans mes choix de vie d'aujourd'hui (une chance que je ne vous ai pas dit que je voulais y aller juste à cause de l'équitation...). Au secondaire, avec tous mes rêves et passions. Au Cégep, où j'ai trouvé ma voie. Au baccalauréat, ces quatre années intensives durant lesquelles j'ai vécu les plus belles expériences. Finalement, à la maîtrise, où votre appui m'a été essentiel.

Papa, pour avoir alimenté mes réflexions, Éline pour tes conseils, maman et Laurent, pour votre écoute et vos visites dans mon petit appartement.

Corinne, Manu et Aurélie qui, malgré la distance, m'ont apporté leur soutien chacun et chacune à leur façon.

Mathieu pour ta présence, ton écoute et toutes nos sorties en forêt.

## RÉSUMÉ

À la suite de plusieurs événements d'érosion dans des évacuateurs de crues de différents aménagements hydro-électriques à travers le monde, Hydro-Québec s'est penchée cette problématique d'érosion concernant ses propres installations. En particulier, la société d'État s'intéresse aux effets des caractéristiques du massif rocheux sur son érodabilité dans le cas des évacuateurs de crues non recouverts, à jet parallèle à la surface du canal. Un canal non recouvert a la particularité d'exposer le massif rocheux directement à la force érosive de l'écoulement. Il existe plusieurs méthodes de calcul basées sur des modèles à la fois expérimentaux et numériques pour déterminer le risque d'érosion de ce type d'ouvrages. Les méthodes de calcul pour l'étude de certains canaux non revêtus ont donné des résultats qui sous-évaluaient ou surévaluaient l'érosion par rapport à l'érosion produite. Deux classes de paramètres ont une incidence sur l'érosion des évacuateurs de crues: les caractéristiques hydrauliques de l'écoulement produisant des pressions sur les blocs rocheux formant le massif rocheux ainsi que les caractéristiques du massif rocheux lui-même, qui pourraient avoir une incidence sur la résistance du rocher face aux pressions générées par l'écoulement. Une revue de littérature exhaustive a été effectuée dans le cadre de ce projet sur le sujet et les résultats montrent que quelques modèles physiques à échelle réduite de canaux d'évacuation ont déjà été conçus. Toutefois, aucun de ces modèles n'offre une étude complète de l'influence des caractéristiques géométriques du massif rocheux sur le potentiel d'érosion. Dans le but d'étudier cette problématique, un modèle réduit de l'évacuateur de crues du barrage Romaine-4 d'Hydro-Québec a été construit dans un laboratoire de l'UQAC. Ce modèle réduit permet d'étudier à la fois les caractéristiques du massif rocheux et les caractéristiques de l'écoulement à l'aide d'une instrumentation adéquate. Une reproduction d'un massif rocheux fracturé sera réalisée à l'aide de neuf blocs de béton, dont un instrumenté de capteurs de pression, disposés dans le canal d'écoulement du modèle réduit. Leur disposition sera variable selon la caractéristique étudiée : leur orientation par rapport à l'écoulement, l'ouverture des joints entre les blocs, leur volume et leur saillie. Dans le cadre de cette étude, seules les caractéristiques de l'ouverture des joints et de la saillie ont été étudiées. Les mesures recueillies permettront d'évaluer l'effet de l'ouverture des joints et de la saillie sur les paramètres hydrauliques autour du bloc instrumenté. Notamment, les résultats permettent de constater que la vitesse de l'écoulement au-dessus des blocs est le paramètre dont la modification est la plus importante pour l'évaluation de la possibilité de soulèvement du bloc. Aussi, ce paramètre est influencé de manière significative par une modification de la saillie. Une diminution de l'ouverture des joints occasionne selon certaines conditions une augmentation de la vitesse dans les joints et l'effet de la hauteur de saillie sur la vitesse de l'écoulement dans les joints dépend de la configuration des blocs en place. Cette étude sera reprise ultérieurement afin de développer une méthode de caractérisation de l'érodabilité du massif rocheux, permettant de prévenir des dommages liés à l'érosion d'un évacuateur de crues excavé dans le roc.

# CHAPITRE 1 INTRODUCTION

## 1.1 MISE EN CONTEXTE

Au Québec, le principal producteur d'électricité est la société d'État Hydro-Québec, qui, avec ses 62 centrales hydro-électriques, permet la production d'une puissance électrique de près de 40 000 mégawatts (Hydro-Québec, 2019). Ces centrales sont conçues soit avec un réservoir, permettant un stockage d'énergie, soit au fil de l'eau, en récupérant l'énergie produite par la rivière. Dans les deux cas, à l'occasion de grandes crues, le volume de l'eau, dans le cas du réservoir, ou le débit, dans le cas du barrage au fil de l'eau, peut devenir trop important pour la capacité de l'ouvrage. Lors de ces événements, le surplus d'eau est évacué par un évacuateur de crues. Parmi les types d'évacuateurs de crues les plus communs, on compte les évacuateurs de crues à jet plongeant et ceux à écoulement parallèle à la surface d'un canal. Ce canal est souvent excavé à même le roc sur lequel le barrage est construit et est considéré à priori résistant à l'érosion. Cependant, plusieurs événements ont démontré que ces structures pouvaient en réalité être sensibles à l'érosion. À titre d'exemple, l'érosion de l'évacuateur du barrage Oroville a causé des dommages atteignant le milliard de dollars américains à la suite d'une crue importante en février 2017. Elle a aussi occasionné l'évacuation de 188 000 personnes vivant en aval du barrage, à cause du risque lié à la rupture de l'évacuateur de crues (Schimdt et al., 2017). En Australie, dans le bassin de dissipation du barrage Paradise, de l'érosion marquée et nécessitant aussi des réparations importantes s'est produite suite à deux crues importantes en 2011 et 2013 (Lesleighter et al., 2016). Le nombre croissant d'épisodes de crues dus aux changements climatiques font de l'érodabilité des évacuateurs de crues un enjeu d'importance. Ayant commencé à observer ce phénomène au sein de ses propres installations, Hydro-Québec s'est associée avec l'Université du Québec à Chicoutimi afin de réaliser une étude dans le but de développer une méthode permettant d'évaluer la sensibilité à l'érosion d'un massif rocheux et ainsi d'assurer la viabilité de ses ouvrages à long terme.

## 1.2 REVUE DE LITTÉRATURE

Il existe quelques méthodes de caractérisation générale de l'érosion des massifs rocheux : des méthodes semi-empiriques, qui regroupent les méthodes comparatives et les formules de prédiction de la profondeur de l'érosion, et des méthodes semi-analytiques (Jalili Kashtiban et al., 2021).

Les méthodes comparatives mettent en relation la résistance du roc à l'érosion avec la capacité érosive de l'écoulement, soit la dissipation de puissance unitaire, ( $\Pi_{UD}$ ), définie de la façon suivante :

$$\Pi_{UD}(\text{kW/m}^2) = \gamma q \Delta E \quad (1.1)$$

Où  $\gamma$  est le poids volumique de l'eau ( $\text{kN/m}^3$ ),  $q$  est son débit unitaire ( $\text{m}^2/\text{s}$ ) et  $\Delta E$  est sa perte d'énergie (J) (Jalili Kashtiban et al., 2021). L'érosion se produit lorsque la force érosive de l'eau, correspondant à la dissipation de puissance unitaire de l'écoulement, devient plus grande qu'une fonction de la résistance à l'érosion du roc ( $K_h$ ) :

$$\Pi_{UD} > f(K_h) \quad (1.2)$$

La résistance à l'érosion du roc est définie par différentes méthodes : l'indice de Kirsten, le « Erodibility Geological Strength Index » (eGSI) ainsi que le « Rock Mass Erodibility Index » (RMEI). Ci-dessous se trouve une brève description de ces indices.

### 1.2.1 INDICE DE KIRSTEN

L'indice de Kirsten (K) est avant tout un indice développé pour mesurer l'excavabilité du sol et du roc. Il est défini de la façon suivante (Kirsten, 1982) :

$$K = M_s K_b K_d J_s \quad (1.3)$$

Avec

$M_s$  : Le nombre de résistance de masse;

$$\text{Pour } UCS \leq 10 \text{ MPa} \quad M_s = 0.78 C_r (UCS)^{1.05}$$

$$\text{Pour } UCS \geq 10 \text{ MPa} \quad M_s = C_r (UCS)$$

UCS est la résistance à la compression uniaxiale du roc ;



$C_r$  est un coefficient de densité :  $C_r = \frac{\gamma_r}{27}$  (Boumaiza, 2019)

Où  $\gamma_r$  est le poids volumique du roc (kN/m<sup>3</sup>)

$K_b$  : Le nombre de la grosseur des blocs;

Où  $K_b = \frac{RQD}{J_n}$  et  $K_d = \frac{J_r}{J_a}$

$K_d$  : Le nombre de la résistance des joints;

$J_s$  : Le nombre de la structure relative des blocs par rapport à l'écoulement.

$J_s$  est déterminé à partir d'une charte<sup>1</sup>, tirée de la détermination de l'indice Q (Barton et al., 1974), tout comme les variables  $J_n$ ,  $J_r$  et  $J_a$ .

L'indice de Kirsten a été utilisé par Van Schalkwyk et al. (1994), Annandale (1995) et Kirsten et al. (2000) pour définir une limite d'érodabilité (Figure 1.1). Comme il est possible de le constater à la figure 1.1, ces fonctions peuvent donner des résultats d'érodabilité différents. Plusieurs critiques sont formulées à l'endroit de l'indice de Kirsten. En particulier, il a été avant tout conçu pour définir l'excavabilité du roc et non son érodabilité. Notamment, les paramètres  $M_s$  et  $J_s$  sont critiqués par Pells (2016) comme étant non représentatifs de l'érodabilité du roc. L'indice de Kirsten a aussi engendré des erreurs d'estimation pour l'excavabilité du roc. Certains paramètres de cet indice seraient à l'origine de cette différence, comme le paramètre  $K_b$  décrivant la grosseur des blocs et la résistance à la compression uniaxiale du roc, utilisée pour calculer le paramètre  $M_s$ . Selon l'indice de Kirsten, une résistance à la compression uniaxiale élevée engendre un paramètre  $M_s$  plus élevé, ce qui vient augmenter la résistance à l'érosion du roc. Pells (2016) fait la remarque que la résistance à l'érosion du roc dépend surtout des caractéristiques de ses familles de joints, comme leur orientation par rapport à l'écoulement, leur persistance et la grosseur des blocs. Pour le paramètre  $K_b$ , il est critiqué en ce sens qu'il ne

---

<sup>1</sup> Disponible dans Kirsten, H. 1982. A classification system for excavation in natural materials. Civil Engineer in South Africa **24**(7): 293-308.

représente pas bien la taille des blocs et que le paramètre  $V_b$ , décrivant le volume des blocs, serait plus représentatif (Boumaiza, 2019).

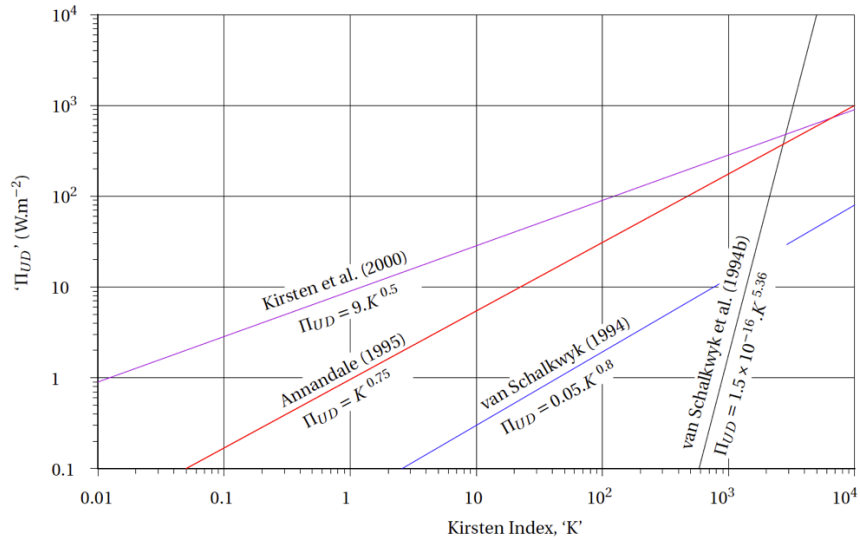


Figure 1.1 : Limites d'érodabilité définies avec l'indice de Kirsten selon différents auteurs. Tiré de Pells (2016)

### 1.2.2 MÉTHODES DE PELLIS

Pells a formulé deux méthodes de caractérisation de la résistance du massif rocheux, le eGSI et le RMEI, basées sur des observations de terrain ainsi que sur des essais à partir d'un modèle réduit.

L'indice eGSI, modifié à partir du « Geological Strength Index » (GSI) (Hoek et al., 1995), tire ses composantes du « Rock Mass Rating » (RMR) (Bienawski, 1976). Le eGSI a la particularité d'inclure un paramètre de l'orientation des blocs par rapport à la direction de l'écoulement, le paramètre «  $E_{doa}$  », ayant une incidence sur l'érodabilité du roc. Ce paramètre varie selon le ratio de fracturation dans le massif rocheux, l'orientation des joints par rapport à l'écoulement, ainsi que les caractéristiques de l'écoulement en présence. L'indice GSI est déterminé à partir d'un tableau visuel duquel une valeur de « qualité du roc » est tirée (Marinos et Hoek, 2000). Le résultat final de l'indice est obtenu en additionnant la valeur du paramètre «  $E_{doa}$  » à la valeur du GSI, selon l'équation 1.4 (Pells, 2016) :

$$eGSI = GSI + E_{doa} \tag{1.4}$$

Le RMEI offre une classification des paramètres du massif rocheux selon un facteur de probabilité (LF) et un facteur d'importance (RF). Les paramètres sont classés de P<sub>1</sub> à P<sub>5</sub> et représentent, respectivement :

- L'isolation cinétique du système;
- La nature de la surface potentiellement érodable;
- Les caractéristiques des joints;
- L'espacement des joints;
- La forme des blocs.

Une fois ces valeurs déterminées à partir d'un tableau d'identification<sup>2</sup>, l'équation 1.5 est utilisée (Pells, 2016):

$$RMEI = [(RF_{P1} * LF_{P1}) * (RF_{P2} * LF_{P2})] * [(RF_{P3} * LF_{P3}) + (RF_{P4} * LF_{P4}) + (RF_{P5} * LF_{P5})] \quad (1.5)$$

Pells a lui-même critiqué ces méthodes, en ce sens qu'elles n'offrent qu'une classification générale de l'érosion, de faible à majeure, plutôt qu'une description plus précise de la profondeur qu'elle atteindra. De plus, cette classification générale est réalisée à partir d'un graphique, dont les limites d'importance de l'érosion sont tracées manuellement selon les résultats obtenus lors de ses essais et lors d'observations sur le terrain. Ces limites engendrent des erreurs de classification des situations d'érosion des évacuateurs de crues étudiés s'élevant à 60% (Boumaiza, 2019).

### 1.2.3 FORMULES SEMI-EMPIRIQUES PRÉDISANT LA PROFONDEUR DE L'ÉROSION

La récente étude de Castillo et Carrillo (2016) a étudié 31 formules de prédiction de l'érosion pour en venir à développer une équation générale (1.6):

$$D_s = Y_0 + Y_s = \Gamma \cdot \frac{q^x H_n^y Y_0^w}{g^v d^z} \quad (1.6)$$

---

<sup>2</sup> Voir Pells, S. 2016. Erosion of Rocks in Spillways. Thesis, Civil and Environmental Engineering, University of New South Wales.

Où  $Y_0$  est le niveau initial du lit (m),  $Y_S$  est la profondeur de l'érosion (m),  $q$  est le débit unitaire (m/s),  $H_n$  est la différence de charge entre l'amont et l'aval (m) et  $g$  est l'accélération gravitationnelle (m/s<sup>2</sup>). Les coefficients de l'équation sont déterminés empiriquement par différentes études (Castillo et Carrillo, 2016).

Les formules semi-empiriques prédisent la profondeur de l'érosion au point d'impact d'un jet plongeant et sont basées sur l'analyse de données d'érosion réelles et sur des expériences en laboratoire. L'équation générale présentée est seulement applicable dans des conditions d'écoulement de type jet plongeant.

#### 1.2.4 MÉTHODES SEMI-ANALYTIQUES

La méthode semi-analytique de Bollaert (2004), le « Comprehensive Scour Model », est composée de trois modules : « Dynamic Impulsion » (DI), « Comprehensive Fracture Mechanism » (CFM) et « Quasi-Steady Impulsion » (QSI), décrivant chacun un procédé d'érosion différent.

##### 1.2.4.1 Dynamic Impulsion (DI)

Le DI est un processus instantané, suivant le principe de la deuxième loi de Newton. Le DI est applicable aux blocs d'un massif rocheux situé au point d'atterrissage d'un jet plongeant et survient lorsque les pressions de soulèvement se propageant dans les fractures sous le bloc ( $F_u$ ) deviennent plus grandes que les forces résistantes à ce soulèvement : le poids du bloc ( $G_b$ ), la résistance au cisaillement des joints ( $F_{sh}$ ) et les forces agissant sur le dessus du bloc ( $F_o$ ). L'éjection du bloc devient plus probable lorsque la hauteur de soulèvement ( $h_{up}$ ) devient plus grande que la moitié de la hauteur du bloc ( $Z_b$ ). Les forces  $F_u$  et  $F_o$  sont définies selon les caractéristiques du jet. Les équations 1.7, 1.8 et 1.9 décrivent le calcul de la hauteur de soulèvement  $h_{up}$  (m).

$$h_{up} = \frac{V_{\Delta tpulse}^2}{2g} \quad (1.7)$$

$$V_{\Delta tpulse}^2 = \frac{(F_u - F_o - G_b - F_{sh})dt}{m_s} \quad (1.8)$$

Où  $dt$  est une intégrale de temps, obtenue avec

$$dt = T_{up} \frac{2L_f}{c} \quad (1.9)$$

Où  $g$  est l'accélération gravitationnelle ( $m/s^2$ ),  $m_s$  est la masse du bloc ( $kg$ ),  $T_{up}$  est un coefficient de temps,  $L_f$  est la longueur du joint ( $m$ ) et  $c$  est la vitesse moyenne des vagues ( $m/s$ ). Le schéma de la figure 1.2 illustre le module DI.

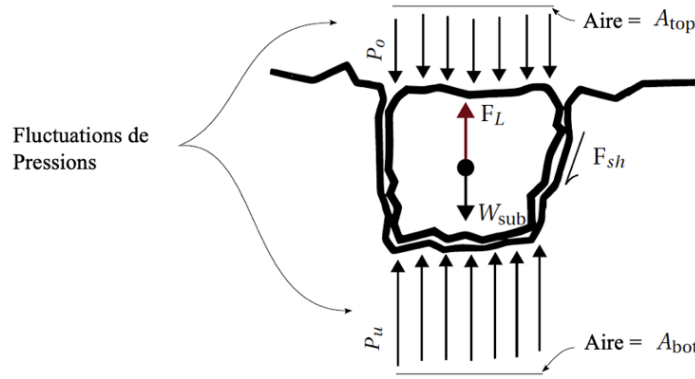


Figure 1.2: Forces agissant lors du processus de soulèvement de blocs (Pells, 2016)

#### 1.2.4.2 Comprehensive Fracture Mechanism (CFM)

Le CFM peut être un processus à la fois instantané et dépendant du temps, en fonction du type de fracture produit. Il est applicable aux fractures fermées qui ne forment pas de blocs, soumises à un écoulement de type de jet plongeant. Ce module suit le principe du mécanisme élastique linéaire. Si la contrainte exercée sur la fracture ( $K_I$ ) ( $MPa/m^{1/2}$ ) est plus petite que la résistance de la fracture ( $K_{IC}$ ) ( $MPa/m^{1/2}$ ), alors le processus de fracturation sera dépendant du temps. Si au contraire  $K_I > K_{IC}$ , la fracturation est instantanée. La contrainte appliquée à la fracture est calculée de la façon suivante :

$$K_I = \sigma_w * f * \sqrt{\pi * L_f} \quad (1.10)$$

Où  $\sigma_w = 0.8P_{max}$ ,  $f$  est un facteur de correction dépendant de la géométrie et de la persistance du joint et  $L_f$  est la longueur de la fracture ( $m$ ).  $P_{max}$  est la pression maximale dynamique se produisant dans les fissures fermées ( $MPa$ ), dépendante des caractéristiques du jet (Jalili Kashtiban et al., 2021). La résistance de la fracture ( $K_{IC}$ ) dépend de la minéralogie de la roche et peut être calculée à l'aide de la résistance à la contrainte en tension ou à la compression uniaxiale (Bollaert, 2010).

### 1.2.4.3 Quasi-Steady Impulsion (QSI)

Le module du QSI est applicable au processus « d'arrachement » des blocs en saillie par un courant parallèle à la surface. Le principe est tiré du module DI, mais seule la force de soulèvement quasi stable ( $F_{QSL}$ ) est considérée. Bollaert (2012) se base sur l'étude expérimentale de Reinius (1986) pour calculer  $F_{QSL}$  (kN) avec les coefficients  $C_{joint}$  et  $C_{surf}$ . Ces coefficients sont obtenus par le rapport entre la pression dynamique obtenue dans le joint ( $C_{joint}$ ) ou à la surface ( $C_{surf}$ ) du bloc et la pression dynamique dans le canal, en considérant la vitesse de l'écoulement dans le canal. Bollaert (2012) mentionne que la différence entre ces coefficients permet d'obtenir un coefficient de soulèvement  $C_{uplift}$  permettant de calculer  $F_{QSL}$  (équations 1.11 et 1.12).

$$F_{QSL} = C_{uplift} L_{bloc} \frac{v_{x,max}^2}{2g} \quad (1.11)$$

$$C_{uplift} = C_{joint} - C_{surf} \quad (1.12)$$

Où  $L_{bloc}$  est la largeur du bloc (m),  $V$  est la vitesse de l'écoulement parallèle au bloc (m/s) et  $g$  est l'accélération gravitationnelle (m/s<sup>2</sup>).

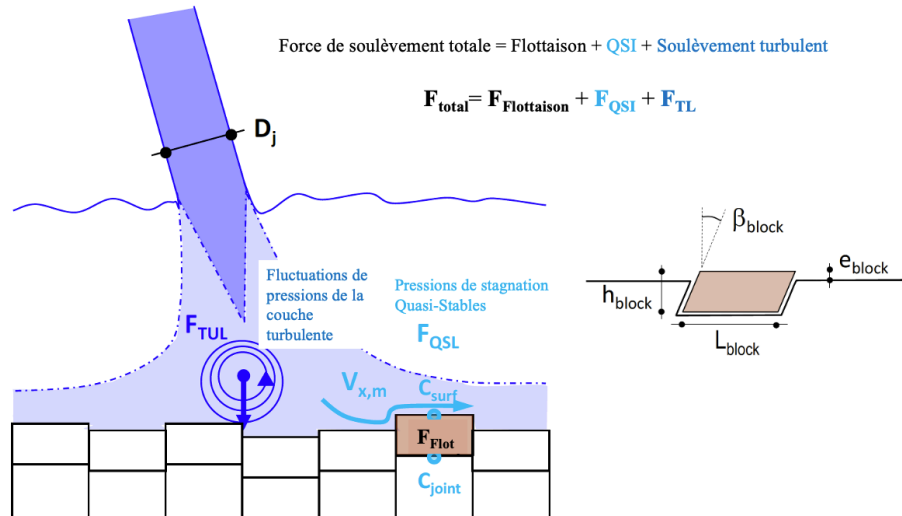


Figure 1.3: Illustration du module QSI, traduit de (Bollaert, 2012)

Cette brève revue de la littérature sur les méthodes existantes de caractérisation de l'érosion montre qu'elles comportent quelques lacunes :

- La différence importante de prévision de l'érosion des méthodes;
- Le décalage important entre la prévision par les méthodes existantes et ce qui a été observé en réalité dans certains cas;
- Les formules semi-empiriques sont seulement applicables aux écoulements de type jet plongeant;
- Parmi les méthodes semi-analytiques, seul le QSI pourrait être applicable aux écoulements de type canal ouvert, pour des blocs en saillie uniquement;
- Parmi les méthodes existantes de caractérisation de l'érosion, très peu sont à la fois applicables au cas de l'érosion des évacuateurs de crues à canal ouvert et suffisamment fiables en matière de prévision de l'érosion.

Les modèles physiques sont des outils importants permettant l'étude du phénomène de l'érosion. Connaître les capacités des modèles physiques existants est primordial pour le développement d'un modèle physique au laboratoire. Le chapitre 2 présente un article de revue de littérature de ces modèles.

Puisqu'aucun modèle physique permettant l'étude simultanée des paramètres géomécaniques relevés par Boumaiza (2019) n'a encore été développé, un modèle réduit de l'évacuateur de crue du barrage ROMAINE-4, à une échelle de 1 :40, sera construit dans un laboratoire de l'UQAC. Ce modèle permettra de pondérer ces paramètres par rapport à leur importance dans le processus de l'érosion en incluant différentes configurations hydrauliques. Ainsi, les résultats seront inclus dans le développement d'une méthode de caractérisation de l'érosion du massif rocheux applicable aux évacuateurs de crue. Aussi, ce modèle permettra de calibrer un futur modèle numérique, qui permettra d'étudier le phénomène d'érosion à l'échelle réelle.

### **1.3 PROBLÉMATIQUE**

Les deux principales catégories de facteurs de l'érosion dans les évacuateurs de crues sont les caractéristiques hydrauliques de l'écoulement et la résistance à l'érosion du massif rocheux. Le seuil d'érodabilité est défini comme étant la limite où la puissance hydraulique ( $P$ ) dépasse la résistance du roc à l'érosion ( $K_t$ ) (Annandale, 1995). Le débit de l'écoulement, sa turbulence et la présence ou non d'un saut hydraulique auront un impact sur les pressions et éventuellement sur l'érosion subie par le massif rocheux. La résistance du massif rocheux à l'érosion dépend de plusieurs paramètres, en particulier de l'orientation et de

l'ouverture des joints, du volume des blocs ainsi que des conditions d'altération du roc et de la saillie des blocs (Boumaiza, 2019). Des chercheurs se sont déjà penchés sur le sujet et en sont venus à formuler des méthodes de caractérisation de l'érosion, qui sont en théorie applicables aux évacuateurs de crues. Ces méthodes ont été développées en se basant sur des essais effectués sur des modèles réduits ainsi que sur l'analyse de situations d'érosion réelles au sein d'ouvrages existants. Elles comprennent la caractérisation hydraulique de l'écoulement ainsi que la caractérisation de la résistance du massif rocheux. Les résultats d'érosion relevés sur des ouvrages existants ont souvent été observés comme étant plus importants que ce que les méthodes de calculs de prévision de l'érosion prévoyaient (Pells, 2016). Une étude plus approfondie, comprenant un modèle physique réduit représentatif d'un évacuateur de crues avec l'analyse des caractéristiques de l'écoulement ainsi que des paramètres de résistance du massif rocheux, permettra d'évaluer l'effet de chacun de ces paramètres sur la distribution des pressions à l'intérieur du massif rocheux et ainsi de pouvoir évaluer leur effet sur l'érosion.

Cette étude servira éventuellement au développement d'une méthode plus précise de prévision et d'évaluation de l'érosion conçue pour les conditions retrouvées dans les évacuateurs de crues à écoulement parallèle à la surface du canal.

## **1.4 OBJECTIFS**

Ci-dessous sont spécifiés l'objectif global ainsi que les objectifs spécifiques de ce projet de maîtrise.

### **1.4.1 OBJECTIF GÉNÉRAL**

L'objectif général de ce projet de maîtrise est de déterminer les effets de l'ouverture des joints et de la saillie des blocs sur les paramètres hydrauliques dans les joints et sur le potentiel de soulèvement des blocs du massif rocheux à partir d'un modèle réduit d'évacuateur de crues en laboratoire. Afin d'atteindre cet objectif général, les sous-objectifs suivants ont été considérés.

### **1.4.2 OBJECTIFS SPÉCIFIQUES**

Les objectifs spécifiques sont précisés comme suit :



- Déterminer les avantages et les inconvénients des modèles physiques existants dans la littérature afin de développer un système d'instrumentation optimal;
- Évaluer l'efficacité des paramètres existants pour l'orientation des joints sur l'érosion en utilisant des situations d'érosion observées dans des projets réels;
- Instrumenter et calibrer le modèle réduit et procéder à sa mise en marche pour la réalisation des essais;
- Déterminer les effets de l'ouverture des joints et de la saillie des blocs sur la vitesse dans les joints du massif rocheux;
- Déterminer les effets de l'ouverture des joints et de la saillie des blocs sur les fluctuations de pression dans les joints du massif rocheux;
- Déterminer les effets de l'ouverture des joints et de la saillie des blocs sur le potentiel de soulèvement des blocs du massif rocheux.

L'ouverture des joints et la saillie des blocs seront analysées et comparées sur le plan de la variation de la pression moyenne de soulèvement produite en fonction de la variation de ces paramètres ainsi que sur le plan de l'amplitude des fluctuations de pressions sur les faces du bloc.

## **1.5 MÉTHODOLOGIE**

La méthodologie suivie pour ce projet de maîtrise est composée de trois parties. La première est en lien avec la revue de littérature, la deuxième concerne l'évaluation de paramètres d'orientation des joints et la troisième concerne la réalisation des essais sur le modèle réduit.

### **1.5.1 ÉTUDE APPROFONDIE DES MODÈLES PHYSIQUES EXISTANTS**

La revue de littérature réalisée a permis d'entreprendre une étude approfondie des modèles physiques existants. Ceci a permis plus particulièrement de considérer les paramètres hydrauliques et les paramètres relatifs aux caractéristiques du roc ayant déjà été mis à l'essai dans un modèle physique, ou encore de considérer ceux n'ayant jamais fait partie d'une étude sur un modèle physique. Dans la revue de littérature, les modèles physiques existants d'évacuateurs de crues sont séparés en deux classes : ceux étudiant principalement les paramètres hydrauliques de l'écoulement et ceux se concentrant sur les paramètres du massif rocheux. Puis, les

modèles faisant partie de la deuxième classe sont une fois de plus classés en deux classes: ceux reproduisant un évacuateur de crues à jet plongeant et ceux reproduisant un évacuateur de crues à jet parallèle. Les modèles sont aussi comparés par rapport aux caractéristiques du massif rocheux ayant été étudiées dans chacun d'eux. Ceci a permis d'avoir une idée précise de ce qui a été étudié auparavant, et aussi de savoir quelles sont les lacunes par rapport aux paramètres du massif rocheux qui ont déjà été étudiés. La revue de littérature réalisée sur les modèles physiques existants a aussi permis de prendre connaissance des mesures réalisées dans le cadre de ces essais antérieurs, et ainsi de les comparer et d'évaluer la méthode et l'instrumentation les plus adaptées à la situation du modèle construit à l'UQAC.

### **1.5.2 ÉVALUATION DES PARAMÈTRES D'ORIENTATION DES JOINTS**

L'évaluation de paramètres d'orientation des joints existants a été ajoutée à ce projet de maîtrise, suite aux délais encourus dans la construction du modèle réduit dus à la COVID. En se servant de la base de données de Pells (2016), trois paramètres d'orientation des joints ont été comparés entre eux. Jumelés à l'indice de qualité du roc GSI (Geological Strength Index), les niveaux de dommages prévus en fonction de la puissance de l'écoulement ont été comparés aux niveaux de dommages réels ayant eu lieu. Cette étude comparative a permis de démontrer qu'aucun des trois paramètres d'orientation des joints évalués jumelés avec l'indice GSI ne retourne sans erreur le niveau de dommages réel. Une meilleure connaissance de l'effet de l'orientation des joints sur l'érodabilité du massif rocheux est donc requise.

### **1.5.3 RÉALISATION DES ESSAIS SUR LE MODÈLE RÉDUIT**

La méthodologie suivie pour la réalisation des essais sur le modèle réduit est présentée en détail au chapitre 4 et un sommaire de cette méthodologie est présenté à la figure 1.4. Les essais sont réalisés avec un modèle réduit d'évacuateur de crues à l'échelle du laboratoire, à échelle 1:40 de l'évacuateur de crues du barrage Romaine-4 d'Hydro-Québec. Neuf blocs de béton sont disposés au centre d'un canal d'écoulement, incliné à 9°. Le bloc du centre est doté de onze entrées d'eau, deux sur chaque face et une sur le dessus, lesquelles seront liées à trois capteurs de pression. Un schéma du modèle réduit et un exemple de bloc instrumenté ayant servi pour les essais sont présentés à la figure 1.5. Afin d'évaluer les effets de l'ouverture des joints et de la saillie sur les paramètres hydrauliques dans les joints, un total de quatre ouvertures de joints, quatre hauteurs de saillie et quatre configurations de saillies différentes ont été mis à l'essai dans le modèle.

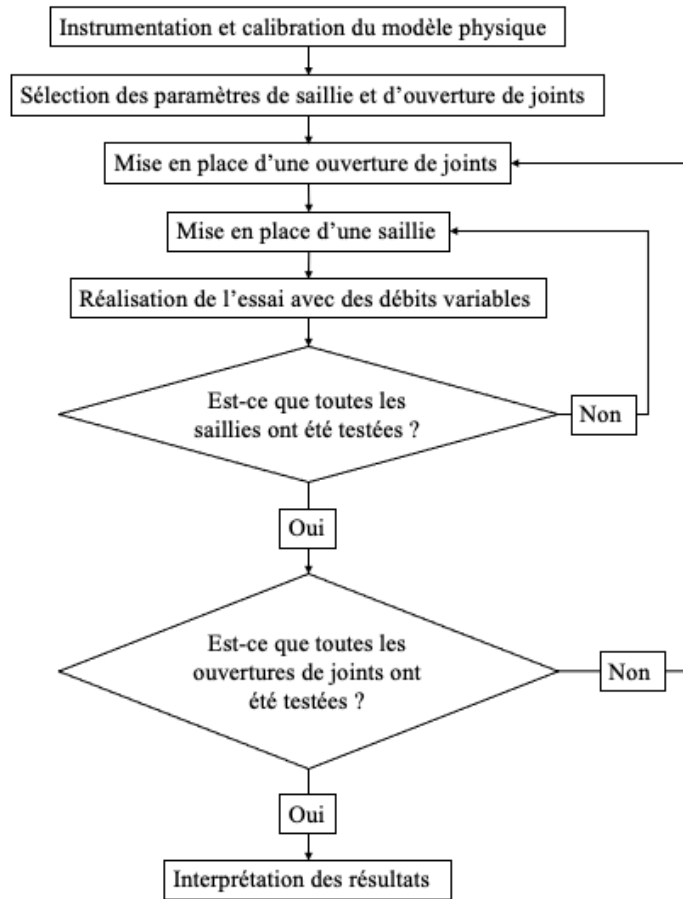


Figure 1.4: Sommaire de la méthodologie suivie pour la réalisation des essais sur le modèle réduit

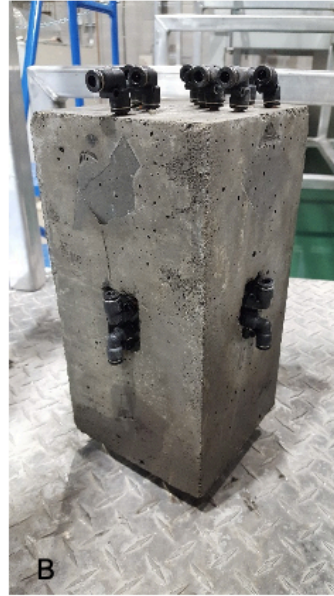
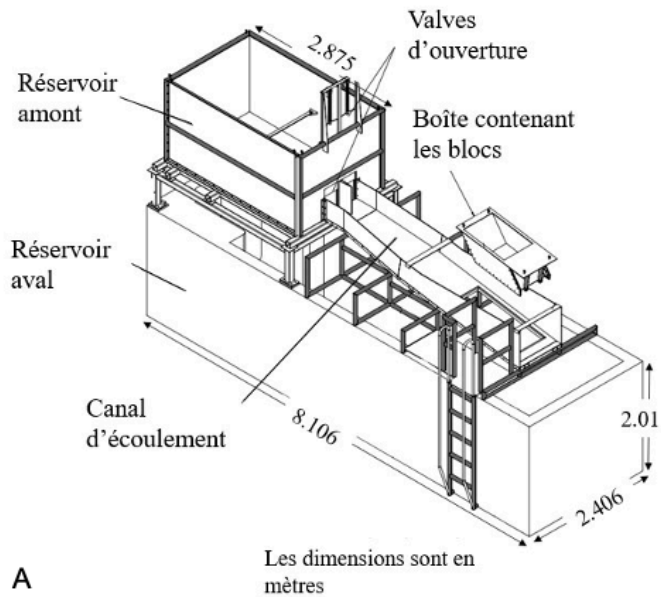


Figure 1.5: **A** Schéma du modèle réduit (Koulibaly, 2021) **B** Bloc instrumenté avec des entrées et sorties d'eau (© Marie-Hélène Wisse)

## 1.6 STRUCTURE DU MÉMOIRE

Ce mémoire présente 5 chapitres comprenant une introduction, les 4 articles préparés au cours du travail de maîtrise formant un chapitre chacun, et une conclusion.

Le chapitre d'Introduction est le **chapitre 1**. Il présente une brève revue de littérature du sujet de maîtrise, la problématique à laquelle la recherche tente de répondre, les objectifs du projet de maîtrise ainsi que la méthodologie suivie pour atteindre ces objectifs.

Le **chapitre 2** répond à l'objectif 1 de ce projet de maîtrise en présentant une revue de littérature approfondie portant sur les modèles physiques existants d'évacuateurs de crues. Il met en lumière les principales caractéristiques de ces modèles physiques et de quelle façon ils sont utiles pour étudier l'érodabilité du massif rocheux.

Le **chapitre 3** répond à l'objectif 2 de ce projet de maîtrise en présentant une étude comparative entre trois paramètres évaluant l'effet de l'orientation des joints du massif rocheux sur son érodabilité dans un évacuateur de crues. Cette étude a été réalisée en appliquant des paramètres d'orientation des joints existants à

une base de données comprenant des informations sur la géologie et l'hydraulique de sections de barrages ayant subi de l'érosion.

Le **chapitre 4** présente un article publié dans la Revue de la Société canadienne de géotechnique, présentant brièvement le modèle réduit et les premiers résultats obtenus.

Le **chapitre 5** répond aux objectifs 3, 4, 5 et 6 de ce projet de maîtrise. L'instrumentation utilisée pour le modèle est détaillée, puis les résultats obtenus avec le modèle réduit sont présentés. Les résultats permettent d'évaluer les effets de l'ouverture des joints et de la saillie des blocs sur les paramètres hydrauliques dans les joints et sur les fluctuations de pression, puis de déterminer la possibilité de soulèvement des blocs du massif rocheux. Ces résultats mènent à une discussion par rapport à la possibilité d'érosion du massif rocheux en fonction des paramètres évalués.

Le **chapitre 6** présente la conclusion de mémoire de maîtrise, ainsi que les principales recommandations pour la suite de la recherche sur le modèle physique réduit en laboratoire.

## **CHAPITRE 2 REVUE DE LITTÉRATURE TRAITANT DES MODÈLES PHYSIQUES EXISTANTS POUR ÉTUDIER L'ÉROSION DU MASSIF ROCHEUX DANS LES ÉVACUATEURS DE CRUES**

Cet article reprend un article dont le premier auteur est l'auteur de ce mémoire. Le chapitre présente une revue de littérature portant sur les modèles physiques existants d'évacuateurs de crues.

Cet article est soumis à la revue *Acta Geotechnica* et en attente d'approbation.

# **A systematic review of existing laboratory models for evaluating the hydrogeometrical parameters of rock mass erosion**

**Marie-Hélène Wisse<sup>a,1</sup>, Ali Saeidi<sup>a</sup> ing. PhD, Esmail Eslami<sup>a</sup> PhD, Marco Quirion<sup>b</sup> ing. PhD, Carl-Oscar Nilsson<sup>c</sup> MSc**

<sup>a</sup> Department of Earth Sciences, Université du Québec à Chicoutimi, 555, boulevard de l'Université, Chicoutimi (Québec), G7H 2B1 Canada

<sup>b</sup> Rock Mechanics, Hydro-Québec, Montréal (Québec), H2Z 1A4 Canada

<sup>c</sup> Dam Safety, Uniper, Östersund, 831 52, Sweden

<sup>1</sup>Corresponding author : Marie-Hélène Wisse, [marie-helene.wisse1@uqac.ca](mailto:marie-helene.wisse1@uqac.ca)

## STATEMENTS AND DECLARATIONS

This work was supported by Hydro-Québec, Natural Sciences and Engineering Research Council of Canada (NSERC), Mitacs, and Uniper.

The authors have no conflict of interest to declare relevant to this article's content.

## ACKNOWLEDGMENTS

The authors would like to thank the research group R<sup>2</sup>Eau for their helpful comments and suggestions and the Natural Sciences and Engineering Research Council of Canada (NSERC) (#CRDPJ 537350 – 18), Hydro-Québec, Mitacs Inc. (# IT22640), and Uniper for research funding.

## DATA AVAILABILITY

Data sharing not applicable to this article as no datasets were generated or analysed during the current study. All papers used for this review article are included in the references.

## CONTRIBUTION STATEMENT

This review article was an idea of Ali Saedi. Marie-Hélène Wisse did the literature search and data analysis and also wrote the first draft of the manuscript. All authors critically revised the work. All authors have read and approved the final manuscript.

## ABSTRACT

Physical flow models are used to study parameters affecting the erodibility of rock in dam spillways. Here we classify these models into two types. The first, which involves studying the hydraulic characteristics of the flow, modifies the characteristics of the flow or the general configuration of the model, such as slope or spillway type. These models characterize the flow using pressure measurements or erosion patterns to study the energy dissipation of water. The second type, which evaluates the geometric characteristics of a rock mass, simulates a rock mass either by blocks or joints and measures the effect of different configurations. These models use either a plunging jet-type flow or an open-channel flow. Among these models, the orientations of joints and protrusions are the most studied parameters; other potentially important parameters remain poorly or unsuccessfully studied. Moreover, most models of the second category consider only a single block, thereby preventing the study of possible interactions between blocks. Although our understanding of the identified hydraulic characteristics affecting erosion is improving, there remains a lack of knowledge about those rock mass characteristics affecting rock erodibility in dam spillways.

Keywords: Erosion, Hydraulic, Physical model, Rock Mass, Scour, Spillway



## 2.1 INTRODUCTION

There are two main types of spillways: those with a flow parallel to the surface and those with a plunging flow. The erosion of the rock mass varies between these spillways types because of differences between the applied hydraulic forces on the rock. In both types, erosion in dam spillways can cause significant damage and lead to substantial financial costs to the owners and safety risks to the public (Hearden, 2018; Pells, 2016; Sawadogo, 2010). The hydraulic characteristics of the flow and the resistance to erosion of the rock mass are the two factors that affect erosion in spillways (Annandale, 1995; Pells, 2016). The water flow rate, the degree of aeration of the flow, flow turbulence, and the presence (or not) of a hydraulic jump will alter hydraulic pressures and possibly favor the erosion of a rock mass (Ervine et al., 1997; Kote et Nangare, 2019; Manso et Schleiss, 2006; Wilkinson et al., 2018). The resistance of the rock mass to this erosion depends on several parameters, including the orientation and opening of joints, joint shear strength, the distribution of uplift pressure, and block volume (Bollaert et Schleiss, 2002; Boumaiza et al., 2019b; Pells, 2016).

The general characterization methods of rock mass erosion can be classified as semi-empirical or semi-analytical (Bollaert et Schleiss, 2003; Jalili Kashtiban et al., 2021; Pells, 2016). Semi-empirical methods have been developed either on the basis of limited data from erosion situations observed around the world or through certain analytical principles and laboratory experiments under very specific conditions (Annandale, 1995; Kirsten et al., 2000; Pells, 2016; Van Schalkwyk et al., 1994). Semi-analytical methods, such as the comprehensive scour model (CSM) (Bollaert, 2004; Bollaert, 2010; Bollaert, 2012; Bollaert et Schleiss, 2002), are based on the analytical concept of erosion and permit assessing the evolution of erosion; however, they require data that can be challenging to obtain (Lesleighter et al., 2016). This second group of methods has been developed for the case of plunging jet spillways and cannot be used to evaluate rock mass erosion in spillways.

Existing methods can produce errors for predicting erosion that exceed 45% (Boumaiza et al., 2021). However, given the limitations of the observed erosion data and the lack of in-depth knowledge about evaluating the effects of hydraulic parameters and the rock mass on erosion, laboratory physical models can be relevant tools for determining the effect of both the rock mass and hydraulic parameters on erosion.

Some physical models in hydraulic and geotechnical engineering can be applied to studying the hydraulic characteristics of flow and erosion phenomena over granular materials (Dargahi, 2003; Tuna, 2012) or a rock mass. The study of rock mass characteristics is vital for developing a better understanding of the hydraulic erosion of rocks. Reinius (1986) proposed one of the first relevant models. His model measured how a block's orientation—in the direction of and opposite to that of the flow—and its protrusion affect water pressure on the block surface. Similarly, Pells (2016) and George et al. (2015) simulated different configurations of the rock mass. By modeling a single block, they measured the effect of its configuration on, respectively, the resulting pressures (Pells, 2016) and displacements (George et al., 2015). Bollaert and Schleiss (2002) focused on the pressure distribution within different joints and built a physical model in which only steel joints were simulated. Water pressure was generated by a vertical jet, and the steel joint was placed at the bottom of the plunge pool. Liu et al. (1998) and Annandale et al. (1998) also used a jet-type flow to evaluate water pressure on a rock mass by modeling either a single block (Liu et al., 1998) or two rows of overlaid inclined blocks (Annandale et al., 1998). Gu et al. (2017) and Kote and Nangare (2019) simulated various spillway channel configurations rather than a rock mass to evaluate the energy dissipation capacity of the channel. Models such as those of Sawadogo (2010) and Wilkinson et al. (2018) simulated a river flow, using small PVC blocks or fractured plaster slabs, and studied the erosion produced in relation to low flow rates. However, none of these abovementioned models could evaluate all relevant rock mass parameters affecting rock mass resistance to erodibility.

Given the limited available data, determining the effect of joint rock mass parameters on erosion and the hydraulic parameters of water flow is crucial for developing new approaches for predicting rock mass erosion. From this perspective, a physical model will significantly help evaluate the effects of these parameters. Therefore, the objective of this paper is to provide an exhaustive review of existing physical models. We emphasize models that investigate the geometrical parameters of the rock mass. Finally, we classify the existing laboratory models into physical models that study erosion on the basis of hydraulic properties and physical models that focus on the rock mass parameters affecting rock resistance to erosion. Finally, we discuss the advantages and limitations of these models to help guide the development of future models of hydraulic erosion of rock in spillways and discuss the suitability and applicability of the existing models to the study of rock erodibility in spillways.

## **2.2 HYDRAULIC FLUME EXPERIMENTS**

The hydraulic flume approach emphasizes the study of hydraulic parameters affecting erosion. Certain models focus on ways to reduce hydraulic power downstream of spillways. Others simulate flow or erosion in given situations. We can classify these hydraulic flume models into two subcategories: models that use pressure measurements and models using erosion patterns to study hydraulic parameters.

### **2.2.1 MODELS USING PRESSURE MEASUREMENTS TO DESCRIBE FLOW**

Several physical models use pressure measurements to evaluate the erosive capacity of flow. These models include those developed by Withers (1991), Manso and Schleiss (2006), Lesleighter et al. (2016), Gu et al. (2017), and Kote and Nangare (2019).

#### **2.2.1.1 Withers' model**

Withers (1991) focused on pressure fluctuations in a plunge pool in relation to flow characteristics and aimed to characterize the magnitude, frequency, and distribution of pressure produced by a plunging jet. In the presented model, a free jet falls from an opening in a vertical pipe, and pressure is measured at different points on the basin surface (Figure 2.1). Ervine et al. (1997) then described the jet's behavior (Figure 2.2). The jet's characteristics depend mainly on the type of opening used, the flow conditions at the outlet of the pipe as it passes through the air, and the conditions at the bottom of the tank. Withers tested 17 independent variables related to fluid mechanics to characterize the flow-generated pressures (Withers, 1991). These variables described the geometry of the exit nozzle (i.e., inclination, diameter, and length to diameter ratio) and its flow conditions (i.e., Reynolds number, flow velocity, and Weber number), flow conditions as the jet traveled through the air (i.e., Froude number, air density to water density ratio, and the air viscosity to water viscosity ratio) and at its landing point, as well as plunge pool geometry (i.e., the depth of tail water to nozzle diameter ratio). Withers tested several configurations: the geometry of the outlet valve, the valve outlet flow conditions, the flow conditions in the air during the water fall, and the geometry of the dissipation basin.

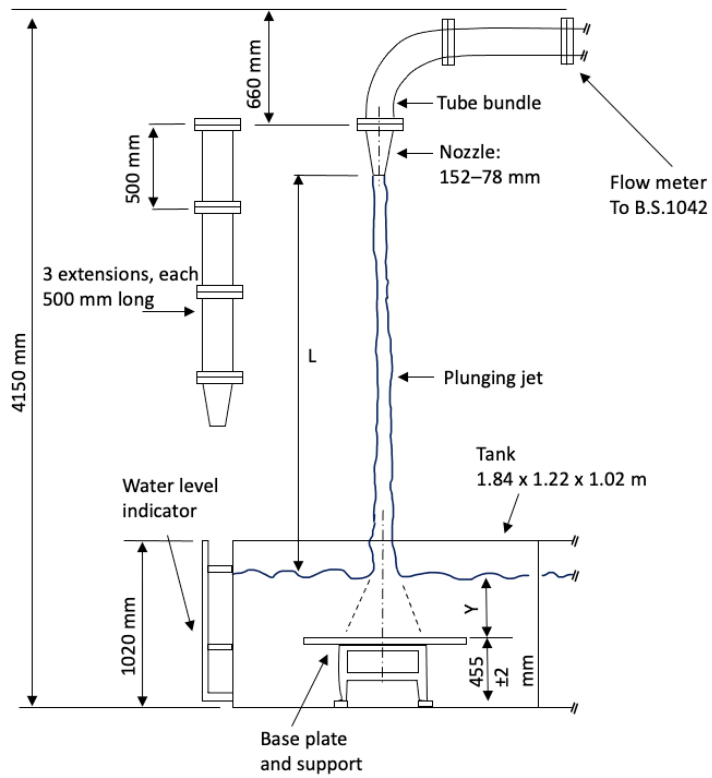


Figure 2.1 : Diagram of Withers' physical model. Redrawn from Withers (1991)

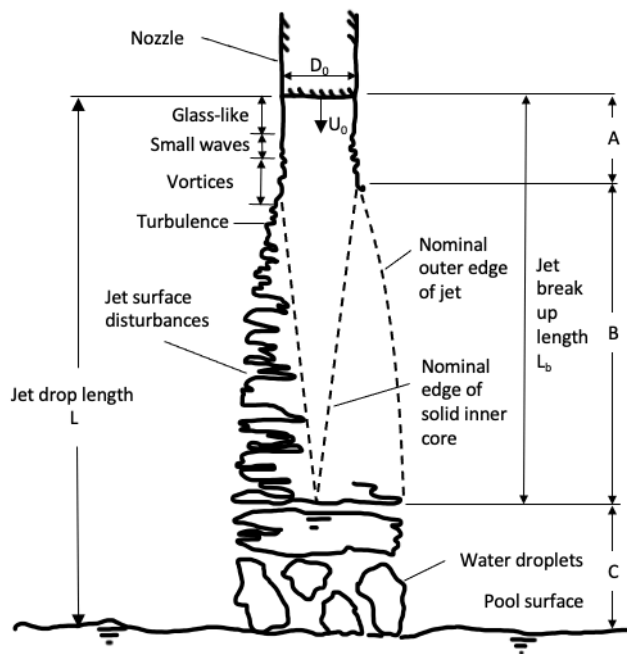


Figure 2.2 : Diagram of the jet's characteristics produced by the model of Ervine et al. Redrawn from Ervine et al. (1997)

The model consisted of a tube leading to a nozzle through which water was pumped at a maximum flow rate of  $60 \text{ L}\cdot\text{s}^{-1}$ . Five pressure sensors were placed around the landing point at the bottom of the pool. The model had a flow velocity capacity of  $25 \text{ m}\cdot\text{s}^{-1}$ . Withers observed a generally constant decrease in pressure as the basin water depth increased, reflecting the cushioning effect of the basin.

Withers' model quantified the pressures generated on the surface of a basin by jets under different conditions. Some weaknesses of the model included the jet being projected vertically rather than having a plunging effect such as those found in spillways, and the model did not directly represent spillway geometry. Nonetheless, the model improved our understanding of the effects of varying types of jets on the pressure distribution generated in a dissipation basin.

### 2.2.1.2 Manso and schleiss' model

Jet dissipation methods cause pressure fluctuations in the dissipation basin, leading to premature erosion (Manso et Schleiss, 2006). These pressure fluctuations caused by the air entrained within the jet remain poorly studied. Most studies have involved basins with a fixed geometry and a flat bottom. Manso and Schleiss (2006), however, included the effects of laterally confined basins. They studied a range of factors, including pressure variations and turbulence within basins of differing geometries, the characteristics of plunging jets, the degree of air entrainment in the basin, the transfer of impact energy to joints in the rock mass, the influence of basin geometry on the propagation of within-joint pressure, and the persistence of the dynamic impact pressures within joints.

The geometric characteristics of the joint sets and the characteristics of the plunging jet both influence erosion patterns in the dissipation basin. The impact pressures transmitted to the rock mass depend on the geometry of the dissipation basin and the flow pattern within the basin and are elements included in Manso and Schleiss's model (Manso et Schleiss, 2006). The physical model used in their study (Figure 2.3) was the same as presented by Bollaert and Schleiss (2002), although the performed tests differed (Table 2.1).

Table 2.1 : Summary of the tests performed in the model of Manso and Schleiss (2006)

Test objective	Test series	
Measure the initial characteristics of the jet	1 <sup>st</sup>	Circular, diameter 72 mm
	2 <sup>nd</sup>	Addition of a honeycomb mesh

Measure the pressures in the basin and the cracks	1 <sup>st</sup>	Flat-bottomed basin
	2 <sup>nd</sup>	Laterally confined basin
	3 <sup>rd</sup>	1D-I and 2D-I joints
Measure the degree of air entrainment in the basin	1 <sup>st</sup>	During the fall
	2 <sup>nd</sup>	At the stagnation point
	3 <sup>rd</sup>	Around the impact point

Manso and Schleiss evaluated the hydraulic characteristics of the jets, the impact pressures within a flat-bottomed basin, the behavior of air entrainment in a flat-bottomed basin, the impact pressures and flow in laterally confined basins, the transient pressures within fractures in flat-bottomed and non-flat-bottomed basins, and the applicability of the results.

This model considered both the pressure distribution and the hydraulic conditions in various basin types and fracture geometries to simulate the pressures acting within rock joints. However, the flow used in the Manso and Schleiss model was a vertical jet, which differs in its landing point angle from that of a plunging jet which have an influence on the water flow direction on the surface of the rock mass. Moreover, the tested joints were always located at the jet's landing point; thus, the effect of the location of joints relative to the landing point of the jet could not be determined.

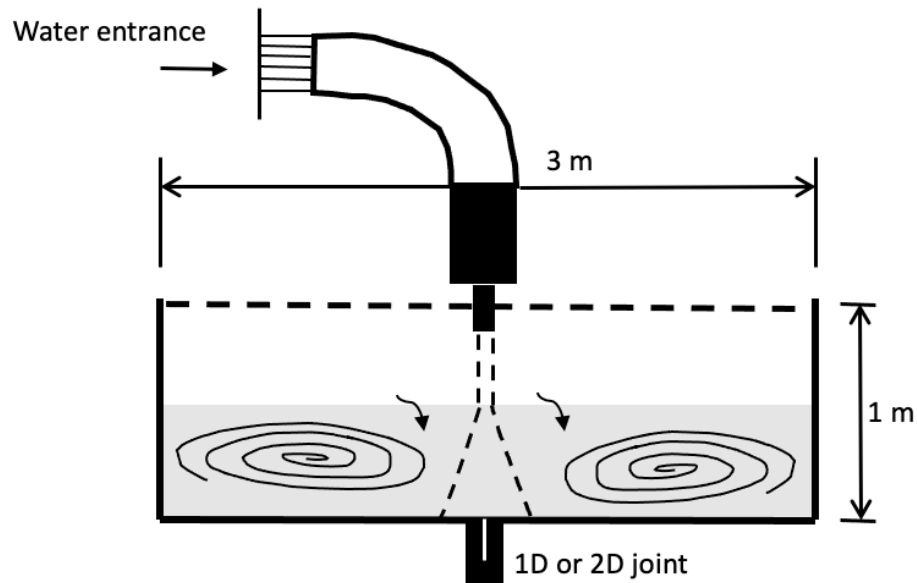


Figure 2.3 : Diagram of the Manso and Schleiss model. Redrawn from Manso and Schleiss (2006)

### 2.2.1.3 Lesleighter et al.'s model

The Paradise Dam, located in Australia, suffered extensive damage to its spillway during major floods in 2011 and 2013 (Figure 2.4) (Lesleighter et al., 2016).



Figure 2.4 : Condition of the Paradise Dam spillway following the 2013 flood. Dashed red lines outline the eroded area. Modified from Lesleighter et al. (2016)

The comprehensive scour model (CSM) (Bollaert et Schleiss, 2005) was used by Lesleighter et al. (2016) to numerically model erosion by studying three modules of the spillway: the plunging jet, the plunge pool, and the rock mass. The plunging jet module described the characteristics of the jet during its fall, and the plunge pool module detailed the evolution of the jet from its landing in the water to the pressures applied to the rock. Finally, the rock mass module illustrated the methods of rock fracturing. These modules influenced all three applications of the CSM: the dynamic impulsion (DI), the comprehensive fracture mechanism (CFM), and the quasi-steady impulsion (QSI) (Bollaert, 2004; Bollaert et Schleiss, 2005; Lesleighter et al., 2016).

Lesleighter et al. (2016) built a 1:70 scale model of the Paradise Dam (Figure 2.5) to obtain transient pressure and water velocity measurements downstream of the spillway. Using sensors placed at the bottom of the dissipation basin, they measured pressures and determined flow speed via the acoustic Doppler velocity

method (Quaresma et al., 2017). This model reproduced the discharge of a flood with an average 1-in-10,000-year return occurrence, equivalent to a model-scale flow rate of  $1,200 \text{ L}\cdot\text{s}^{-1}$  at maximum capacity.

The measurements of the maximum and dynamic pressures and the velocities at the bottom of the basin for the various flows served as input data for the numerical model. Lesleighter et al. (2016) validated their model by comparing the outputs of their simulation of the 2013 flood with the erosional profile and pressures observed in the field. The numerical model determined the possible damage from larger floods. The authors also modeled and projected floods having 1-in-200, 1-in-500, 1-in-1000, and 1-in-10,000-year return periods.

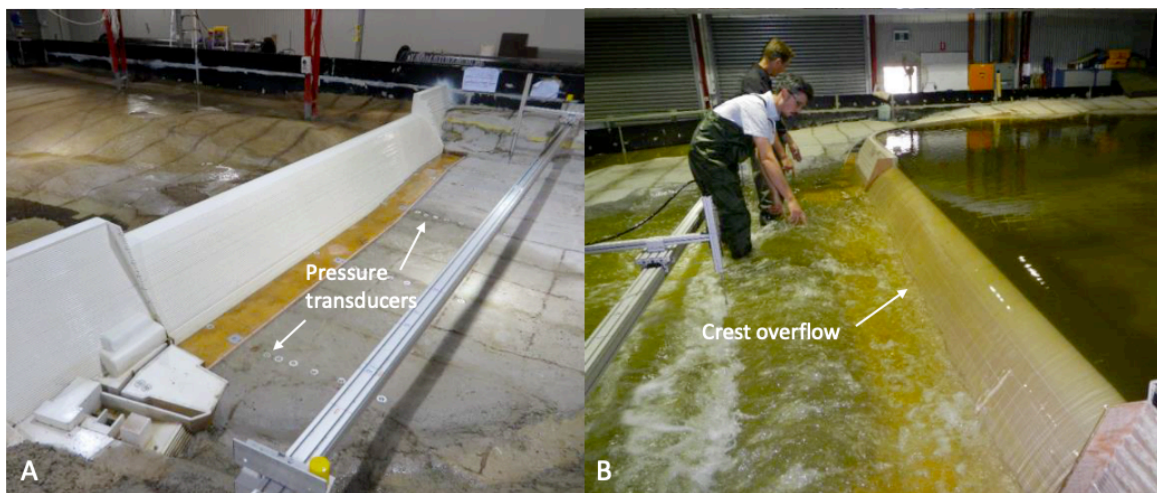


Figure 2.5 : **A** Arrangement of pressure transducers and **B** Lesleighter et al.'s physical model during testing. Modified from Lesleighter et al. (2016)

Lesleighter et al.'s model (2016) provided hydraulic input values for their numerical model. It does not physically model the site's geology, block geometry, or the pressure between the joints of the blocks. The CSM nonetheless allowed these values to be calculated and produced fairly accurate erosion profiles. However, the input values and model calibration are specific to the Paradise Dam situation, and the results cannot be generalized to other dams.

#### 2.2.1.4 Gu et al.'s model

Gu et al. (2017) aimed to validate the *Smoothed Particle Hydrodynamic Model*, a mesh-free numerical model used to model flow in an open-channel spillway, using a physical model. This numerical model is applicable to different spillway types and geometries and provides a better understanding of pressure



distribution and energy dissipation. Gu et al. (2017) applied the model to help design the stairs in stepped spillways to produce more efficient energy dissipation and protect the downstream basin from erosion. A 1:40 scale model of the Dahua Dam spillway, China, was constructed to study flow characteristics (Figure 2.6) and verify the numerical model. The numerical model reproduced the dam at a 1:10 scale.

The percentage of energy dissipation obtained for the three spillway configurations of the experimental and numerical models were similar, with errors below 10%. It shows that the numerical model effectively reproduces the flow in the experimental model. The 45-step spillway was the most energy-dissipating setup, with a dissipation of 81% and 85% for the experimental and numerical models, respectively. A 31-step spillway produced a dissipation of 76% for the experimental model and 82% for the numerical model, whereas the respective experimental and numerical model energy dissipation values for a 62-step spillway were 75% and 81%. By optimizing the number of steps and their dimension, it would be possible to optimize energy dissipation in a stepped spillway according to its characteristics (flow conditions, spillway length and slope, ...).

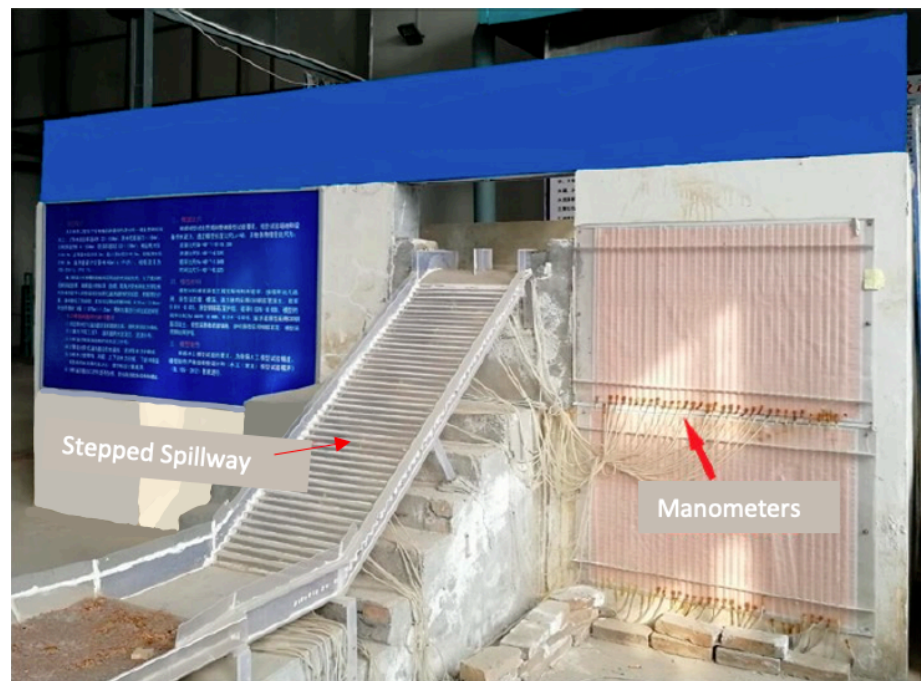


Figure 2.6 : Gu et al.'s physical model of a stepped spillway. Modified from Gu et al. (2017)

Gu et al.'s (2017) model provided a flexible configuration for multiple geometries, surface flow visualization, and a pressure distribution profile. By increasing the dissipation of energy along the chute, the

hydraulic power was reduced when the flow reached the dissipation basin. Manometers determined the pressure distribution, allowing a quantitative analysis of energy dissipation in relation to spillway configuration. Modeling the flow also helps the understanding of the pressure distribution along the chute.

#### **2.2.1.5 Kote and nangare's model**

At the Kadhakwasla Dam, India, energy dissipation issues have caused erosion in the spillway and the dissipation basin. Energy dissipation in stepped spillways depends on the ratio of critical water depth of the flume to stair height in laboratory tests (Chamani et Rajaratnam, 1999). A ski jump at the end of the spillway is necessary to reduce the length of the dissipation basin where the downstream water depth results in the formation of a hydraulic jump (Kote et Nangare, 2019).

The Kote and Nangare's model (2019) was built at a 1:33 scale of the Kadhakwasla Dam spillway, and they tested an ogee-shaped spillway and a stepped spillway (Figure 2.7). For the stepped model, 12 steps—each 40 mm high, 33 mm wide, and angled at 50°—were built. The model's ski jump and dissipation basin were reproductions of those at the Grand Coulee and Angostura dams in the United States. The tests were carried out at hydraulic loads of 4 m and 6 m and respective flow rates of 5.3 L·s<sup>-1</sup> and 6.5 L·s<sup>-1</sup>. The channel had a constant inclination of 37°.

The first step in their methodology was to verify the effectiveness of plain and slotted roller buckets. They tested each bucket with a load of 4 m and 6 m and photographed the resulting hydraulic jump. They also measured the distance between the location where the water landed and the end of the structure. The slotted roller bucket produced the best energy dissipation for both hydraulic loads.

Kote and Nangare (2019) then proceeded by testing the two hydraulic loads and flow rates with four spillway types: ogee plain roller bucket (OPRB), ogee slotted roller bucket (OSRB), stepped plain roller bucket (SPRB), and stepped slotted roller bucket (SSRB) (Kote et Nangare, 2019). They observed that the OPRB dissipated sufficient energy when the load was low (i.e., at 4 m). However, for the 6 m high load, the SSRB was the optimal choice, producing an energy dissipation of 83% for the 6 m head.

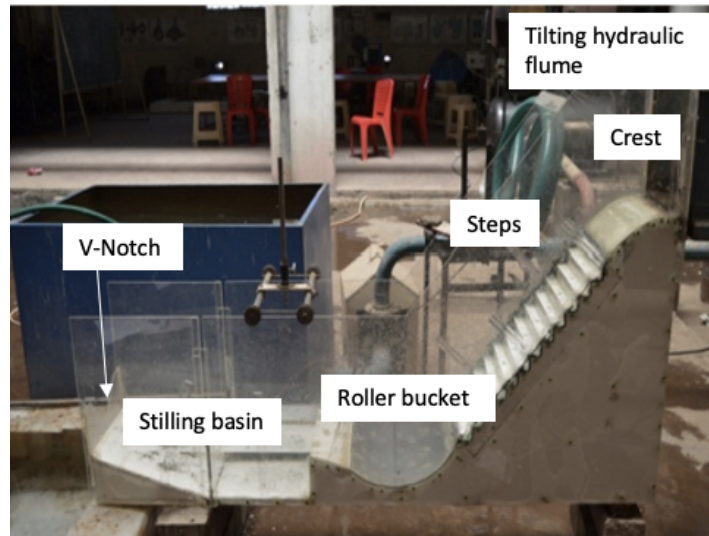


Figure 2.7 : Kote and Nangare’s physical model for the stepped plain roller bucket spillway. Modified from Kote and Nangare (Kote et Nangare, 2019)

A positive aspect of this model was the comparison of different types of spillways in regard to the energy dissipation efficacy and the length of the produced hydraulic jump. Greater energy dissipation of the falling water resulted in the less downstream damage produced by this water. Moreover, a hydraulic jump that falls farthest from the dam is less likely to damage the dam itself (Kote et Nangare, 2019). This study used piezometers to measure water pressure, and therefore its energy, when it fell. However, the used flow rates were relatively low considering the scaled model’s design discharge of  $410 \text{ L}\cdot\text{s}^{-1}$ , when flow rates of only  $5.3 \text{ L}\cdot\text{s}^{-1}$  and  $6.5 \text{ L}\cdot\text{s}^{-1}$  were used. Therefore, these flows did not represent the hydraulic conditions of an actual emergency spillway.

## 2.2.2 MODELS USING EROSION PATTERNS TO QUALIFY FLOW

The physical models in the section use the erosion patterns in simulated rock masses to express the erosion capacity of flow. These models include those developed by Sawadogo (2010), Tuna (2012), and Wilkinson et al. (2018).

### 2.2.2.1 Sawadogo’s model

Sawadogo (2010) tackled the problem of erosion in South African dam spillways built in low-cohesion sedimentary rocks, e.g., sandstone, or in fault zones. This study aimed to develop a mathematical model to predict the depth and erosion rate in this geological context. Sawadogo’s mathematical model combined both

hydraulic parameters and selected rock mass parameters using the methods of Annandale (1995) and Van Schalkwyk et al. (1994) to define rock erodibility.

Sawadogo (2010) applied two types of equations in his two-dimensional mathematical model: those defining flow behavior and those describing sediment transport. He ignored vertical hydraulic movements and used the sediment transport formula of Wu (2001) as well as the formulas of Wang and Jia (Sawadogo, 2010). To calibrate the mathematical model, Sawadogo built a flume model and placed 10,000 PVC cubes in six horizontal layers to simulate sedimentary layers (Figure 2.8). The registered erosion profiles were used to calibrate the mathematical model.

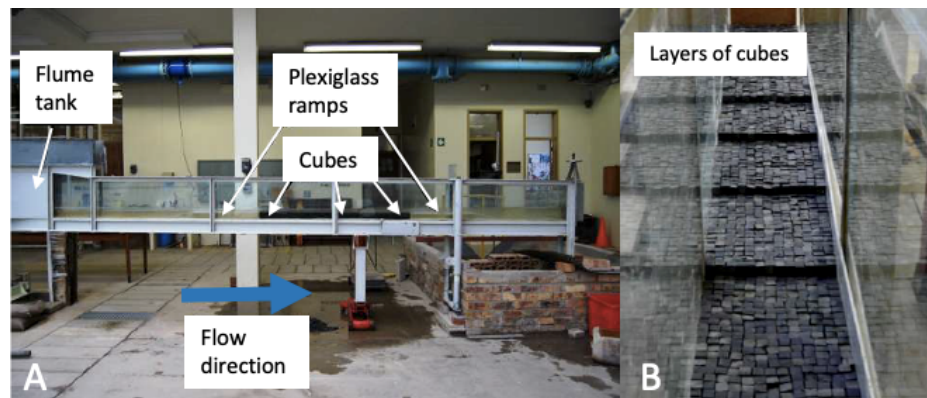


Figure 2.8 : **A** Overview of Sawadogo's physical model **B** Six layers of cubes. Modified from Sawadogo (2010)

Sawadogo modeled the actual conditions at the Mokolo Dam, South Africa. This dam is built in sandstone, and a large flood in 1996 caused significant damage to the dam's spillway. The general profile given by the final model, combining numerical simulations and physical experiments, corresponded well with observations. Nonetheless, the model underestimated erosion by 4 m in some parts of the spillway channel (Figure 2.9) (Sawadogo, 2010).

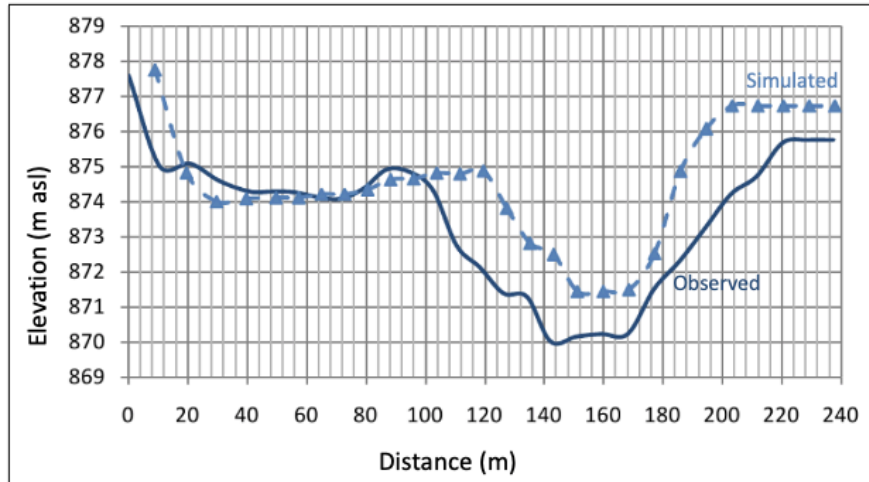


Figure 2.9 : Comparison of the numerical model output and field measurements. Modified from Sawadogo (2010)

Sawadogo’s physical model focused on the erosion of identical cubic blocks arranged along an inclined channel. In actual spillways, rock block shape can be relatively heterogeneous, and the blocks can show some interblock cohesion. Sawadogo used a maximum slope angle of 3.5%, a much lower slope than found in existing spillways. This limitation is important because the erosion observed in his model was greatest at higher slopes because of the increasing hydraulic gradient. The main benefit of Sawadogo’s model is that it considered the interaction between a large number of blocks in varying flows.

#### 2.2.2.2 Tuna’s model

Few studies have examined the effect of the geometric shape of erosion in the dissipation basin of a spillway (Tuna, 2012). Tuna (2012) aimed to determine the effect of spillway angle on the shape and depth of erosion in granular sediments downstream of the spillway. The study investigated three regimes of air entrainment during water fall: the skimming flow, transitional flow, and nape flow regimes. All three occur in stepped spillways at different locations and at different flow rates, depending on the spillway angle and water load.

At the bottom of the stairs of the channel, the dissipation basin was filled with a non-cohesive granular material to allow a measurement of the depth of flow-related erosion and the obtained erosion geometry. They used two types of granular material, one having a  $d_{50}$  of 3.17 mm and a uniformity coefficient of 0.55, the second having a  $d_{50}$  of 9.94 mm and a uniformity coefficient of 0.73. The energy dissipated along the stairs was

measured from the erosion caused in the basin and not according to the measured pressures. The rock mass was not modeled during the tests.

During the tests, Tuna varied the parameters one at a time and measured the dimensions of the formed scour in the three directions (x, y, and z) in the granular sediments of the dissipation basin. Tuna tested changes in spillway slope, step height, and flow velocity. The test was stopped once the erosion had stabilized. The stepped spillway dissipated 70%–80% of the water’s total energy as it fell.

The most influential parameters affecting the depth and extent of erosion were flow rate and spillway slope. A 30° channel produced less erosion than for the 40° and 50° slopes. Lower flows also produced less erosion. The erosion depth decreased as the downstream water level increased, and Tuna concluded that a 30° stepped spillway was most efficient for dissipating flow energy. The variable geometry of Tuna’s model was a clear advantage of this model, as it allows this model to be adapted to other contexts to determine the most energy-dissipating geometry for a given spillway.

### 2.2.2.3 Wilkinson et al.’s model

The objective of Wilkinson et al.’s model (2018) (Figure 2.10) was to assess the possibility of uplift without protrusion and evaluate the degree of uplift in relation to flow velocity and turbulence. A 1 cm thick plaster mosaic, fractured randomly prior to testing, simulated the rock mass. Channel slope varied between 0.493% and 1.24%. Steps (0.8 cm high) could also be added to produce a hydraulic jump landing on a plaster test area.

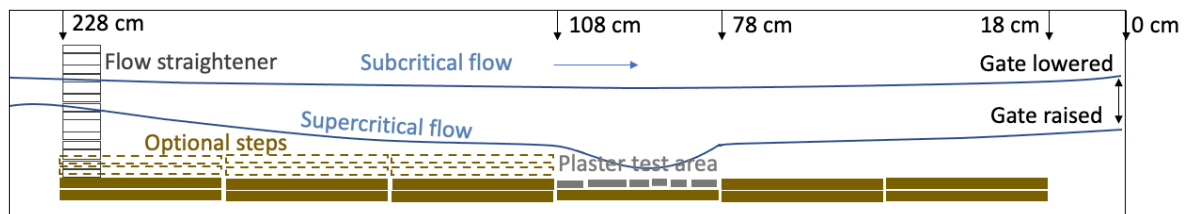


Figure 2.10 : Diagram of Wilkinson’s physical model. Redrawn from Wilkinson et al. (2018)

They performed three series of tests. The first involved variations in the channel slope and the presence/absence of steps. The second involved using three layers of plaster, rather than a single layer, modeled

with a constant channel slope. Finally, the final test measured the displacement of one of the three plaster slabs in the center of the channel using particle image velocimetry (Quaresma et al., 2017).

Wilkinson et al. (2018) identified three main lifting mechanisms: 1) The change in the hydraulic gradient, caused by a difference in hydraulic load induced by the hydraulic jump, varied the hydraulic gradient in the joint under the block to produce an uplift force; 2) Directly under the hydraulic jump, the turbulence was highest. This induced very unstable and variable pressures on the sides and under the block to cause the block to oscillate and eventually be ejected. 3) The recirculation of water upstream of the block produced a pressure exerted within vertical joints, eventually causing the uplifting of the block.

The flow conditions in Wilkinson et al.'s model (2018) were very similar to those found within a river, characterized by low slopes and low flows, rather than the flow conditions of a spillway. This model focused on the phenomenon of plucking, the uplifting of blocks due to the uplift pressure generated by water. The rock mass studied in this model was in two dimensions with plaster slabs placed along a channel section, not in three dimensions as an actual rock mass. Moreover, the study results were based on the movement of the slabs, and pressure distribution along the channel was not measured.

### **2.2.3 ROBERTS' MODEL**

To determine how to dissipate the plunging jet from the Loskop Dam, South Africa, Roberts (1943) tested different methods of jet dissipation on a scale model (Figure 2.11). Roberts (1943) hypothesized that a small-diameter jet breaks up in a spray faster than a large-diameter jet, in which water particles remains together for a longer distance. He explained this phenomenon via the resistance of the air (or the amount of energy per unit volume of the flow), and the model required a strong flow to test the various hypotheses.

The model scale was 1:10 of the Loskop Dam. The channel section was 0.61 m wide, and one side of the dam was built using transparent materials to allow photography of the jets. Roberts compared the jets of each test by placing a grid in front of the jet to serve as a reference in photographs taken of the jet. The step in the weir was also removable so that tests could be performed applying different configurations. The flow rate reached  $311 \text{ L}\cdot\text{s}^{-1}$ .

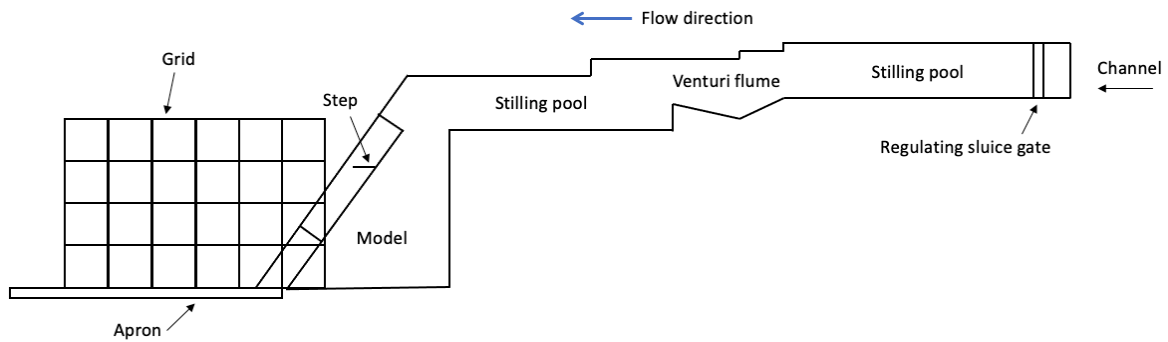


Figure 2.11 : Diagram of the flume section used for Roberts' study. Redrawn from Roberts (1943)

The first tests measured the ability of the water jet to jump when the flow velocity exceeded a critical velocity or when flow over the step was sufficiently repelled away from the spillway. In these tests, the jet formed further away from the dam. The second series of tests aimed to separate the flow by placing triangle-shaped wedges of varying geometries on the step. Some of the water would thus be projected upward, passing over the wedge, whereas another part would be ejected downward, passing directly over the step. These first two tests did not generate significant changes in flow.

In contrast, the third test saw Roberts (1943) introducing a thin divider onto the step to split the flow into two jets that merged in the air. This setup favored energy dispersion, as the split flow came back together on the step and produced a spray to favor energy dissipation. A final test determined how the divider worked under various hydraulic loads and evaluated its impact on flow. Roberts tested 300 different geometric and hydraulic configurations to determine the ideal divider dimensions (height, width) and position above the step of the divider in relation to the water depth upstream. Roberts' model (1943) identified an energy-dissipating solution for a specific spillway geometry relying on observations made on the geometric shape of the jet. This solution is also applicable to other dams having the same type of spillway. Nonetheless, these tests represented qualitative analyses.

#### 2.2.4 SUMMARY

We can summarize the characteristics of existing hydraulic flume models and classify the methods (Table 2.2) using six parameters found to be common among the physical models: model type, model configuration, flow type, channel or flow inclination, analysis method and if the physical model can be used to



calibrate a theoretical or a numerical model. We then compare flow rates among the models and indicate how the results were obtained.

Table 2.2 : Summary of methods studying the hydraulic characteristics of the flow

Model	Model type	Configuration <sup>a</sup>	Flow rate <sup>b</sup>	Slope <sup>b</sup>	Method of analysis	Valid. <sup>c</sup>
Roberts (1943)	1:10 scale of the Loskop Dam ogee spillway	<b>Fixed</b>	<b>High</b> 311 L·s <sup>-1</sup>	To scale	<b>Qualitative</b> From images	<b>No</b>
Withers (1991)	Jet flowing from the nozzle	<b>Variable</b> Valve types	<b>Low</b> 60 L·s <sup>-1</sup>	Vertical 90°	<b>Quantitative</b> Pressure measurements around the jet's landing point	<b>No</b>
Sawadogo (2010)	10,000 cubes in layers in an inclined channel	<b>Fixed</b> Cube configuration	<b>Low</b> 5.2 L·s <sup>-1</sup>	<b>Low</b> Max 3.52%	<b>Qualitative</b> Erosion pattern within the blocks. Depth and rate of erosion	<b>Yes</b>
Tuna (2012)	Stepped spillway, basin made in granular sediments	<b>Variable</b> Inclination, Water load upstream and downstream	<b>Average</b> 20–100 L·s <sup>-1</sup>	<b>Realistic</b> 30°–50°	<b>Qualitative</b> Geometry of erosion formed in granular sediments. Depth of erosion	<b>No</b>
Lesleighter et al. (2016)	1:70 scale of the Paradise Dam ogee spillway	<b>Fixed</b>	<b>Very high</b> 1200 L·s <sup>-1</sup>	To scale	<b>Quantitative</b> Pressure and velocity of flow	<b>Yes</b>
Gu et al. (2017)	1:40 scale model of the Dahua Dam stepped spillway	<b>Variable</b> Number of stairs <b>Fixed</b> Inclination, Water load	<b>Low</b> 11.88 L·s <sup>-1</sup>	To scale	<b>Quantitative</b> Pressure and velocity of flow along the spillway <b>Qualitative</b> Flow path on the spillway	<b>Yes</b>
Wilkinson et al. (2018)	Riverbed Slabs representing fractured rock mass	<b>Variable</b> Inclination	<b>Low</b> 3.5 L·s <sup>-1</sup>	<b>Low</b> 1%	<b>Qualitative</b> Uplift pattern	<b>No</b>
Kote and Nangare (2019)	1:33 scale of Kadhakwasla Dam stepped and ogee spillway	<b>Variable</b> Spillway type Ski jump type Types of spillway and roller bucket	<b>Low</b> 5.3, 6.5 L·s <sup>-1</sup>	To scale	<b>Quantitative</b> Piezometers along the spillway Energy dissipation	<b>No</b>

<sup>a</sup>Configuration indicates whether it is possible to modify the model to test different setups (variable) and the parameters that can be adjusted. <sup>b</sup>Values presented in *Flow rate* and *Slope* are the maximum values used for these parameters, and the qualitative description of flow e.g., high, is in relation to the other presented models. <sup>c</sup>Valid. indicates whether the physical model makes it possible to use or validate a numerical or theoretical model

## **2.3 MODELS THAT INCLUDE THE STUDY OF THE GEOMETRICAL PARAMETERS OF THE ROCK MASS ON EROSION**

The models presented in this section incorporated the geometric parameters of the rock mass into their erodibility studies. To evaluate erosion, authors have used these models to study the distribution of the pressure applied by the flow on instrumented blocks by varying, for example, joint orientation, block size, shape, and protrusion. We can classify these models according to whether they study rock mass characteristics from a plunging jet or an open-channel flow.

### **2.3.1 PLUNGING JET MODELS**

The first category of this group of physical models are the physical models using a plunging jet to simulate flow. These models include those developed by Annandale et al. (1998), Liu et al. (1998), and Bollaert and Schleiss (2002).

#### **2.3.1.1 Annandale et al.'s model**

This experiment addressed the hypothesis that rock erosion occurs when the erosive force of water exceeds the resistance of the rock. Annandale et al. (1998) defined the resistance capacity of rock by an index of erodibility, and the erosive force of water is described by the unit stream power dissipation. Their physical model comprised a plunge pool into which two layers of inclined blocks were placed. A jet fell at 15° from a rectangular opening situated 4.57 m above the basin in which the blocks were placed. The water level in the basin above the blocks remained a constant 0.192 m depth (Figure 2.12).

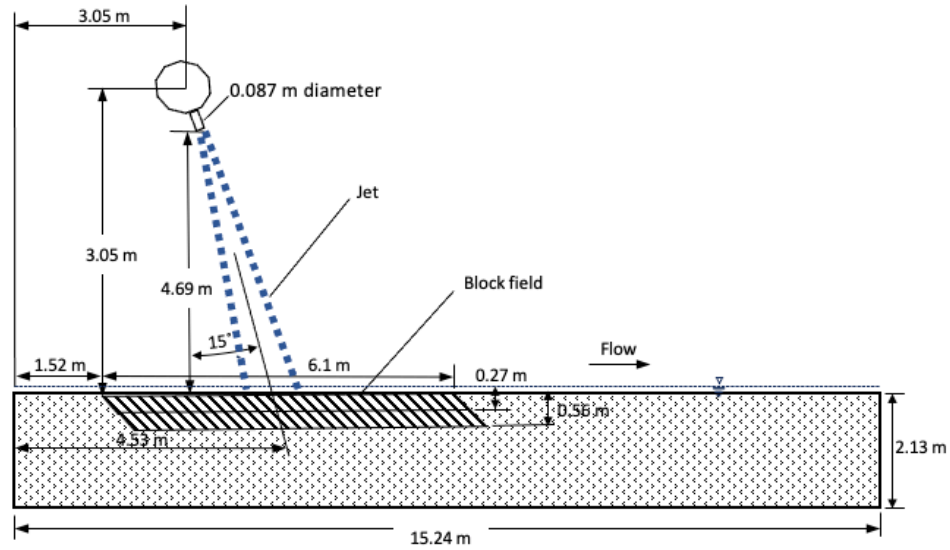


Figure 2.12 : Diagram of Annandale's physical model. Redrawn from Annandale et al. (1998)

Annandale et al. (1998) theoretically determined the erosive force of water and the rock resistance to erosion of their experimental model. Rock mass erosion resistance was determined using the Kirsten index (Kirsten, 1982). The calculated theoretical result corresponded to that measured in the model. Moreover, Annandale (1995) had previously defined an erodibility limit corresponding to the point where the erosive force of the water exceeded the rock's resistance to erosion. Annandale et al.'s model (1998) determined the limit at which erosion began, and this point corresponded to Annandale's erodibility limit (1995).

Annandale et al.'s model (1998) reproduced the erosional conditions of a jet landing into a plunge pool. Energy was measured in the basin using piezometers placed on the rock surface and between the two layers of blocks; this setup allowed for determining the pressure distribution within the modeled rock mass. The model studied the relationship between the rock's erodibility limit and flow power. Neither the configuration of the rock nor the flow varied. Moreover, the application of the results for spillways cases remained debatable.

### 2.3.1.2 Liu et al.'s model

Liu et al. (1998) studied the problem of erosion occurring through hydrofracturing in plunge pools having a plunging-jet flow. This hydrofracturing is caused by fluctuating pressures and their propagation within the rock mass through joints. The block is ejected if the lifting force is greater than the other forces applied to

the block, such as drag and block weight. The same principle then applies to the immediately underlying block and so forth until significant erosion occurs.

Liu et al. (1998) used the theoretical model of Rinaldo and Fiorotto (1992), who developed one-dimensional equations to describe the propagation of pressures in a rock joint from tests on scale models. The equations state that the pressure distribution, shaped like a symmetrical bell, reaches its maximum within the joint, midway between its upstream entry and its downstream exit. In reality, this pressure produces several small variations, and the method of Rinaldo and Fiorotto (1992) describes only the overall tendency (Liu et al., 1998).

To validate the theoretical model and obtain more data on the pressure fluctuations within a joint, Liu et al. (1998) built a physical model (1:100 scale) of a spillway of the Three Gorges Dam, China (Figure 2.13). It was designed according to Froude's similarity criterion. The dam-specific discharge rate was  $174 \text{ m}^2 \cdot \text{s}^{-1}$  when applying Froude's similarity criterion. In the model, a block was positioned at the jet landing point and linked to a pressure sensor to measure the uplift pressures.

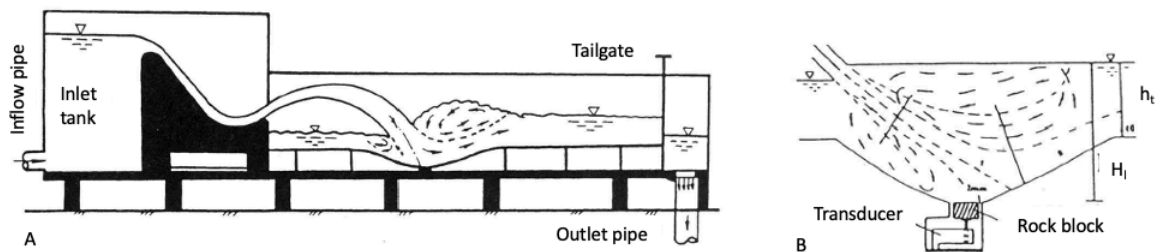


Figure 2.13 : **A** Diagram of Liu et al.'s physical model **B** a larger view of the test section. Taken from Liu et al. (1998).<sup>3</sup>

The tests were carried out using the same flow rate, varying only the downstream water load. Several volumes of blocks were tested, from 2 cm (l) x 2 cm (w) x 2 cm (h) to 6 cm (l) x 6 cm (w) x 4 cm (h). The lifting forces were measured by pressure sensors located under the blocks during the tests. Liu et al. (1998) determined that the measured pressure distribution followed a Gaussian probability function, with an

<sup>3</sup> Experimental investigation of fluctuation uplift on rock blocks at the bottom of the scour pool downstream of Three-Gorges spillway. Journal of Hydraulic Research © International Association for Hydro-Environment Engineering and Research, reprinted by permission of Taylor & Francis Ltd, <http://www.tandfonline.com>

asymmetry coefficient ( $C_s$ ) and a peak coefficient ( $C_e$ ) near 0 and 3.0, respectively, when the basin water height ( $h_t$ ) was 37.05 cm. The Gaussian probability density function with a mean value of zero of fluctuating uplift is defined by Equation (2.1).

$$p(x) = \frac{1}{\sigma_f \sqrt{2\pi}} \exp\left(-\frac{x^2}{2\sigma_f^2}\right), \quad (2.1)$$

where  $p(x)$  is the probability of fluctuating uplift,  $\sigma_f$  is the mean root square value for fluctuating uplift, and  $x$  is the experimental value of fluctuating uplift.

Liu et al. (1998) demonstrated that the uplift pressure fluctuations decreased as the downstream water load increased. Moreover, a larger block size decreased the maximum force being applied to a block. As the block size decreased, the maximum force increased until it reached an asymptotic value where it tended to become constant with decreasing block size. The maximum force recorded exceeded the hydraulic buoyancy by 65%, implying that the average lifting force was not responsible for the lifting of the block.

Liu et al.'s model (1998) was a scale reproduction of a dam spillway with a plunging-jet flow type. The study of pressure variations was carried out on a block representing a rock mass, of which only the dimensions varied. The pressure distribution under this block, captured by a pressure sensor, provided quantitative results. The water depth in the basin also varied during the tests to study the impact of depth on the pressure distributed under the block. The flow rate remained constant throughout the tests.

### 2.3.1.3 Bollaert and schleiss' model

Bollaert and Schleiss' (2002) physical model was built to match Bollaert's theoretical model describing erosion processes under a plunging jet (Bollaert, 2004) (Figure 2.14). Their physical model aimed to assess the variations and intensity of uplift pressures on an individual block. Two steel plates represented the rock mass, with various openings representing a joint. Steel was used to prevent erosion of concrete or rock, given the large water flow rates used. Rock joints were simulated by different configurations of steel plates in one and two dimensions. The jet was directed vertically, directly onto the joint. Pressure distribution was measured within the joint and on the basin surface. Three to seven sensors were used in the joints, depending on the joint configuration. Bollaert and Schleiss (2002) selected jet diameters of 0.072 m and 0.057 m and ten

flow rates ranging from 30 to 120 L·s<sup>-1</sup> for the 0.072 m diameter jet and seven flow rates ranging from 20 to 80 L·s<sup>-1</sup> for the 0.057 m diameter jet. Flow rates were increased in 10 L·s<sup>-1</sup> increments. Both a cylindrical and convergent exhaust outlet opening was used. The ventilation rate varied from 60% to 70% and was scaled to that of the dam. The drop height of the jet varied between 0.03 m and 0.70 m, and the geometry of the basin did not vary. Water depth in the basin went from submerged to nonsubmerged conditions. Table 2.3 summarizes the tests carried out for the five types of joints, as detailed in Figure 2.15.



Figure 2.14 : Bollaert and Schleiss' physical model, as modified from Bollaert and Schleiss (2002)

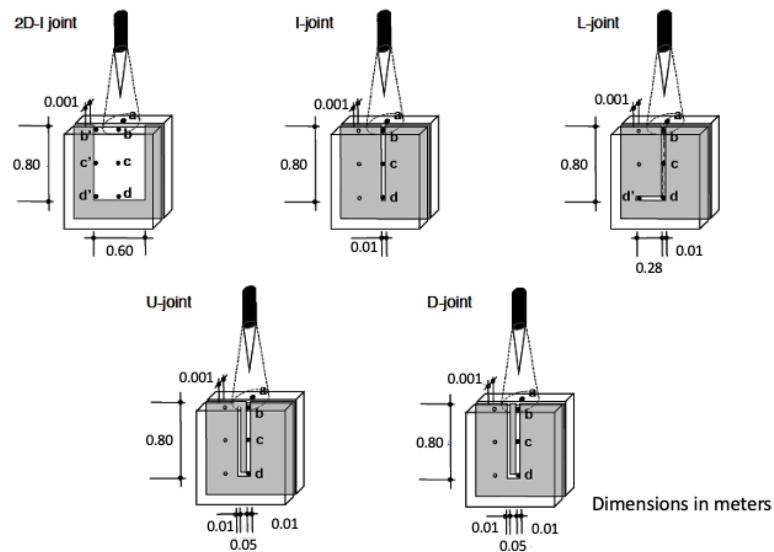


Figure 2.15 : Joint types and location of pressure sensors in the physical model of Bollaert and Schleiss. Modified from Bollaert and Schleiss (2002)

Turbulence influenced the air content of the jet, which altered the pressure fluctuations. For both types of nozzles, the jet's turbulence characteristics were measured at its initial exit point. The pressures were also measured at the bottom of the basin and within the 2D-I joint. Finally, the tests were carried out with the different types of joints at the bottom of the basin.

Table 2.3 : Summary of tests carried out for each joint in the Bollaert and Schleiss model (2002)

<b>Joint type</b>	<b>Nozzle</b>	<b>Jet diameter (mm)</b>	<b>Number of sensors</b>
2D-I	Cylindrical	57 and 72	7
1D-I	Cylindrical	57 and 72	4
1D-I	Convergent	72	4
L	Cylindrical	57 and 72	5
L	Convergent	72	5
U	Cylindrical	57 and 72	3
D	Cylindrical	57 and 72	3

In their two-dimensional model, all joints were 1 mm thick, whereas in reality the joint openings in a rock mass vary in size. This model provided the study of the distribution of pressure generated by a vertical jet in different joint geometries. The pressures were measured with sensors, allowing a quantitative analysis. Only a single joint was studied for each test, and the joint was always located directly under the jet. Because the jet was vertical, the jet did not exactly simulate the flow conditions found in spillways.

### **2.3.2 OPEN-CHANNEL FLOW MODELS**

The second category of this class of physical models are the physical models using an open-channel flow to simulate water flow. These models include those developed by Reinius (1986) (based on the study of Montgomery (1984)), Wang and Jiang (2010), George et al. (2015), and Pells (2016).

#### **2.3.2.1 Reinius' model**

Reinius (1986) observed erosion problems in the spillways and dissipation basins related to rock uplift. He was interested in how joint orientation and rock mass protrusion affected the generated pressures on the rock mass. Montgomery (1984) focused on the erosion mechanism of high-velocity flow along irregularities in the rock mass, in particular on the pressures generated by the high flow rate within the joints of the rock mass. A rock mass contains joints in which water circulates and can produce pressure variations that induce uplift pressures. If these pressures are greater than the joint shear strength, the effective weight of the block, and the

water pressure above the block, the block will move and eventually be ejected. The resistance of a block to erosion depends on its size, shape, and the degree of abrasion of the joint. The authors hypothesized that the shear strength of the fracture might be of less importance depending on its orientation relative to the flow and when several blocks undergo uplifting at the same time.

The designed model had a flow channel in which several concrete blocks were aligned (Figure 2.16). The third block was instrumented with piezometers on each of its faces to measure the pressures under which the block was subjected. The pressure was measured on the thrust face, the lee side face, and under the block. Eight tests were performed on the blocks (Table 2.4).

Table 2.4 : Summary of the test program of Reinius (1986)

Test #	Dip (°)	Protrusion (mm)	Flow rate (L·s <sup>-1</sup> )	Froude number	Water depth (mm)
1	0	+2	40–145	3.6–6.3	34–248
2	0	–2	40–145	3.4–6.2	35–68
3	2.6	+6.8	40–145	3.7–6.5	32–65
4	9	+23.5	65–130	1.7–3.0	50–100
5	17.5	+45.1	50–180	1.5–3.2	60–120
6	33.5	+82.8	50–200	1.1–3.6	80–140
7	87.1	–7.6	40–145	3.9–6.9	32–66
8	72	–46.4	50–200	1.5–4.3	50–140

The most critical dips in terms of calculated pressure coefficients were those between 10° and 15° upstream. The thrust face of the block was subjected to the highest pressure, followed by the face under the block. The lee side always recorded weak pressures, often negative. When the block dipped downstream, the pressures recorded on all its faces were very low. The upstream dip orientation produced the highest pressures.



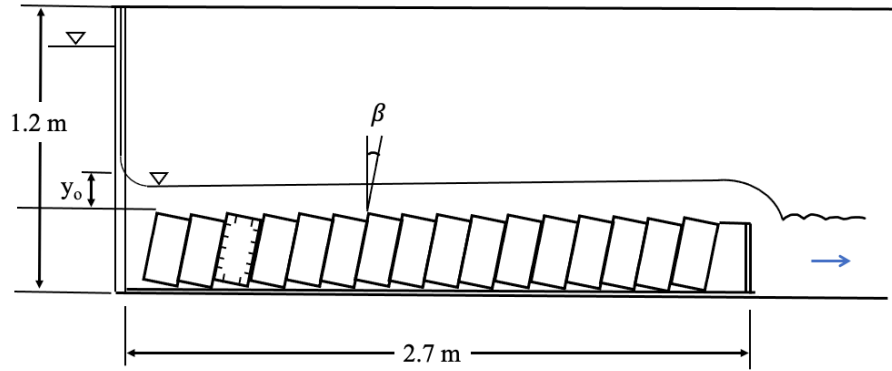


Figure 2.16 : Diagram of the physical model used in both the Reinius and Montgomery studies. Rebuilt from Reinius (1986)

Montgomery's (1984) testing program included the location of the instrumented block in the channel, the joint opening between the blocks, and the control of water circulation in the joints (Table 2.5). All tests were performed at flow rates between  $40 \text{ L}\cdot\text{s}^{-1}$  and  $145 \text{ L}\cdot\text{s}^{-1}$ . All tests but one were carried out in supercritical flow.

Table 2.5 : Block displacement tests performed by Montgomery (1984)

Test number	Froude number	Block displacement	Protrusion height (mm)	Block angle (°)	Location of block from gate (cm)	Joint width (mm)	Circulation of flow through joints
1	3–6.2		1.6	0	40	1	Yes
2	3–6.2		2.2	0	40	1	Yes
3	2. –3.6		1	+3.5	162	1	Yes
4	3. –6.8		2	0	40	0.75	No
5	3.2–6.8		2	0	40	0.75	No
6	3.2–6.8		7.2	+2.6	40	0.75	No
7	3.2–6.8		7.7	-2.9	40	0.75	No
8*	3. –6.8		2	0	40	3	No

\*All tests were carried out in supercritical flow except for Test 8.

Reinius' model (1986) focused on the pressure distribution obtained with various block layouts to assess the effect of water pressure on rock mass parameters. The advantage of their approaches was the consideration of the pressure between the joints of the blocks for various dips, thereby providing a view of how hydraulic forces act during the block lifting. However, only a single joint orientation was studied, i.e., perpendicular to the flow. In reality, joints are found in all directions, and a full understanding of the effect of this parameter remains to be established. Neither Reinius (1986) nor Montgomery (1984) varied joint openings; the latter applied sealed joints when joint opening varied. Therefore, water cannot circulate, and no pressure variation can be measured in these cases. Montgomery's study concluded that rock protrusion and high flow rate—especially under supercritical flow conditions and at the foot of a hydraulic jump—were the main factors affecting rock erosion. Finally, the channel of this model was kept horizontal, whereas open-channel spillways are inclined structures.

#### **2.3.2.2 Wang and Jiang's model**

Wang and Jiang (2010) aimed to assess friction reduction techniques. These have been studied previous studies and included strategies for adding polymers to the water and covering a spillway surface with silicone oil. They performed a test in an open-channel flume (Figure 2.17) and used a 1:100 scale model of the Xiluodu Dam spillway, China. Their tests involved either adding a polymer to the water at different concentrations (0–300 mg·L<sup>-1</sup>) or coating the channel surface with dimethyl silicone oil. In the laboratory, Wang et al. compared dredging reduction techniques with pressure loss measurements translated into friction coefficients. On average, the relative frictional resistance decreased by 8.2% when silicone oil was applied to the channel surface. Nonetheless, applying dimethyl silicone oil in practice is a more viable solution than adding a polymer to water.

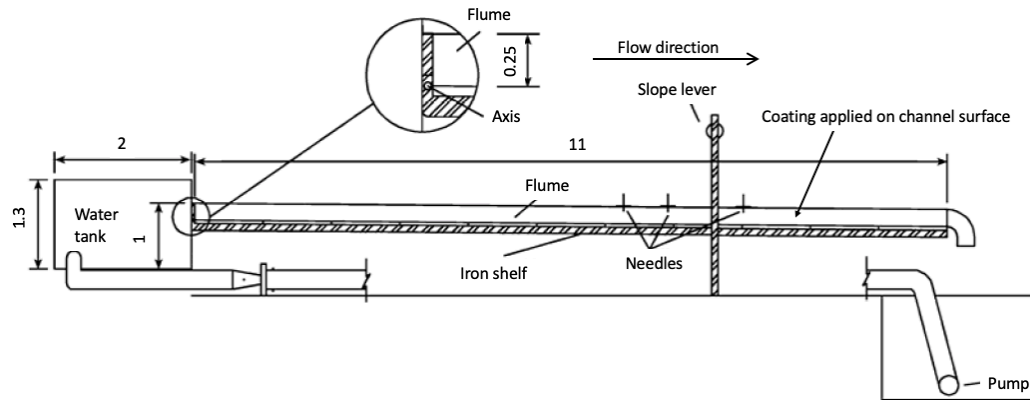


Figure 2.17 : Diagram of the physical model, modified from Wang and Jiang (2010)

Flow velocity along the spillway reflected the effectiveness of silicone oil application. Flow velocity increased up to 4% when the channel was covered, demonstrating that covering a channel offers an effective technique for reducing friction. This study highlighted that the reduction of friction is an important parameter for reducing erosion, although, for our purposes (uncovered spillways), the results of this study are not fully applicable.

### 2.3.2.3 George et al.'s model

Most existing studies focus on the pressures acting on one or more cubic blocks. Therefore, George et al. (2015) aimed to determine the distribution of pressure and the induced displacements for a tetrahedral block having faces oriented in all directions, as generally observed in a natural rock mass.

The flume model (Figure 2.18) had a channel inclined at a constant 21% slope. The block was placed in a mold located downstream of the channel. The horizontal orientation of this rotational mold could be varied from  $0^\circ$  to  $180^\circ$ . The block was instrumented with pressure and displacement sensors, and water speed and depth were both controlled. A total of nine flow rates are used for the experiments, varying between 0 and  $0.3 \text{ m}^3 \cdot \text{s}^{-1}$ . The tests were carried out with either low (2%) or high (7%) turbulence. Three blocks of similar geometry were tested with various protrusions: 0, 1.5, and 4 mm.

A consistent critical orientation was observed (between  $60^\circ$  and  $90^\circ$ ) for a minimum block ejection speed. At this orientation, the block offered the most resistance to flow. A similar conclusion was drawn for the least critical orientation (between  $0^\circ$  and  $15^\circ$ ). At this latter orientation, the block presented itself in profile to the flow, and therefore offered the least resistance. For turbulence and protrusion, these parameters did not

change the critical orientation of the block, only the average ejection speed. Moreover, the blocks without protrusion were not ejected.

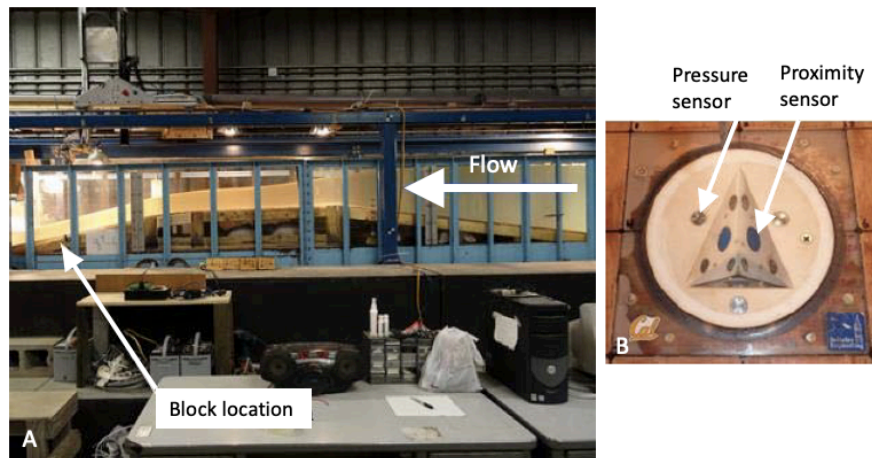


Figure 2.18 : **A** Physical model used in George et al.'s experiment **B** example of an instrumented block. Modified from George et al. (2015)

George et al.'s model (2015) focused on the pressures and displacements induced in the rock mass of a spillway. It mimicked flow conditions along the spillway channel, with a slope of the same magnitude as found in actual settings. The advantage of this model was that it considered the hydraulic pressures acting on a block with faces in the three directions at different horizontal orientations and protrusions. However, the dip of the block and the inclination of the channel slope did not vary. Furthermore, only one block was studied, which limited the interpretation when considering a rock mass with joints in which the blocks interact. Finally, the joint opening was held constant between the block and its mold; therefore, it was impossible to evaluate the effect of different joint openings, an element of great importance for calculating uplift pressure.

#### 2.3.2.4 Pells' model

Pells (2016) studied the effects of selected rock mass characteristics, including joint orientation and opening and rock protrusion, on rock mass erodibility. He also determined the effects of the hydraulic characteristics of a flow on the pressure induced in a rock mass. In his model (Figure 2.19), he represented the rock mass as an instrumented cubic block placed in the center of the flow channel. The block was instrumented with pressure and force sensors, and its horizontal orientation and dip could be varied. The block was placed within a cavity in the center of the channel, allowing for 1 mm spacing around the block. A 50 mm space under

the block could also be produced. Pells' tests aimed to evaluate the effect of hydraulic parameters on the pressures and forces applied to the block. This physical model permitted an assessment of the effects of variable arrangements of the block in the channel, i.e., block protrusion, horizontal orientation, vertical orientation, and an opening under the block.

Pells (2016) found that rock protrusion has a marked impact on the lifting force, and a negative or positive protrusion of even a few millimeters markedly increased the lifting force. The horizontal orientation affected the lifting force only if the block had a significant protrusion greater than 5 mm and was oriented at least  $22^\circ$  to the current. An upstream dip produced a significantly greater impact on the uplift force than a downstream dip or no dip. Moreover, the effect of the opening under the block did not alter the lifting force. Therefore, verifying the effect of joint opening requires a very different setup.

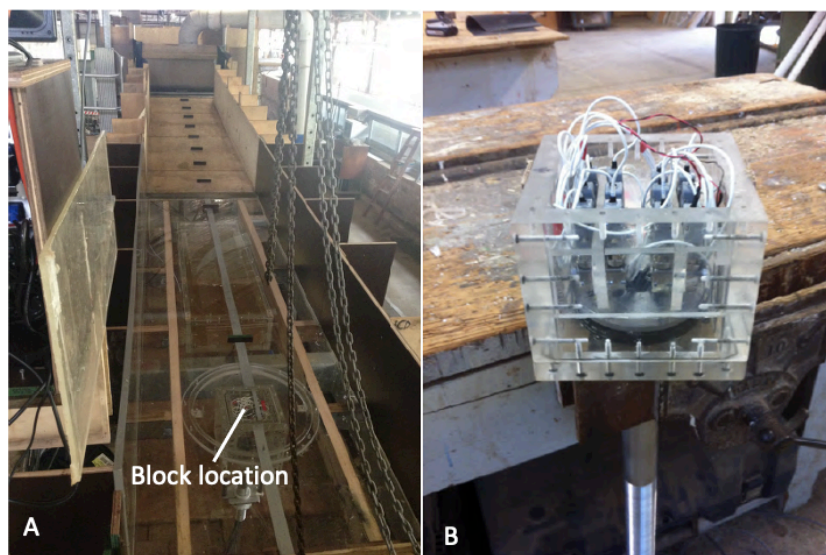


Figure 2.19 : **A** Pells' flow channel **B** the instrumented block used in Pells' model. Modified from Pells (2016)

The advantages of Pells' model (2016) include studying the effect of both the horizontal and vertical orientations of the block on the hydraulic forces and pressures. He also measured the effect of the block's protrusion and various hydraulic configurations on the pressure distribution. However, only one block was modeled, rendering it impossible to assess the effects of hydraulic pressure acting between the joints of the blocks. Moreover, Pells (2016) wished to assess the effect of joint opening by creating an opening under the

block. However, the results were inconclusive because the joint openings alongside the block did not vary, and thus the effect of the joint opening could not be determined.

### 2.3.3 RONG ET AL.'S MODEL

Rong et al. (2020) aims to analyze the nonlinear flows in a fracture depending on its geometry. They used Brazilian-type fracturing of 50 samples of granite blocks of 200 mm × 100 mm × 100 mm. The geometry and opening of each fracture were analyzed using 3D scanning to an accuracy of 10 μm. The edges of the joints were sealed with silicone to ensure one-direction flow, and the samples were then placed within a cell into which water was injected at flow rates varying between 0 and 200 mL·min<sup>-1</sup> (Figure 2.20). The differential pressures between the inside and the outside of the cell were continually measured by a pressure gauge during the tests. Each fracture was analyzed in regard to the roughness and geometry parameters and was tested with ten different flow rates to compare the effect of the characteristics of the joint on the pressure generated in relation to the flow rate. The joint opening was kept constant for all tests using bolts but was not specifically measured.

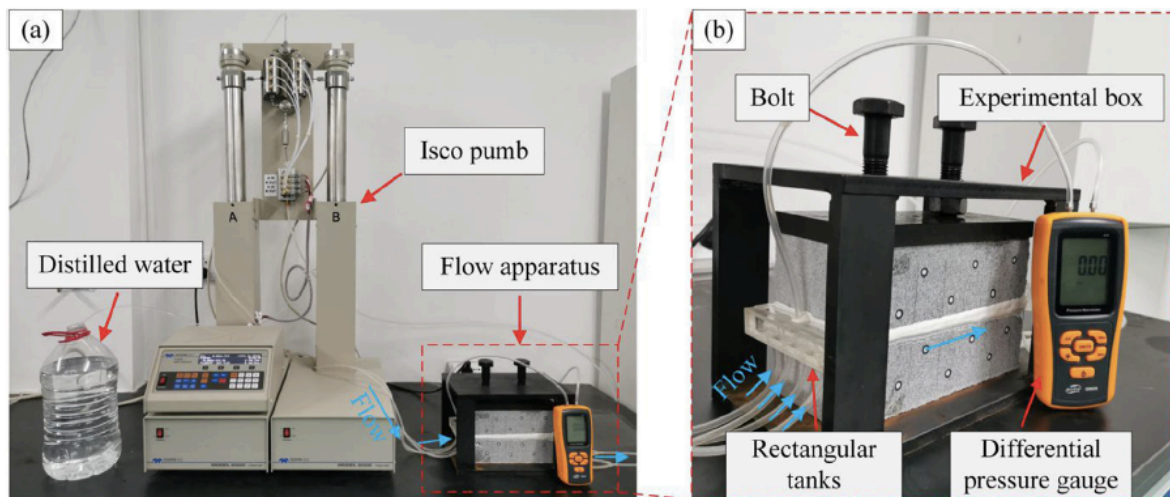


Figure 2.20 : **A** Rong et al.'s experimental setup **B** example of a modeled joint. Taken from Rong et al. (2020)<sup>4</sup>

<sup>4</sup> Reprinted from Journal of Hydrology, Vol 589, Guan Rong, Jie Tan, Hongbin Zhan, Renhui He, Ziyang Zang. Quantitative evaluation of fracture geometry influence on nonlinear flow in a single rock fracture, Page 4, Copyright (2020), with permission from Elsevier.

This method was applicable to individual fractures with an opening on 1 mm (opening size remained fixed throughout the test). The flow rates used during the tests were low ( $<1 \text{ L} \cdot \text{min}^{-1}$ ). To apply these results to an actual spillway, we must know the flow rate in rock mass joints within an unlined spillway.

#### **2.3.4 SUMMARY**

We can summarize the characteristics of existing models and classify the methods (Table 2.6) using five parameters found to be common among the physical models: model type, model configuration, flow type, channel or flow inclination, and analysis method. We indicate whether the model was a scale model of an existing prototype and, if so, indicate the scale. The configuration indicates how it is possible to modify the model, and we present the maximum values used for channel flow and inclination. We then compare flow among the models and indicate how the results were obtained.

Table 2.6 : Summary of the characteristics of the methods, including rock mass geometrical characteristics

Method	Model type	Configuration <sup>a</sup>	Flow <sup>a</sup>	Slope <sup>a</sup>	Analysis method
Montgomery (1984)	Open-channel flow, set of blocks	<b>Variable</b> Dip of blocks Joint opening <b>Fixed</b> Block size and shape	<b>High</b> 250 L·s <sup>-1</sup>	Horizontal	<b>Quantitative</b> Pressure measured on one block face
Reinius (1986)	Open-channel flow, set of blocks	<b>Variable</b> Dip of blocks <b>Fixed</b> Joint opening Block size and shape	<b>High</b> 311 L·s <sup>-1</sup>	Horizontal	<b>Quantitative</b> Pressure measured on one block face
Annandale et al.(1998)	Plunging jet into a plunge pool, two layers of blocks	<b>Fixed</b> Block disposition Jet characteristics	<b>Very high</b> 3400 L·s <sup>-1</sup>	15° jet flow Blocks in a horizontal basin	<b>Quantitative</b> Pressure measured on the basin surface and between block layers
Liu et al. (1998)	1:100 scale model of the Three Gorges Dam spillway jet flow spillway, one block	<b>Variable</b> Block size and shape Flow characteristics <b>Fixed</b> Joint orientation and opening	<b>Average specific discharge:</b> 174 L·s <sup>-1</sup>	<b>At scale</b>	<b>Quantitative</b> Pressure measured under the block
Bollaert and Schleiss (2002)	Vertical jet in a basin, steel joints	<b>Variable</b> Flow characteristics Types of joints <b>Fixed</b> Joint orientation	<b>Average</b> 120 L·s <sup>-1</sup>	Vertical	<b>Quantitative</b> Pressure measured in the joints and on the basin surface
Wang and Jiang (2010)	Open-channel flow and 1:100 scale of the Xiluodu Dam stepped spillway	<b>Fixed</b> Configuration of spillway Flow rate <b>Variable</b> Spillway slope	<b>Maximal velocity</b> in the 1:100 scale model: 38 m·s <sup>-1</sup>	<b>Channel: low</b> 1.44%–2.62% <b>Model: to scale</b>	<b>Quantitative</b> Channel: Pressure Model: Flow velocity
George et al. (2015)	Open-channel flow, one tetrahedral block	<b>Variable</b> Block orientation <b>Fixed</b> Channel slope Block size and shape	<b>High</b> 300 L·s <sup>-1</sup>	<b>Realistic</b> 21°	<b>Quantitative</b> Block displacement and ejection speed
Pells (2016)	Open-channel flow, one cubic block	<b>Variable</b> Block orientation and protrusion Flow characteristics <b>Fixed</b> Joint opening	<b>High</b> 350 L·s <sup>-1</sup>	<b>Low to medium</b> 4.6° and 11.1°	<b>Quantitative</b> Pressure measurements and forces on the block faces
Rong et al. (2020)	Fractured granite blocks	<b>Fixed</b> Minor differences between samples	<b>Low, but small scale</b> 0.2 L·min <sup>-1</sup>	<b>Non-applicable</b>	<b>Quantitative</b> Pressure gradient

<sup>a</sup>Configuration indicates whether it is possible to modify the model to test different setups (variable) and the parameters that can be adjusted. <sup>b</sup>Values presented in Flow and Slope are the maximum values used for these parameters, and the qualitative description of flow e.g., high, is in relation to the other presented models.



## 2.4 DISCUSSION

The existing physical models relating to the study of erosion can be divided into two categories: those studying the hydraulic characteristics of the flow and those studying the effect of different rock and hydraulic parameters on the pressure applied to the rock mass. Each has its advantages and disadvantages. The first-category models mainly study the effects of varying hydraulic configurations, such as slope, flow rate, and flow turbulence, and assess various spillway configurations, such as the number of stairs and the type of ski jump. Some of these models used pressure measurements on flat surfaces or stairs without joints or blocks. In contrast, others used the produced erosion patterns to assess the effects of varying flow parameters. Thus, they did not specifically evaluate the effect of geometric parameters on erosion, although their objectives often included the study of erodibility or ways to reduce erosion downstream from spillways. Consequently, only models in the second category considered rock mass parameters affecting erosion.

The models presented in the second section focus more specifically on the effects of rock mass characteristics on its erodibility. Suitable models must include the pressure distribution according to specific parameters, such as joint orientation, their opening, block volume and their protrusion, to produce a better characterization of a rock mass. Boumaiza et al. (2021), using observational data, concluded that six rock mass parameters are important in the erosion process. These parameters, listed from most important to least important, are joint condition, the nature of the potential erodible surface, block volume, joint opening, joint orientation, and the rock mass deformation module. We have studied the ability of existing models to measure the effect of these six parameters in the erosion process. We also added the parameter of protrusion, which has a marked effect in the physical models that we reviewed. Because the deformation modulus is the least important parameter in rock mass erodibility and no physical models have yet to study this parameter, we removed this element from any consideration (Table 2.7). We note that some parameters, such as joint orientation and block protrusion, are studied much more than other parameters. Most of the effects of the other parameters remain poorly studied.

Table 2.7 : Models characterizing the effects of the geometrical parameters of the rock

Type	Model	Joint orientation	Joint opening	Block volume	Joint condition	NPES	Protrusion
Plunging jet	Annandale et al. (1998)						
	Liu et al. (1998)			X			
	Bollaert et Schleiss (2002)		X				
Open-channel flow	Montgomery (1984)	X					X
	Reinius (1986)	X					X
	Wang and Jiang (2010)					X	
	George et al. (2015)	X					X
	Pells (2016)	X					X
Other	Rong et al. (2020)				X		

#### 2.4.1 INFLUENCE OF JOINT ORIENTATION AND PROTRUSION

The interaction between joint orientation and protrusion of blocks has been considered by, among others, George et al. (2015), Reinius (1986), and Montgomery (1984). George et al. (2015) studied only one block. Reinius (1986) and Montgomery's (1984) respective studies used several blocks arranged within the channel; however, in both cases only a single block was instrumented. Pells' model (2016) consisted of a single block, although he could vary the parameters individually. Despite joint orientation and protrusion impact being modeled in the laboratory, further studies are required that consider more than one instrumented block to assess interactions between blocks. Studies of other parameters, such as joint opening, block volume, joint condition, and the nature of the potentially erodible surfaces remain limited.

#### 2.4.2 INFLUENCE OF JOINT OPENING

The joint opening parameter was discussed by Bollaert and Schleiss (2004; 2002) and Montgomery (1984). Bollaert and Schleiss (2002) modeled flow as a vertical jet, which does not replicate the conditions of a plunging-jet spillway. Furthermore, the studied joints were composed of steel and did not properly represent the rock texture, and only one joint was modeled at a time. Montgomery's study (1984) of joint openings suffered from the joints being sealed where their openings varied; therefore, hydraulic flow between the joints was prevented. Moreover, neither model studied pressure fluctuations when the joint length and aperture ratio increased.

### **2.4.3 INFLUENCE OF BLOCK VOLUME**

Liu et al.'s plunging jet flow model (1998) used rock block size as a variable. Their model could determine pressure variations experienced by blocks of variable size at the point of impact of a plunging jet in relation to varying heights of water fall at the point of impact. However, this model had some drawbacks. For example, pressure was only measured under the block, not along the block sides or upper surface. According to the erodibility criteria of the dynamic impulsion module of the comprehensive scour model (Bollaert, 2004), uplift forces must be compared with resisting forces to assess rock erodibility. Resisting forces include the hydraulic forces applied to the top of the block, block weight, and joint shear resistance. Moreover, the block was not displaced upstream or downstream of the point of impact, thus preventing any assessment of the effect of pressure variations related to the horizontal flow caused by the impact of the jet in the basin.

### **2.4.4 INFLUENCE OF JOINT CONDITION**

Rong et al. (2020) examined joints in relation to their geometry. They used boulders sourced from the same granite deposit to ensure consistent roughness and weathering of the material; only fracture geometry varied. Their model was nonetheless limited by only varying joint geometry and applying a relatively low flow (Table 2.6). However, because a single fracture was studied in their model, the flow scale was representative of the fracture scale. Rong et al. (2020) modeled a fracture at the centimeter scale. Nonetheless, it remains uncertain how to extrapolate and apply this small scale to joints at the metric scale, as pressure varies along the full length of the joint. A more thorough investigation of this scaling issue is required for applying the effects of joint geometry to the scale of unlined spillways.

### **2.4.5 NATURE OF POTENTIALLY ERODIBLE SURFACE**

Wang and Jiang (2010), in their study of the nature of a potentially erodible surface, demonstrated that smoother surfaces are subjected to less erosion. Coatings applied to a spillway surface reduce friction; nonetheless, the conclusion of this latter study is not as relevant for this review, as we are focused on the parameters affecting the erosion within uncovered spillways.

#### **2.4.6 FLOW TYPES**

Flow type, as identified in Table 2.4, can influence the effects of the studied rock mass. Plunging jet flows have the particularity of creating an impact point where the jet reaches the water downstream. This point of impact is where the erosion potential is greatest, and the pressure conditions are particular to this location. In contrast, open-channel flows do not present a particular point of impact. By flowing along the channel, this type of flow creates different conditions of pressure variations from those of the plunging jet. Models of an open-channel flow have demonstrated that joint orientation and protrusion are frequently studied together; however, other important parameters remain neglected. An exception is the study of NPES by Wang and Jiang (2010). Thus, these models do not present a complete study of rock erodibility parameters. In particular, block volume and joint conditions have yet to be investigated using an open-channel flow.

#### **2.5 CONCLUSIONS AND FUTURE CHALLENGES**

Two main types of flume models exist for studying erosion in spillways: flume models focused on hydraulic characteristics and models evaluating the geometric characteristics of the rock mass. For models of geometric features, joint orientation was the most frequently discussed parameter in the studies of Montgomery (1984), Reinius (1986), Pells (2016), and George et al. (2015). However, these studies only measured the pressure applied to a single block. Few models have focused on the effect of joint opening variation. The exceptions are Pells (2016), who investigated the impact of an opening under a block, and Montgomery (1984), who varied joint openings around a sealed block. The model of Liu et al. (1998) was the only model that recorded uplift pressures for different block sizes and shapes; however, this model was for a plunging jet flow. For uncovered spillways, characterized by an open-channel flow, there remains a lack of information. Flume model studies should include the effect of the identified rock mass characteristics on hydraulic erosion. Moreover, understanding the interaction among these parameters within a given model is vital for improving our understanding of the hydraulic erosion of rock.

### **CHAPITRE 3 COMPARAISON DE PARAMÈTRES D'ORIENTATION DES JOINTS ET LEUR EFFET SUR L'ÉRODABILITÉ DU MASSIF ROCHEUX DANS LES ÉVACUATEURS DE CRUES**

Ce chapitre reprend un article dont la première auteure est l'auteure de ce mémoire. Le chapitre présente et compare trois paramètres décrivant l'effet de l'orientation des joints du massif rocheux sur son érodabilité.

L'article est soumis à la revue *Quaterly Journal of Engineering Geology and Hydrogeology* et en attente d'approbation.

# COMPARISON OF EXISTING JOINT ORIENTATION PARAMETERS AND THEIR EFFECT ON ROCK ERODIBILITY IN DAM SPILLWAYS

**Marie-Hélène Wisse\*<sup>1</sup>, Ali Saeidi<sup>1</sup>, Marco Quirion<sup>2</sup>**

<sup>1</sup>Applied Sciences, Université du Québec à Chicoutimi, 555 Boul. de l'Université, Chicoutimi, QC, G7H 2B1

<sup>2</sup>Rock Mechanics, Hydro-Québec, 75 Boul. René-Lévesque W, Montréal, QC, H2Z 1A4

\*Corresponding author (e-mail: [marie-helene.wisse1@uqac.ca](mailto:marie-helene.wisse1@uqac.ca))

## ACKNOWLEDGMENTS

The authors would like to thank the research group R<sup>2</sup>Eau for their helpful comments and suggestions.

## AUTHORS CONTRIBUTION

**Marie-Hélène Wisse:** Conceptualization, Validation, Visualization, Formal analysis, Investigation, Methodology, Writing – Original Draft, Writing – Review and Editing

**Ali Saeidi:** Conceptualization, Methodology, Resources, Writing – Review and Editing, Supervision, Project administration, Funding acquisition, Validation

**Marco Quirion:** Writing – Review and Editing, Supervision, Funding acquisition

## FUNDING

This work was supported by the Natural Sciences and Engineering Research Council of Canada (NSERC) (#RDCPJ 537350 – 18), Mitacs Inc. (# IT22640), Hydro-Québec and Uniper.

## DATA AVAILABILITY STATEMENT

All data generated or analysed during this study are included in this published article: (Pells, 2016).

## ABSTRACT

Rock mass erosion in unlined spillways causes significant structural damage and necessitates expensive repairs. The rock mass is made up of blocks, formed by various arrangements of joint sets. The volume and the protrusion of these blocks, as well as the orientation, the opening and the roughness of the joints, are all features that can affect rock erodibility. Most of these features are incorporated in parameters developed for rock mass characterization. Three joint orientation parameters are compared in this article using a database containing geological and hydraulic information on scoured spillways. According to the detailed methodology, the data is first classified according to rock quality using the  $GSI_{chart}$  index. Then, for each  $GSI_{chart}$  class, the data is distributed according to the damage level, stream power and the selected joint orientation parameter. This study shows that no joint orientation parameter is currently able to accurately represent the effect of joint orientation on erosion of excellent- to poor-quality rock mass. Moreover, this study shows that the  $GSI_{chart}$  index is not appropriate to analyse rock erosion, since some relevant parameters for evaluating rock erodibility are not considered.

## KEYWORDS

Joint orientation, erosion, rock mass, hydraulic, unlined spillway

### 3.1 INTRODUCTION

Hydroelectricity production requires the construction of dams. For safety, emergency spillways are built as part of these dams to carry away excess water. These spillways are excavated into the bedrock, which exposes the rock mass to the erosive power of water flow. In some cases, rock mass erosion in unlined spillways has been shown to cause damage to the dam's structure. The erosion process occurs in all quality rock mass and is affected by rock mass features and flow characteristics. In the field of rock mechanics, several methods for evaluating rock mass erodibility have been developed, such as those of Kirsten (1982), Van Schalkwyk (1994), Annandale (1995) Kirsten et al. (2000), Bollaert (2004; 2010; 2002) and Pells (2016). These methods fall into two main categories: semi-analytical and semi-empirical (Jalili Kashtiban et al., 2021). The main existing semi-analytical method is the one of Bollaert (2004; 2010; 2002), the Comprehensive Scour Model (CSM). Methods of Kirsten (Kirsten, 1982), Van Schalkwyk (1994), Annandale (1995), Kirsten et al. (2000) and Pells (2016) are classified as semi-empirical. Semi-empirical methods define a threshold where erosion in rock mass occurs, i.e., when the stream power becomes greater than the rock's resistance to erosion. Several researchers have sought to find methods to define rock mass resistance to erosion according to its characteristics, such as block size, joint orientation, uniaxial compressive strength, joint opening, joints roughness and joint shear strength. Boumaiza et al. (2021) have developed a methodology to identify the relative impact of each of these features on the hydraulic erodibility of rock. It was found that joint orientation influences a rock mass's resistance to erosion when subjected to flow power. This article focuses on semi-empirical methods involving a parameter that describes the effect of joint orientation within the flow. Methods involving joint orientation parameters that are compared in this paper are described below.

The Kirsten index (N) is designed to assess the ease of excavating with a bulldozer (Kirsten, 1982). This index has also been used to evaluate the erodibility of the rock mass. However, this application has been criticized. Van Schalkwyk (1994), Annandale (1995), and Kirsten et al. (2000) used the Kirsten index to define a rock erodibility limit. This limit depends on the rock's resistance to erosion, determined using Kirsten's index, and on the erosive capacity of the flow (Jalili Kashtiban et al., 2021). Kirsten's index is presented in equation (3.1).

$$N = M_s K_b K_d J_s \quad (3.1)$$



Where  $M_s$  is the uniaxial compressive strength of the rock,  $K_b$  refers to the block size,  $K_d$  refers to the shear strength and  $J_s$  is the joint orientation parameter.  $J_s$  defines a value of the rock's vulnerability to erosion as a function of the joint spacing ratio and the joint orientation within the flow. The Kirsten index was originally designed to define the ease with which a rock mass can be excavated. Since its inception, there has been a lot of criticism of this method. In particular, its application to erodibility situations has been questioned by several authors and some of the parameters used have been shown not to provide a satisfactory estimate of what they represent (Boumaiza, 2019; Pells, 2016). Boumaiza et al's study (2019a) reveals that the estimation of orthogonal joint sets when calculating  $J_s$  is inadequate and that a better approximation of the angle between joint sets should be considered. Pells (2016) notes that the  $M_s$  and RQD factors of Kirsten's index have a much greater impact on the final value of Kirsten's index. The maximum values of  $M_s$  and RQD are 280 and 100, and their minimum values are 0.87 and 5, respectively. In contrast, the maximum and minimum values of the  $J_s$  parameter are 1.50 and 0.37. The overall impact of the  $J_s$  parameter on Kirsten's index is low.

Pells (2016) proposed two new methods to assess rock mass erodibility: the Rock Mass Erodibility Index (RMEI) and the Erodibility Geological Strength Index (eGSI) (equation 2). It is in the eGSI that he introduces  $E_{doa}$  as a new parameter to evaluate the effect of joint orientation on rock mass erodibility.  $E_{doa}$  makes it possible to evaluate rock resistance to erosion according to joint orientation and joint spacing ratio. The value of  $E_{doa}$  is added to the GSI index developed by Hoek et al. (1995)

$$eGSI = E_{doa} + GSI_{chart} \quad (3.2)$$

Pells (2016) used Marinos and Hoek's (2000) chart to calculate  $GSI_{chart}$ .

The two main parameters that evaluate the effect of joint orientation are  $E_{doa}$  and  $J_s$ . Reinius (1986) and Montgomery (1984) studied the effects of the joint orientation of a row of blocks placed in a horizontal flow channel. Pressure was measured at various locations on an instrumented block. Along with different block dispositions, such as orientation and protrusion, and various flow rates, pressures applied to the block were measured and the uplift pressure coefficient  $C_{up}$  was obtained.

$J_s$ ,  $E_{doa}$  and  $C_{up}$  do not report the same effect of joint orientations on rock mass erodibility. In order to determine the parameter that best represents the effect of joint orientation on rock mass erodibility, a method was used to assess the applicability and the effectiveness of each joint orientation parameter to classify rock mass according to its vulnerability to erosion. This paper covers the methodology used to define the parameter that best represents the effect of joint orientation, presents a summary of the existing parameters, considers the results obtained and ends with a discussion on the significance and validity of these results.

### 3.2 MATERIALS AND METHODS

The database used in this study was developed by Pells (2016). It includes the description, geomechanical features and several geomechanical parameters of the rock mass in 24 dams located in South Africa and Australia. Flow strength, flow direction and erosion damage levels are also documented. For each dam, the spillway is separated into different sections depending on the damage level. For each section, the following geomechanical parameters of joint sets are described: opening, spacing, persistence, dip, orientation and roughness. The rock is also evaluated with the Kirsten index factors:  $RQD$ ,  $J_n$ ,  $J_r$ ,  $J_a$ ,  $J_s$  and  $M_s$ . In total, the database contains information on a total of 114 sections spread across 24 dams. This information was reported in the form of consultant reports, technical documents and observations made by geologists over the years.

The first step of the methodology is to develop the database.  $E_{doa}$  and  $J_s$  are determined by Pells (2016) for each section.  $C_{up}$  is determined according to the most critical joint orientation of each data set. Rock mass quality is assessed by  $GSI_{chart}$  rock resistance index, which is determined by Pells (2016). Stream power and damage levels are also defined by Pells (2016).

The methodology used to compare joint orientation parameters was inspired by Boumaiza et al. (2019b). Each parameter must first be divided into classes: joint orientation parameters,  $GSI_{chart}$ , stream power and damage level. For each  $GSI_{chart}$  class, a graph of the mean stream power class in relation to the damage level class is produced. Joint orientation parameters are then plotted, according to the joint orientation parameter class. It is then possible to compare the effectiveness of the joint orientation parameter selected according to the damage level recorded. The methodology is summarized in Figure 3.1.

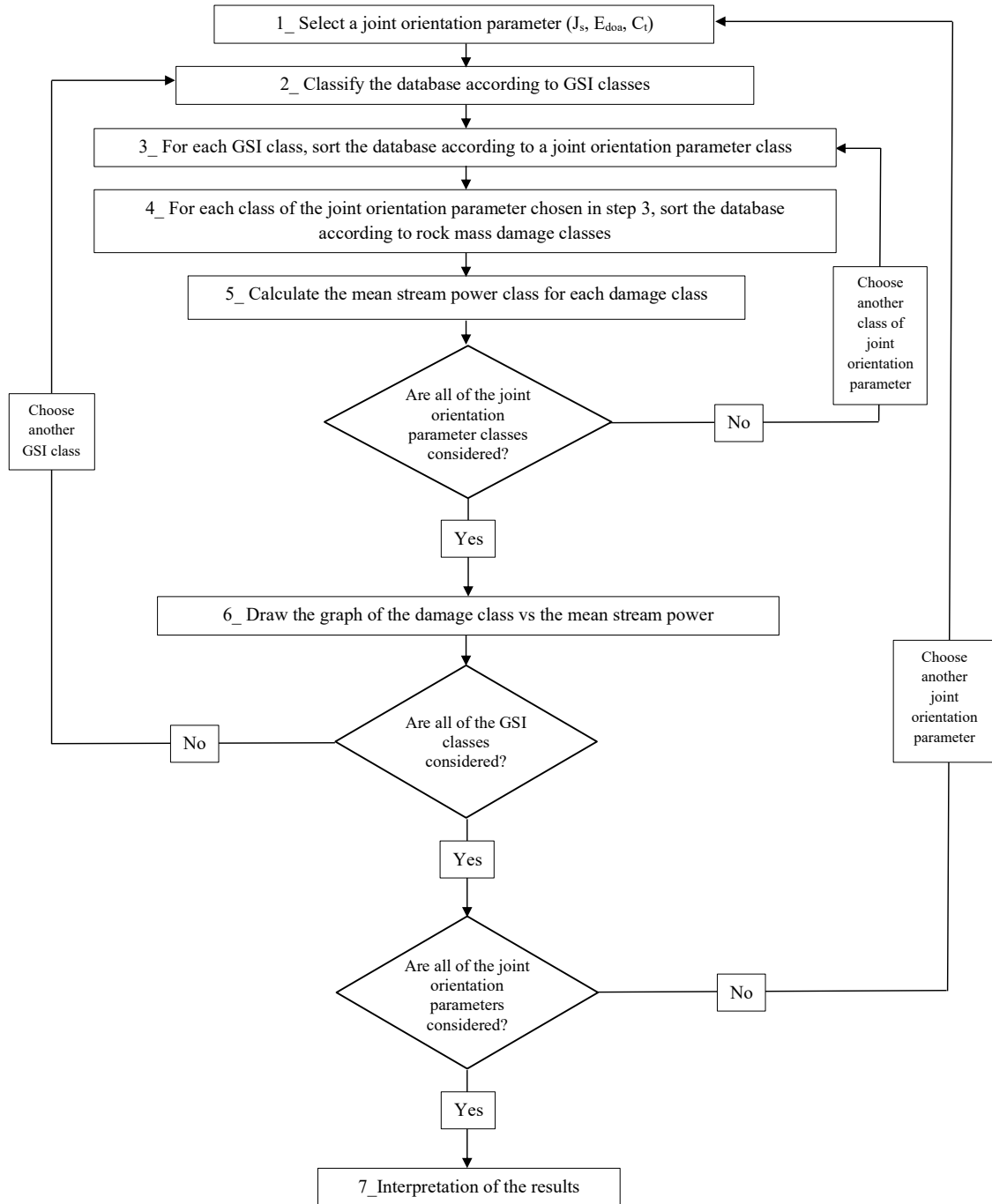


Figure 3.1 : Methodology for comparing joint orientation parameters

### 3.2.1 STEP 1 – SELECTION OF A JOINT ORIENTATION PARAMETER

Step 1 consists of selecting one joint orientation parameter from those presented ( $E_{doa}$ ,  $J_s$  or  $C_{up}$ ). The following steps will be performed according to the selected parameter.

### 3.2.2 STEP 2 – CLASSIFY THE DATABASE ACCORDING TO GSI<sub>CHART</sub>

The goal of this step is to combine data with the same rock quality index. GSI<sub>chart</sub> values are assigned a class from 1 to 4, according to RMR classification (Bieniawski, 1989). Classes are assigned according to the separation shown in Figure 3.2.

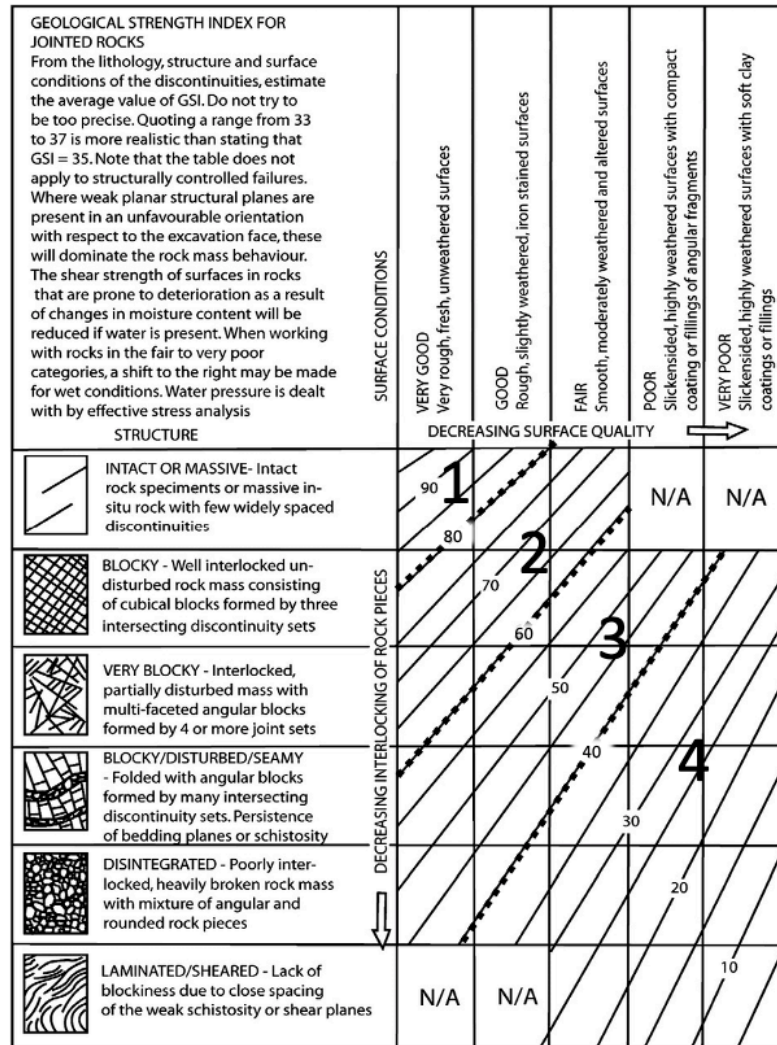


Figure 3.2 : GSI determination chart and class separation modified from Marinos and Hoek (2000)

### 3.2.3 STEP 3 - CLASSIFY THE JOINT ORIENTATION PARAMETER CHOSEN FOR EACH GSI CLASS

The goal of this step is to group the data into different classes according to the value of the joint orientation parameter previously chosen.

Classification of  $J_s$  was done by Boumaiza et al. (2019b) by statistically distributing Pells'(2016) database. Classification of  $J_s$  is detailed in Table 3.1.

Table 3.1 :  $J_s$  proposed classification (Boumaiza et al., 2019b)

<b>Class</b>	<b><math>J_s</math></b>	<b>Description</b>
1	0.4 - 0.6	Highly vulnerable to erosion
2	0.6 - 0.8	Very vulnerable to erosion
3	0.8 - < 1	Moderately vulnerable to erosion
4	1	Less vulnerable to erosion
5	> 1	Minimally vulnerable to erosion

Classification of  $E_{doa}$  was done by Boumaiza et al. (2019b) by statistically distributing Pells'(2016) database. Classification of  $E_{doa}$  is detailed in Table 3.2.

Table 3.2 :  $E_{doa}$  proposed classification (Boumaiza et al., 2019b)

<b>Class</b>	<b><math>E_{doa}</math></b>	<b>Description</b>
1	0 to -5	Minimally vulnerable to erosion
2	-5 to -10	Less vulnerable to erosion
3	-10 to -15	Moderately vulnerable to erosion
4	-15 to -25	Highly vulnerable to erosion

Classification of  $C_{up}$  is presented in Table 3.3. It was done by statistically distributing Pells'(2016) database and based on the effect that this parameter has on erosion.

Table 3.3 :  $C_{up}$  proposed classification

<b>Class</b>	<b><math>C_{up}</math></b>	<b>Description</b>
1	< 0	Minimally vulnerable to erosion
2	0 - 0.1	Less vulnerable to erosion
3	0.1 - 0.4	Moderately vulnerable to erosion
4	0.4 - .5	Very vulnerable to erosion
5	> 0.5	Highly vulnerable to erosion

### 3.2.4 STEP 4 – CLASSIFICATION OF DAMAGE LEVEL

The goal of this step is to assemble data with the same damage level class from data with the same  $GSI_{chart}$  class and joint parameter class. The damage level classes were defined using Pells' classification (2016). The damage categories depend on the depth of the erosion and its general extent. The classification proposed by Pells (2016) is presented in Table 3.4.

Table 3.4 : Proposed classification of damage levels (Pells, 2016)

Class	Scour depth	General extent $m^3 100m^{-2}$	Damage description
1	<0.3	<10	Negligible
2	0.3 - 1	10 - 30	Minor
3	1 - 2	30 - 100	Moderate
4	2 – 7	100 - 350	Large
5	>7	>350	Extensive

### 3.2.5 STEP 5 – CLASSIFICATION OF THE STREAM POWER

The goal of this step is to group together all data with the same  $GSI_{chart}$  class, the same joint orientation parameter class and the same damage class. Mean stream power is calculated using this data. A classification of stream power classes had already been proposed by Boumaiza et al. (2019b) However, this classification did not sufficiently account for the highest stream power, which is greater than  $100kW/m^2$ . This is why a modified classification is proposed, as shown in Table 3.5.

Table 3.5 : Proposed stream power classification. Modified from Boumaiza et al (2019b)

Class	Unit Stream Power ( $[u]_{ud}, kW m^{-2}$ )	Description
1	< 2.5	Very Low
2	2.5 - 10	Low
3	10 - 25	Moderate
4	25 - 50	High
5	50 - 100	Very High
6	> 100	Extreme

When all the classes of the chosen joint orientation parameter have been evaluated, continue with step 6. Otherwise, start over with a new joint orientation parameter class in step 3.

### **3.2.6 STEP 6 – DRAW THE DAMAGE CLASS GRAPH AS A FUNCTION OF THE MEAN STREAM POWER CLASS FOR THE CHOSEN JOINT ORIENTATION PARAMETER**

This step aims to visually compare the effect of each joint orientation parameter on rock mass erodibility. In total, four graphs will be built for each joint orientation parameter, with each graph representing one  $GSI_{chart}$  class. The Y-axis represents the damage level class and the X-axis represents the mean stream power class for each class of the joint orientation parameter with the same damage class and  $GSI_{chart}$  class.

If all  $GSI_{chart}$  classes are considered for the same joint orientation parameter, continue with the next joint orientation parameter and repeat steps 1 to 6. Otherwise, choose a new  $GSI_{chart}$  class and repeat steps 2 to 6.

### **3.2.7 STEP 7 – INTERPRET THE RESULTS**

This step involves interpreting the results obtained and determining which joint orientation parameters best represent the effect of joint orientation on rock mass erodibility.

## **3.3 THEORY**

In the following section, the three joint orientation parameters introduced are presented in detail.

### **3.3.1 PRESENTATION OF THE $J_s$ PARAMETER**

The  $J_s$  parameter describes the effect of joint orientation on rock mass excavatability according to the direction of excavation. Kirsten (1982) mentions that it is easier to excavate a rock whose joints dip in the same direction as the excavation rather than the opposite direction. In Kirsten's study (1982), some assumptions are made to evaluate  $J_s$ : joint sets are considered orthogonal and only the two less spaced joint sets are considered. Since Kirsten's index is used to assess rock mass erodibility rather than excavatability, in this article,  $J_s$  is considered to be a joint orientation parameter for rock mass erodibility. The joint spacing ratio ( $r$ ) is defined by the ratio of  $S_{\psi}$ , the spacing between joints dipping in the opposite direction of ripping (m), and  $S_{\theta}$ , the spacing

between joints dipping in the direction of ripping (m) (Figure 3.3). The joint spacing ratio presented in equation 3.3 is necessary to determine  $J_s$ .

$$r = S_\psi / S_\theta \quad (3.3)$$

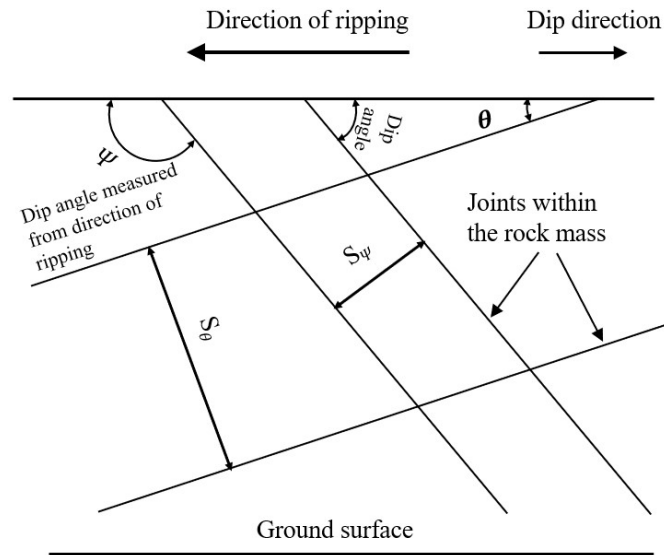


Figure 3.3 : Sketch of a fractured rock mass. Rebuilt from (Kirsten, 1982)

$J_s$  values can be found from Table 3.6. The first step in defining  $J_s$  is to define the closest spaced joint set oriented perpendicular to the flow. Then, depending on the dip direction of this joint set (whether it is in the same or opposite direction of the flow), the value of  $J_s$  will be found either in the upper section (for  $0^\circ$ ) or in the lower section (for  $180^\circ$ ) of Table 6. With the joint spacing ratio and the dip of this joint set, it is possible to find a value for  $J_s$ . When joint orientation has no effect on rock mass erodibility,  $J_s$  is equal to 1.  $J_s$  value will decrease below 1 if joint orientation increases the rock's vulnerability to erosion. If joint orientation increases the rock's resistance to erosion, the  $J_s$  value will increase to above the value of 1.



Table 3.6 : Relative ground structure number ( $J_s$ ) proposed values rebuilt from Kirsten (1982)

Dip direction of closer spaced joint set (°)	Dip angle of closer spaced joint set (°)	Ratio of joint spacing (r)			
		1:1	1:2	1:4	1:8
180/0	90	1	1	1	1
0	85	0.72	0.67	0.62	0.56
0	80	0.63	0.57	0.50	0.45
0	70	0.52	0.45	0.41	0.38
0	60	0.49	0.44	0.41	0.37
0	50	0.49	0.46	0.43	0.40
0	40	0.53	0.49	0.46	0.44
0	30	0.63	0.59	0.55	0.53
0	20	0.84	0.77	0.71	0.68
0	10	1.22	1.10	0.99	0.93
0	5	1.33	1.20	1.09	1.03
0/180	0	1	1	1	1
180	5	0.72	0.81	0.86	0.90
180	10	0.63	0.70	0.76	0.81
180	20	0.52	0.57	0.63	0.67
180	30	0.49	0.53	0.57	0.59
180	40	0.49	0.52	0.54	0.56
180	50	0.53	0.56	0.58	0.60
180	60	0.63	0.67	0.71	0.73
180	70	0.84	0.91	0.97	1.01
180	80	1.22	1.32	1.40	1.46
180	85	1.33	1.39	1.45	1.50
180	90	1	1	1	1

### 3.3.2 PRESENTATION OF THE $E_{DOA}$ PARAMETER

Pells (2016) added the  $E_{doa}$  parameter to the rock quality index GSI<sub>chart</sub> (Marinos et Hoek, 2000) to consider joint orientation and joint spacing effects on rock erosion, as GSI<sub>chart</sub> does not take them into account.  $E_{doa}$  is based on the results of laboratory tests on a physical model, erosion, geological and hydraulic data of dam sites, and on the theory of block uplift. Pells used the model of the  $J_s$  parameter to develop  $E_{doa}$ . However,  $E_{doa}$  is more precise, considering different parameters such as flow types, channel slopes and various joint spacing ratios (r): 1: 1, 1: 2, 1: 4, 1: 8, 1:20. For a flow parallel to the surface,  $E_{doa}$  presents negative values,

with a maximum value of 0 and a minimum value of -23 (Figure 3.4). Therefore, joint orientation cannot have a positive effect on the resistance to erosion of the rock, as for the  $J_s$  parameter.

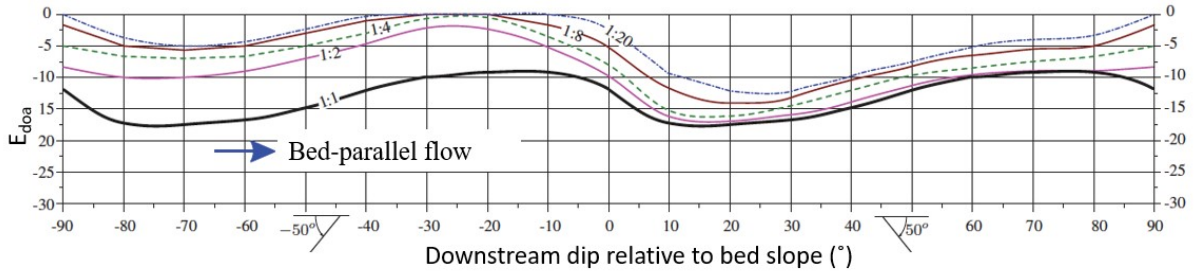


Figure 3.4 :  $E_{doa}$  values for a horizontal channel (Pells, 2016)

### 3.3.3 PRESENTATION OF THE $C_{UP}$ PARAMETER

Reinius' (1986) and Montgomery's (1984) laboratory experiments made it possible to obtain different values of pressure acting on an instrumented block placed in a horizontal flow channel, among an alignment of non-instrumented blocks (Figure 3.5). The block was instrumented with 14 piezometers, which were used to measure the hydraulic head at different points (Figure 3.6). The blocks, dimension was  $15 \times 15 \times 30 \text{ cm}^3$ . This study considers various flow rates, water loads above the block and block dips. As shown in Figure 3.4 and Figure 3.5, the  $\beta$  angle is calculated from the vertical, whereas the dip is calculated from the horizontal. In order to compare the parameters, a  $90^\circ$  correction was made to transform  $\beta$  values into dip values.

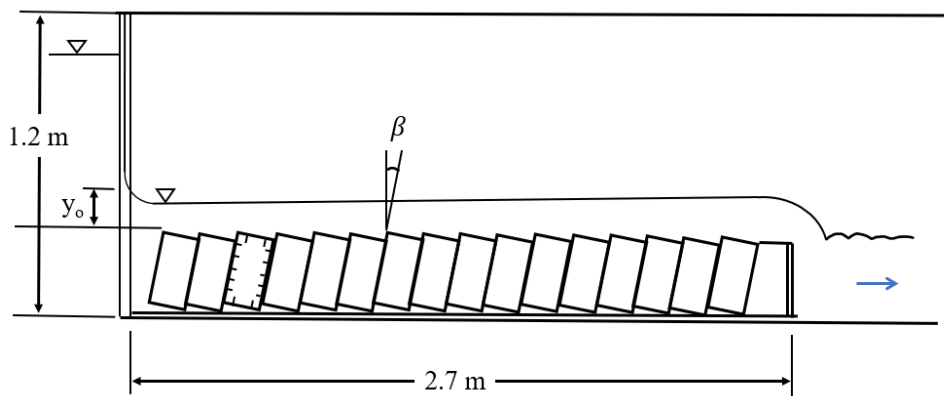


Figure 3.5 : Experimental setup. Reworked from Reinius (1986)

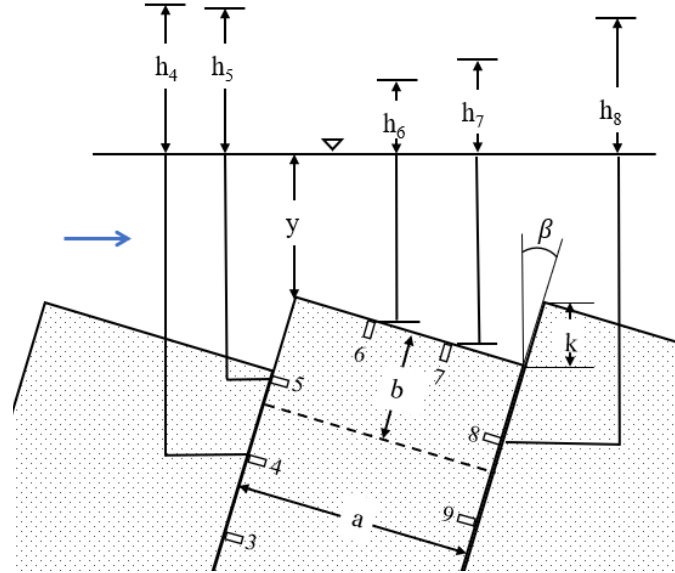


Figure 3.6 : Simulated fracture between piezometers 5 and 8. Dynamic pressures are also shown. Reworked from Reinius (1986)

Using piezometer data, a dimensionless pressure coefficient  $c$  was obtained (equation 3.4).

$$c = \frac{h}{U^2/2g} \quad (3.4)$$

Where  $h$  represents the dynamic pressure reading (m),  $U$  represents the velocity of water ( $\text{m s}^{-1}$ ) and  $g$  represents the gravitational acceleration ( $\text{m s}^{-2}$ ).

The dynamic pressure reading  $h_d$  is obtained from the water head recorded by the piezometer, from which the static pressure, the height of water from the piezometer, is subtracted (equation 3.5).

$$h_d = h_t - h_s \quad (3.5)$$

Where  $h_t$  is the piezometer reading, i.e., the total water pressure, and  $h_s$  is the static pressure, the water load above the block.  $C_{\text{up}}$  parameter was calculated with the mean value of the pressure coefficients at piezometers 5 and 8, when considering a block of thickness  $b$  (Figure 3.6).

### 3.4 RESULTS

#### 3.4.1 CLASSIFICATION OF THE $GSI_{\text{chart}}$ INDEX

According to the classes shown in Figure 3.2,  $GSI_{\text{chart}}$  data distribution is presented in Figure 3.7. The Y-axis represents the total data for each  $GSI_{\text{chart}}$  class.

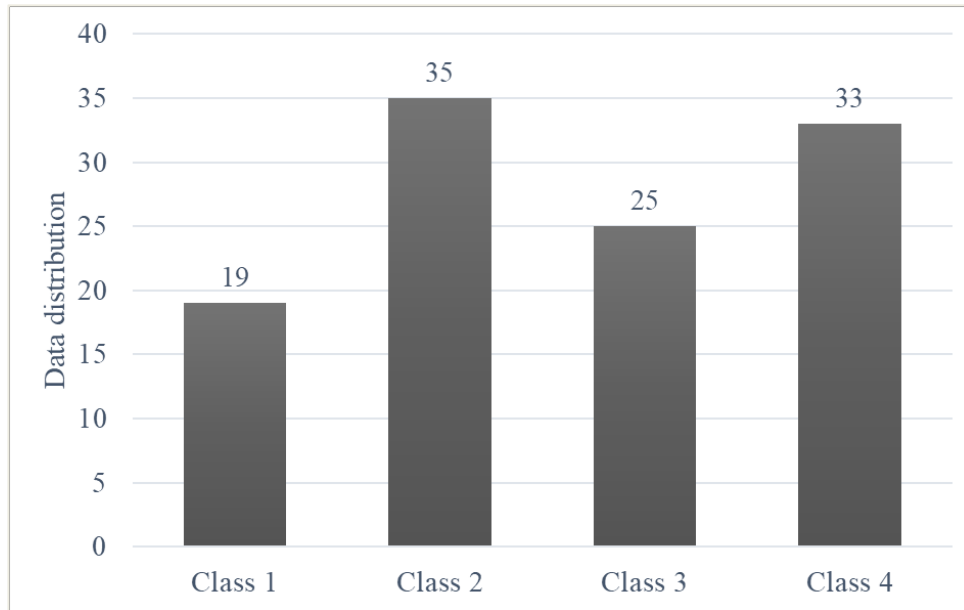


Figure 3.7 : Distribution of data by  $GSI_{\text{chart}}$  class

#### 3.4.2 CLASSIFICATION OF THE $J_s$ PARAMETER

Data classification for the  $J_s$  parameter was performed according to the classes described in Table 3.1. Figure 3.8 shows the data distribution for each  $J_s$  class. Class 4 of  $J_s$  has significantly more data than the other classes. This class corresponds to a  $J_s$  equal to one, representing joint orientation having no impact on Kirsten's index, i.e., having no impact on rock resistance. The Y-axis represents the total data for each  $J_s$  class.

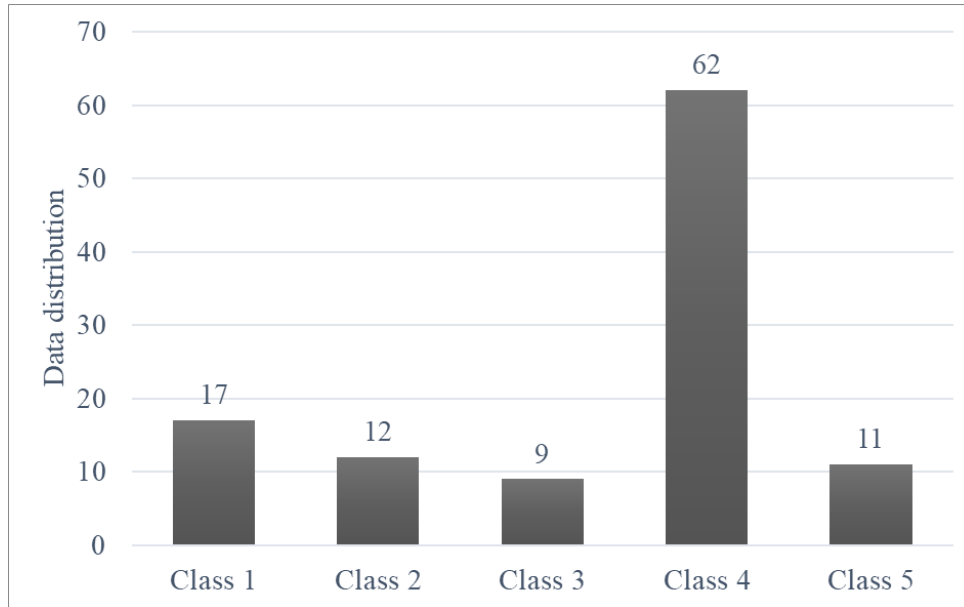


Figure 3.8 : Distribution of  $J_s$  classes of Pells (2016) case studies data

### 3.4.3 CLASSIFICATION OF THE $E_{DOA}$ PARAMETER

Data classification according to the  $E_{doa}$  parameter was done according to classes described in Table 3.2. Figure 3.9 shows the data distribution for each  $E_{doa}$  class. The  $E_{doa}$  of class 1 has significantly fewer data than the other classes. This class corresponds to a situation where  $E_{doa}$  has the least effect on rock mass resistance to erosion. The Y-axis represents the total data for each  $E_{doa}$  class.

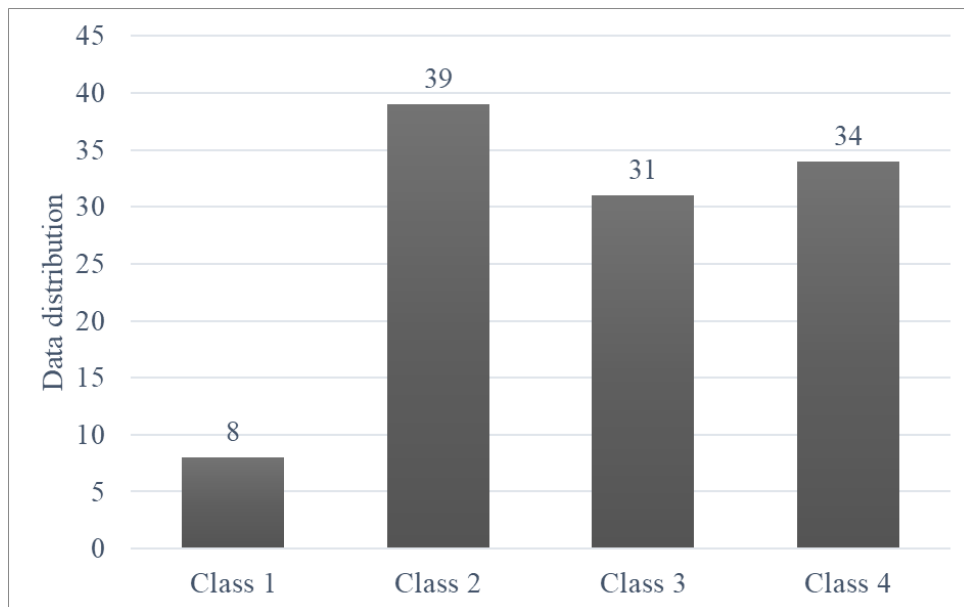


Figure 3.9 : Distribution of  $E_{doa}$  classes of Pells (2016) case studies data

### 3.4.4 CLASSIFICATION OF THE $C_{UP}$ PARAMETER

In order to assess a  $C_{up}$  value for each data set available, each joint set was analyzed according to its orientation in relation to the flow. Only joint sets not parallel to the flow were considered. A joint set must have a difference of orientation of at least  $20^\circ$  to be considered valid for this analysis. Then, according to Reinius' study (1986), for each data set, the most critical joint set was chosen. The most critical joint set is the one with the highest  $C_{up}$  value. Figure 3.10 illustrates the distribution of the data according to the  $C_{up}$  parameter and the orientation  $\beta$  ( $^\circ$ ) of the block. Only the most critical  $C_{up}$  values were retained for each data set.

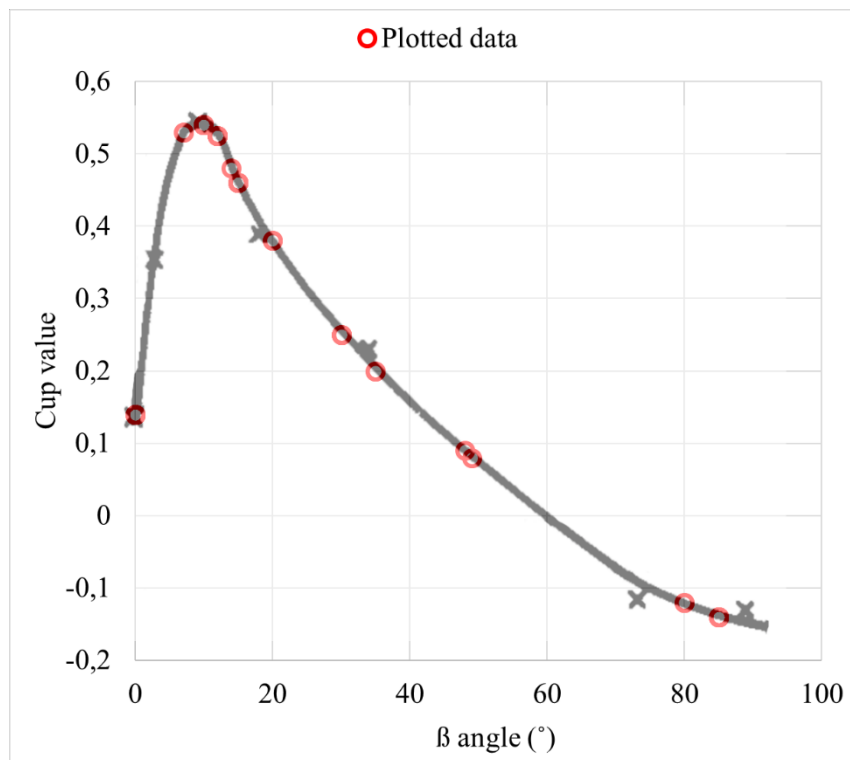


Figure 3.10 : Distribution of the data according to Reinius' study (1986)

Figure 3.11 shows the data distribution according to these two situations. The Y-axis represents the total data for each  $C_{up}$  class.

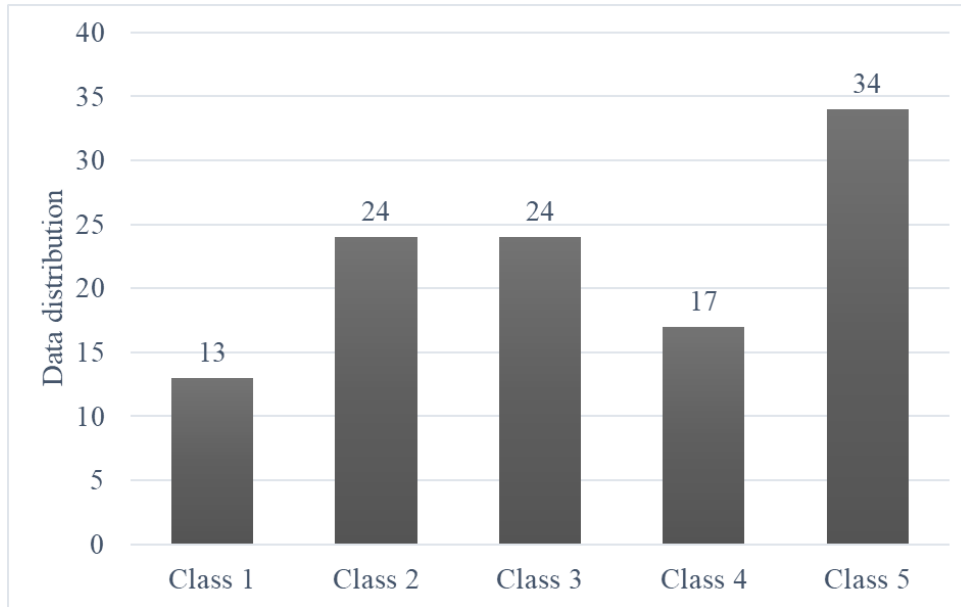


Figure 3.11 : Distribution of Pells (2016) data by  $C_{up}$  classification

### 3.4.5 EFFECTS OF $J_s$ ON ROCK MASS EROSION

The effects of the  $J_s$  parameter are shown in Figure 3.12 (a-d). The Y-axis represents the mean stream power class and X-axis represents the damage level class. The bubble sizes represent the amount of data for each bubble.  $J_s$  of class 1 ( $J_{s1}$ ) is defined by a joint orientation increasing the rock mass erodibility and  $J_s$  of class 5 ( $J_{s5}$ ) represents a joint orientation increasing rock mass resistance to erosion. If  $J_s$  correctly represents the effects of joint orientation on erosion, a high  $J_s$  class should produce less damage than a lower class. In addition, the relation between damage classes and the mean stream power class should be linearly increasing.

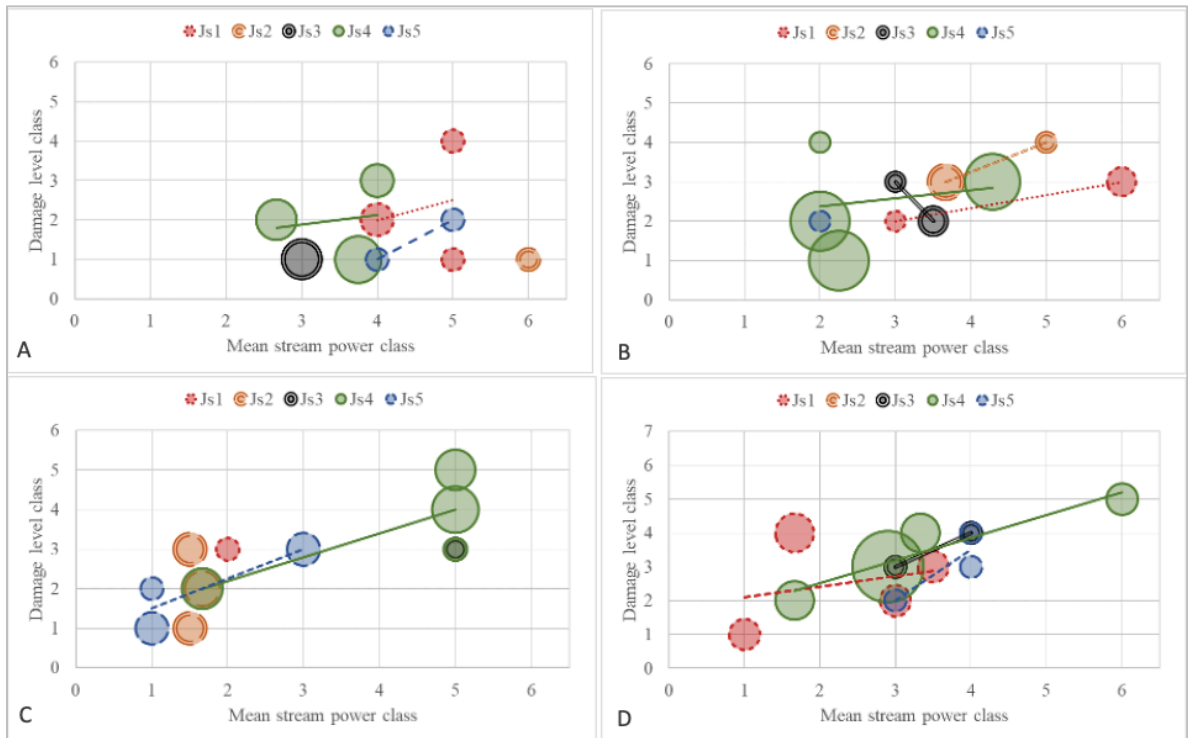


Figure 3.12 : Results of the effects of the  $J_s$  parameter on the rock's vulnerability to erosion. Lines represent the linear approximation of the data distribution **A**  $GSI_{chart}$  class 1 **B**  $GSI_{chart}$  class 2 **C**  $GSI_{chart}$  class 3 **D**  $GSI_{chart}$  class 4

For all  $GSI_{chart}$  classes, the majority of the  $J_s$  classes do not show the expected relation between them. Indeed,  $J_s$  of class 1 never show more damage than  $J_s$  of class 2. We can, however, observe in Figure 12 b) that the  $J_s$  of class 2 show more damage than the  $J_s$  of class 4, and for stream power class above 3, more damage than  $J_s$  of class 3. Some correlation is observed for  $J_s$  of class 4 and 5.  $J_s$  of class for shows indeed more erosion vulnerability than  $J_s$  of class 5, supposed to show erodibility resistance. We can also observe that the majority of the classes show the expected relation between the damage level and mean stream power class, which is observed to be increasing, as expected.

### 3.4.6 EFFECTS OF THE $E_{DOA}$ PARAMETER

The effects of the  $E_{doa}$  parameter are shown in Figure 3.13 (a-d). If the  $E_{doa}$  parameter correctly represents the effects of joint orientation on erosion, a higher  $E_{doa}$  class should produce more damage than a lower class. In addition, the relation between damage classes and the mean stream power class should be linearly increasing.



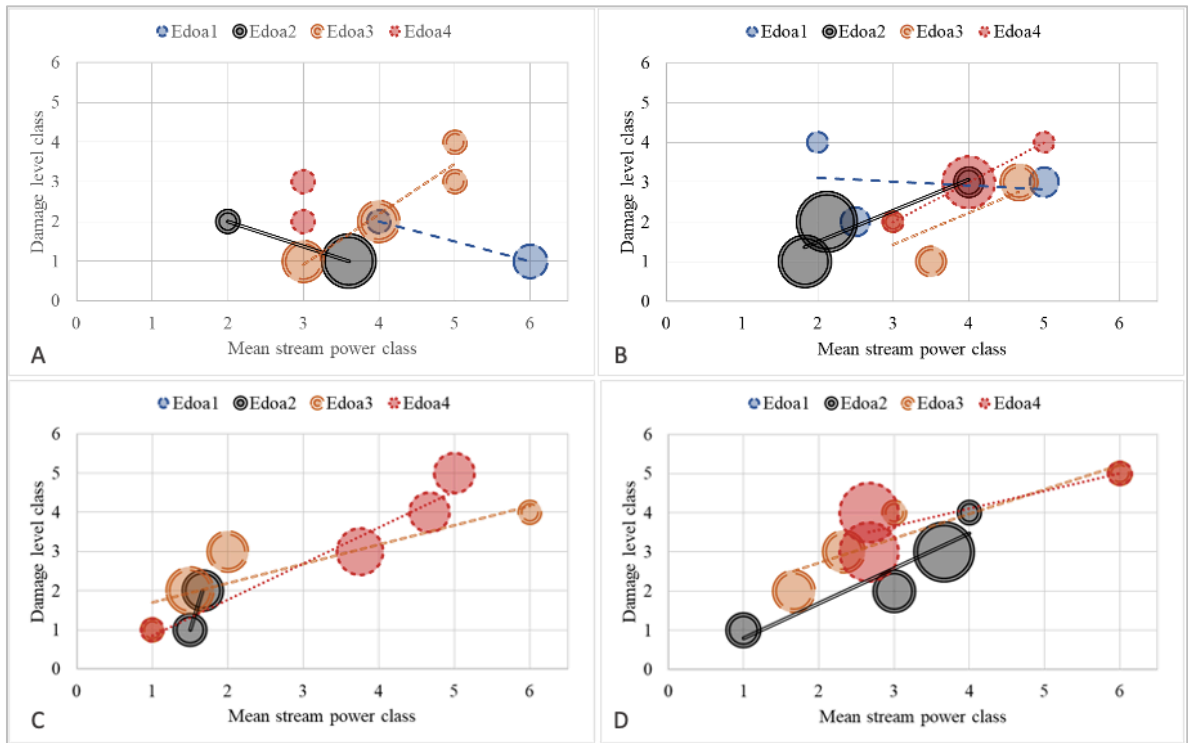


Figure 3.13 : Results of the effects of the  $E_{doa}$  parameter on the rock's vulnerability to erosion. Lines represent the linear approximation of the data distribution **A**  $GSI_{chart}$  class 1 **B**  $GSI_{chart}$  class 2 **C**  $GSI_{chart}$  class 3 **D**  $GSI_{chart}$  class 4

For high rock quality, corresponding to a  $GSI_{chart}$  of class 1, the  $E_{doa}$  parameter does not show the expected logical relation. For a  $GSI_{chart}$  of class 1, in Figure 3.13 (a), the relation between the damage level and the mean stream power class for  $E_{doa}$  of class 1 and class 2 is reversed, when it should be increasing. Aside from this aspect, the relationships between the  $E_{doa}$  classes are not respected, with a larger class showing less damage than a smaller class for low to medium stream power. For high stream power, the relation between higher  $E_{doa}$  classes is more respected, with higher classes showing more damage than lower classes. For a  $GSI_{chart}$  of class 2, in Figure 3.13 (b), the order of damage level versus  $E_{doa}$  classes is respected from a mean stream power of class 4. Lower stream power classes may not generate enough energy for the joint orientation to have a notable impact on rock erosion. The same pattern is observed for  $GSI_{chart}$  of class 3, where good relation between  $E_{doa}$  happens when stream power mean class reaches 3.  $GSI_{chart}$  class 4 in Figure 3.13 (d) shows that  $E_{doa}$  classes have a logical relationship, both in terms of the order of the  $E_{doa}$  classes and of the relationship between damage and stream power.

### 3.4.7 EFFECTS OF THE $C_{up}$ PARAMETER

The effects of the  $C_{up}$  parameter are shown in Figure 3.14. The Y-axis represents the damage level and the X-axis represents the mean stream power class. If the  $C_{up}$  parameter correctly represents the effects of joint orientation on erosion, higher classes should show more damage than lower  $C_{up}$  classes. In addition, the relation between damage classes and mean stream power should be linearly increasing.

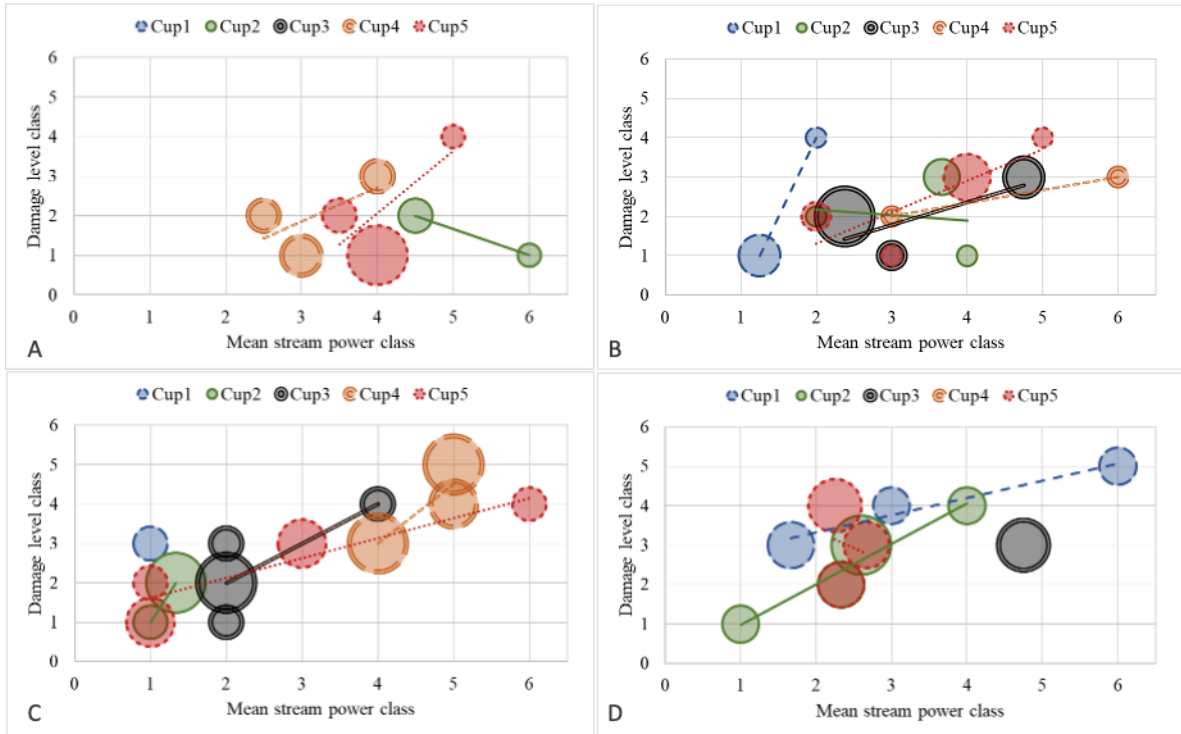


Figure 3.14 : Results of the effects of the  $C_{up}$  parameter on the rock's vulnerability to erosion. Lines represent the linear approximation of the data distribution **A**  $GSI_{chart}$  class 1 **B**  $GSI_{chart}$  class 2 **C**  $GSI_{chart}$  class 3 **D**  $GSI_{chart}$  class 4

For the  $GSI_{chart}$  classes 1 and 2, i.e., for good-quality rock mass, the results show an acceptable classification of the  $C_{up}$  parameter. It is generally observed that higher  $C_{up}$  classes generate higher damage level, for high stream power classes. However, for lower-quality rock mass, for  $GSI$  classes 3 and 4, correlation between damage and  $C_{up}$  classes is no longer observed. It is also noted that relation between stream power and damage is generally increasing.

### 3.4.8 COMPARISON OF RESULTS

In general, the parameter classification results improve as the mean stream power classes increase. For the  $E_{\text{doa}}$  parameter, its classification also improves when the  $GSI_{\text{chart}}$  increases. An increase in the  $GSI_{\text{chart}}$  classes, according to the classification proposed in this article, occurs when the quality of the rock mass decreases. Thus, joint orientation would have a greater impact on erodibility for a lower quality rock subjected to high hydraulic pressures. However, this is counterintuitive, since in a very low-quality rock mass, i.e., for a  $GSI_{\text{chart}}$  below 40, corresponding to a  $GSI_{\text{chart}}$  of class 4, the rock is crushed and joint orientation is not distinguished easily. Joint orientation is best distinguished when rock mass quality is high. Results show correlation between joint orientation and damage level when  $GSI_{\text{chart}}$  is of class 1 and class 2, for high stream power, only for the  $C_{\text{up}}$  parameter. No joint orientation parameter presents an accurate relationship between damage level and joint orientation effect for a good quality rock mass. For all  $GSI_{\text{chart}}$  classes, solely  $J_s$  classes 4 and 5 show correlation with damage classes. These classes describe joint orientation that would either have no effect or have a positive effect on rock resistance to erosion.

### 3.5 DISCUSSION

There are several methods used to classify the effect of joint orientation of a rock mass on its erodibility. These methods offer different classifications, hence the need to evaluate these methods and compare their accuracy.

The errors in the classification of the  $J_s$  parameter developed by Kirsten (1982) can be explained by four factors, namely the assumption that joints are orthogonal to each other, the fact that  $J_s$  parameter has been developed to characterize the excavatability of the rock rather than erodibility, the fact that this parameter was developed only theoretically, and the poor amount of data for all  $J_s$  classes except for  $J_s$  of class 4 (Figure 3.8). Boumaiza et al's study (2019a) shows that the approximation of orthogonal joints leads to significant errors when calculating Kirsten's index when the joint sets considered are in fact non-orthogonal.  $J_s$  is obtained with the direction of the closer spaced joint set and the apparent dip of the closer spaced joint set with relation to the direction of the flow. However, the apparent dip is calculated considering the two joint sets as being orthogonal. If they are in fact non-orthogonal, this apparent dip will change along with the  $J_s$  value. In addition, Kirsten's index, considering the  $J_s$  parameter, was developed to characterize the excavatability of a rock mass. The force

considered when excavating a rock mass is that of a bulldozer, whose force applied by the excavator acts only at a specific point and is directed at a specific angle. The study of erodibility by hydraulic power involves a hydraulic force acting on all the faces of the blocks of the rock mass, particularly with an uplift force that acts under the block. Since this parameter was developed thoroughly theoretically, some inconsistencies may have appeared, like the fact that joint orientation can have a positive effect on rock resistance to erosion. Since this methodology was applied on a limited data set, data was unequally distributed through  $J_s$  classes, which resulted in too few data for four of  $J_s$  classes out of five.

The  $E_{doa}$  parameter was developed by Pells (2016). It is based on the  $J_s$  parameter, the results of tests on a scale model, real erosion situations that have taken place in dams and on the kinematics of block uplift. Pells' (2016) physical model has flaws regarding the analysis of joint orientation effects. Indeed, only one block is modelled, not allowing to measure the effect that joint orientation could have on a series of blocks and joints, where water could flow, and therefore create variable uplift pressure. Also, only a few orientations were tested, that is  $0^\circ$ ,  $22^\circ$  and  $45^\circ$  horizontally and  $0^\circ$ ,  $11^\circ$  and  $22^\circ$  vertically. Horizontal and vertical orientations correspond to direction and to dip direction, respectively. The  $E_{doa}$  parameter also considers orthogonal joints, which presents the same problem as for the  $J_s$  parameter. Pells (2016) built his database with erosion and dam data coming from different sources. Since Pells (2016) did not collect all the data himself, some errors or different interpretations coming from different sources could have been included, especially regarding more qualitative parameters, such as  $GSI_{chart}$ . An analysis of the results demonstrates that the  $E_{doa}$  parameter offers the best classification of the effect of the joint orientation of the rock mass on erosion. However, the database used to build the  $E_{doa}$  parameter was used for this study, which could introduce bias into the results of  $E_{doa}$ .

The  $C_{up}$  parameter of Reinius (1986) is exclusively based on the pressure results obtained from a scale model. The advantage of the  $C_{up}$  parameter is that it is the only parameter based exclusively on laboratory tests. It is therefore possible to precisely understand its origin. The physical model used consisted of an alignment of blocks, one of which was instrumented with piezometers. The uplift pressure parameter is not calculated directly from the pressures measured under the block, but is calculated as the mean value of the pressure coefficients of piezometers 5 and 8. Moreover, pressure variation was not measured as a variable dependent of time, more as a fix value for each model setup. The  $C_{up}$  parameter yields opposite results than the  $E_{doa}$  parameter, with a better

correlation for high GSI classes. In Reinius'(1986) experiments to development the  $C_{up}$  parameter, the rock mass was modelled with concrete blocks. These blocks thus represent a rock mass of high quality, which corresponds with GSI classes 1 and 2. Therefore, the  $C_{up}$  parameter may only be applicable to good GSI classes. Unlike  $E_{doa}$  and  $J_s$ ,  $C_{up}$  does not consider joint spacing. The joint spacing considered for  $C_{up}$  parameter is the one used in Reinius'(1986) experiments, which is has a fix value for all tests. According to  $E_{doa}$  and  $J_s$ , joint spacing does not radically change the impact of joint orientation, but it does change the value slightly. Additionally, joint orientation testing by Reinius (1986) was limited. The block was always placed vertically in the model, with varying dips from the vertical of  $0^\circ$ ,  $9^\circ$ ,  $17.5^\circ$ , and  $33.5^\circ$  in the opposite direction of the flow and varying dips from the vertical of  $2.9^\circ$  and  $18^\circ$  in the same direction of the flow. These tests allowed Reinius (1986) to extrapolate his results to all cases. However, the  $C_{up}$  parameter would need to be further developed in order to be applied to all cases of joint orientation.

This study reveals some probable inconsistencies with the  $GSI_{chart}$  determination in relation to joint orientation. Considering the joint orientation parameters analyzed, results show that joint orientation has much less of an effect on good-quality rock mass than on lower-quality rock mass. However, joint orientation is much more distinguishable on a good quality rock mass.  $GSI_{chart}$  is determined using block structure and joint condition. When considering  $GSI_{chart}$ , the same  $GSI_{chart}$  value is determined for a "very blocky" rock mass with a good joint condition (rough and not altered) as for a "massive" rock mass with a medium joint condition (smooth and altered), which could explain the issue regarding the effect of joint orientation. To effectively compare the effect of joint orientation, rock mass should be classified according to the same class of structure and the same class of joint condition. Moreover, in our analysis with  $GSI_{chart}$ , joint orientation and stream power does not consider all parameters as having an effect on rock mass erosion, such as NPES and joint opening. Boumaiza et al(2021) revealed a classification of the most relevant parameters to study rock mass hydraulic erodibility. From the most to the least important, his study obtained the following classification: joint condition ( $K_d$ ), nature of the potentially erodible surface (NPES), block volume ( $V_b$ ), joint opening ( $J_o$ ), joint orientation ( $E_{doa}$ ) and rock mass deformation module ( $E_{rm}$ ). Our study does not consider NPES, which includes the block's protrusion, nor does it consider joint opening or rock deformation module. It would be interesting to include NPES and  $J_o$  in an index of rock quality, as they have more importance for rock mass hydraulic erosion than joint orientation. Furthermore, joint condition and block volume have the same weight when determining

$GSI_{chart}$ , when, according to Boumaiza et al,(2021) joint condition is the most important parameter for rock mass hydraulic erodibility, when block volume is in third position. Therefore, when studying rock mass hydraulic erodibility, a rock quality index that takes this classification into account should be considered.

### 3.6 CONCLUSION

Hydroelectric facilities require the excavation of an emergency spillway in the bedrock, which exposes the rock mass to hydraulic erosion. Joint orientation is known as a relevant geomechanical parameter to evaluate rock mass erodibility. The method used in this article to evaluate the parameters describing the effects of joint orientation on rock mass erodibility is based on the one used by Boumaiza et al.(2019b) The results show that the  $E_{doa}$  parameter is the joint orientation parameter with a classification that is closest to expectations, based on the  $GSI_{chart}$  index of rock quality, mean stream power and damage level. The  $E_{doa}$  parameter shows good correlation when the rock is of medium to low quality. Good results for the  $E_{doa}$  parameter may be influenced by the fact that the database used to determine this parameter is the same used to analyze the accuracy of this parameter. This leaves room for potential bias. Regarding the  $J_s$  parameter, the classification obtained is not representative of the damage level. However, little data is available for  $J_s$  classes 1, 2, 3 and 5, since the majority of data falls under  $J_s$  class 4. Regarding the  $C_{up}$  parameter, for high stream power, results generally show correct correlation for  $GSI_{chart}$  classes 1 and 2. Unlike the  $E_{doa}$  and  $J_s$  parameters,  $C_{up}$  does not consider spacing ratio of joint sets, which could help increase the accuracy of the results for this parameter.

Good-quality rock mass can have a variety of structures, from massive to very blocky, with a joint condition ranging from rough and non-altered to smooth and altered. In this study, some parameters that have a significant impact on rock mass erodibility were disregarded, such as NPES,  $J_o$  and  $E_m$ . A rock quality index that includes these parameters and considers their relative importance would be useful to develop in order to correctly analyze joint orientation parameters and rock mass erodibility.

## **CHAPITRE 4: ÉTUDE DE L'ÉROSION DU MASSIF ROCHEUX DANS LES ÉVACUATEURS DE CRUES NON RECOUVERTS À L'AIDE D'UN MODÈLE RÉDUIT EN LABORATOIRE**

Ce chapitre présente un article dont le premier auteur est l'auteur de ce mémoire. Le chapitre présente brièvement le modèle réduit lors des essais et montre les premiers résultats obtenus.

Cet article a été publié dans le magazine de la Société Canadienne de Géotechnique.

# STUDYING ROCK MASS HYDRAULIC EROSION IN UNLINED SPILLWAYS USING A SCALED PHYSICAL MODEL

Marie-Hélène Wisse<sup>1</sup>, Aboubacar Sidiki Koulibaly<sup>1</sup> and Ali Saeidi<sup>1</sup>

<sup>1</sup>Applied Sciences, Université du Québec à Chicoutimi, 555 Boul. de l'Université, Chicoutimi, QC, G7H 2B1

## AUTHORS CONTRIBUTION

**Marie-Hélène Wisse:** Conceptualization, Validation, Methodology, Visualization, Formal analysis, Investigation, Methodology, Writing – Original Draft, Writing – Review and Editing

**Aboubacar Sidiki Koulibaly:** Design of the scaled physical model, Writing – Review and Editing

**Ali Saeidi:** Conceptualization, Resources, Writing – Review and Editing, Supervision, Project administration, Funding acquisition, Validation



## ABSTRACT

Physical flow models are used to study parameters affecting the erodibility of rock in dam unlined spillways. Among the existing physical models, the parameters of joint orientation and of protrusion are the most studied. However, other rock mass parameters have an important contribution in the erosion mechanism but they were given less attention in existing research or, when studied, mixed results were obtained. In addition, the majority of models simulate rock mass considering a single block, which cannot simulate possible interactions between blocks. To address this problem, a scale model that simulates an existing spillway was built in a UQAC laboratory. This model is a 1:40 scale of the existing spillway. The model is equipped with a pump allowing a constant flow at velocities between 3 m/s and 5 m/s which allows reaching flow rates between 290 L/s and 460 L/s. The water flows along a 9° inclined channel design to insert concrete blocks that are placed in a manner that represent the fractured rock mass. The blocks are instrumented with pressure sensors to measure the pressure applied to each of their faces. The model is also equipped with cameras to observe the behaviour of the blocks subjected to the water pressure. The physical model makes it possible to vary several rock mass and hydraulic parameters, such as joint orientation, joint opening, protrusion, block volume and shape, joint roughness, flow rate and velocity, as well as channel roughness to evaluate their impact in the rock erosion process.

#### 4.1 UNLINED SPILLWAY EROSION

Dams are structures used to retain water, either for irrigation or for energy production in the case of hydropower plants. Dams must have an emergency spillway to release excess water in the reservoir during periods of floods. When the spillway floodgates open, water flows at an impressive flow rate and can erode the excavated bedrock spillway channel located downstream. In some cases, erosion to the channel can extend upstream reaching the concrete structure and damage its foundation, leading to expensive repairs. Figure 4.1 shows the spillway floodgate structure and excavated bedrock channel (outlined in red) of Hydro-Québec's Romaine-4 dam.



Figure 4.1 : Photograph of Romaine-4 spillway outlined in red (© Hydro-Québec)

Two main factors interact to control bedrock erosion: hydraulic erosive forces and bedrock resistance to erosion (Jalili Kashtiban et al., 2021). Hydraulic erosive forces are characterized as the unit rate of energy dissipation as well as the water power. The resistance of the rock mass can be defined by different indexes. Commonly used resistance indexes are the Kirsten Index (Kirsten, 1982) the erodibility Geological Strength Index (eGSI) (Pells, 2016), and the Rock Mass Erodibility Index (RMEI) (Pells, 2016). Several researchers have studied the relation between water power and rock resistance. These studies have led to the development of methods to evaluate a spillway channel's erodibility potential. However, in some cases, the results obtained with these methods over or underestimate the erosion potential. Each of these methods uses different limits or domains to assess the erosion potential. Other methods, using a physics-based approach, also exist but the parameters required are not limited to water power and rock resistance, because they address rock, air and water

physical interactions. Their application is complex and not directly applicable to parallel flow channel spillways. To increase our knowledge of erosion mechanisms in unlined spillway channels, and to contribute to the development of assessment methods to prevent erosion, more knowledge is needed in this field of rock mechanics.

Reduced-scaled physical models are typically used to obtain preliminary data to study phenomena that are difficult to study on a real scale. The data obtained from a physical model can then be used to calibrate a numerical model of a full-sized model. Few open channel spillway physical models have been constructed, and they have been mainly used to study the hydraulic characteristics of the flow rather than the rock mass resistance to erosion. Previous physical models used to study rock resistance to erosion either did not simulate a proper rock mass (i.e., made up of many blocks) or did not study the main rock mass parameters affecting its resistance to erosion, mainly joint opening, joint orientation, block volume, block shape and protrusion.

This article presents the design and preliminary test results of a scaled physical model of an open channel spillway that was built in a laboratory of Université du Québec à Chicoutimi (UQAC).

#### **4.2 DESIGN OF A SCALED PHYSICAL MODEL**

The Scaled Physical Model was designed at a scale of 1:40 of the Romain IV dam's spillway. Figure 4.2 shows a sketch and Figure 4.3 shows a photograph of the scaled physical model.

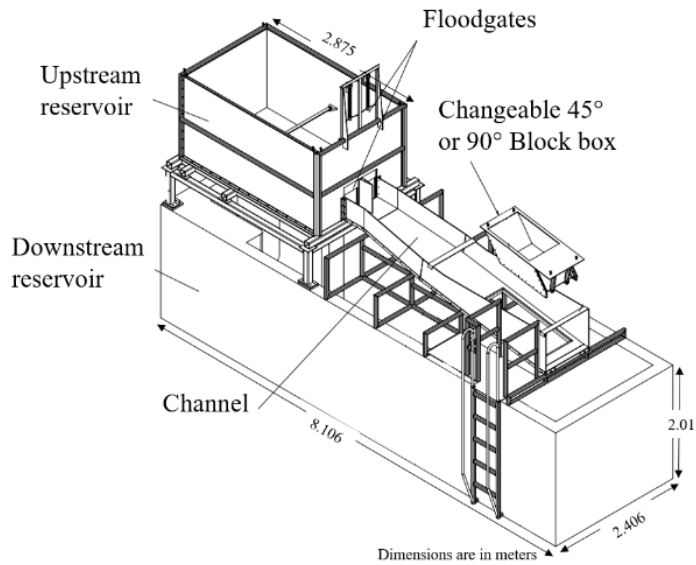


Figure 4.2 : Sketch of the 1:40 scaled physical model, modified from (Koulibaly, 2021)

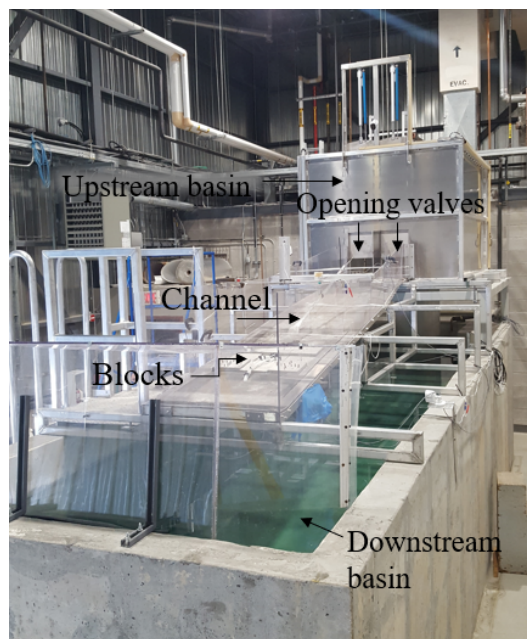


Figure 4.3 : Photograph of the scaled physical model (© Marie-Hélène Wisse)

The model was equipped with a pump, which pumped water vertically into the upstream reservoir and allowed a natural overflow effect from this reservoir. Two adjustable floodgates, as in the real spillway, allowed water to flow, at a specific flow rate down the channel. The channel had a slope of  $9^\circ$ . At the downstream end of the channel was a box containing solid concrete blocks simulating the rock mass. The arrangement of these blocks can be varied, either perpendicular to the channel or with an angle of  $45^\circ$  to the channel, to study the geomechanical parameters related to joint orientation. To date, nine blocks of two different dimensions (15 x

15 x 30 cm<sup>3</sup>) and (20 x 20 x 30 cm<sup>3</sup>) have been tested. The shape and the volume of the blocks are changeable by molding new blocks in various molds. Openings and protrusions between and under the blocks were managed with bolts drilled into the blocks, maintaining a constant opening and protrusion during each test. The centre block was instrumented with twelve pressure sensors, two on each face. A high-speed camera and a displacement sensor allowed measuring the displacement of the blocks during the tests.

### 4.3 PRELIMINARY TESTS RESULTS

To date, tests with varying joint openings and protrusions have been carried out. The first test was performed with a joint opening of 2.5 cm around the central block and on the sides of upstream and downstream blocks. The central block had a dimension of 15 x 15 x 30 cm<sup>3</sup>. As a comparison, the second test was performed with a joint opening of 0.5 mm, using only bigger blocks of 20 x 20 x 30 cm<sup>3</sup>. For all tests the blocks were oriented perpendicular to the channel. For all tests where blocks had no protrusion, the joint opening under the block was 0.7 cm, for the top of the blocks to be flush with the channel surface. Finally, to measure the effect of protrusion, for the third test the middle row of blocks was lifted an additional 2.8 cm from the channel surface, while otherwise maintaining the configuration of the second test.

For the results, we expected that the static pressure, equal to the height of the water table, would be the minimum value. The flow velocity was maintained at 3.4 m/s for all tests. For the first and second tests, the water height varied between 2 and 3 cm above the central instrumented block. For the third test, the protrusion of the middle row caused a hydraulic jump above the blocks. A pressure higher than the static pressure, implies a dynamic pressure, which depends on the water velocity. Figure 4.4 shows the total pressure measured on sensors C and D, which are located on the upstream and downstream faces of the block, respectively. Sensors C1 and D1 were 5 cm from the top of the block and sensors C2 and D2 were 5 cm from the bottom of the block.

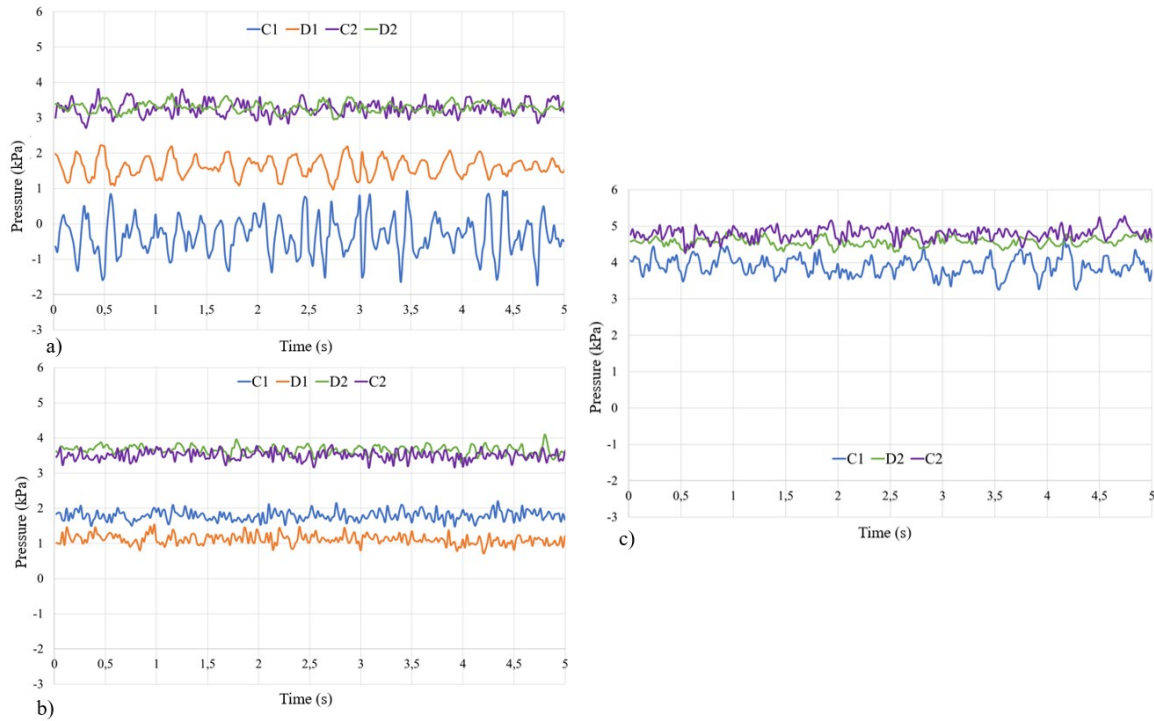


Figure 4.4 : Pressure measured on sensors C1, C2, D1 and D2. **a)** Test one. Joint opening of 2.5 cm, no protrusion; **b)** Test two. Joint opening of 0.5 mm, no protrusion; **c)** Test three. Joint opening of 0.5 mm, protrusion of the middle row of 2.8 cm upwards

For tests one and two, with joint openings of 2.5 cm and 0.5 mm with no protrusion (Figure 4.4ab), pressures measured lower on the faces of the block (C2 and D2) were very similar. However, for pressure sensors located closer to the top of the block (C1 and D1), pressures measured varied much more for a 2.5 cm joint opening than for a 0.5 mm joint opening. Thus, joint opening may have less effect on the pressure deeper in the rock mass than closer to the surface.

Test three, with protrusion of the middle row of blocks (Figure 4.4c) , showed higher pressures for sensors C1, C2 and D2. For sensor C1, the pressure measured was twice that for the test without protrusion (Figure 4.4b). Due to the hydraulic jump caused by the protrusion, no pressure was measured at sensor D1. It is interpreted that the greater pressure measured for the test with protrusion resulted from the higher dynamic pressures caused by the increase of the flow velocity in the joints. The range of pressure variation is very similar to tests with or without protrusion with the same lateral joint opening (Test two vs Test three).

#### **4.4 FURTHER ONGOING TESTS**

Further tests are being conducted where the first row of blocks has protrusion from the channel surface. For these tests, all nine blocks were lifted from the bottom of the box. From very preliminary results of these further tests obtained so far, protrusion as well as joint opening show to be important parameters for hydraulic rock mass erosion. Further tests will study these two parameters jointly to understand their mutual effects.

#### **4.5 DISCUSSION**

The scaled physical model allows a variety of hydraulic conditions and geomechanical parameters to be tested. A hydraulic jump can be created by increasing the blocks' protrusion; channel roughness can be changed by adding obstacles on the channel surface upstream of the blocks; and flow velocity and flow rate can be adjusted with a pump and by adjusting the opening valves of the reservoir. Turbulence and air entrainment vary with all the previous hydraulic parameters.

The scaled physical model also allows testing of hydraulic limit conditions used for numerical modelling. The five important geomechanical parameters identified by Boumaiza et al. (2019b) for rock mass hydraulic erosion can be tested in this model, namely: joint shear strength, nature of the potentially erodible surface (NPES), block volume, joint opening, block shape and joint orientation. NPES is represented by the protrusion. These geomechanical parameters can be combined to evaluate their mutual effect. The results obtained with the scaled physical model can be used as a calibration for a numerical model.

#### **4.6 CONCLUSION**

This article describes a scaled physical model, built on a scale of an actual hydroelectric dam spillway that reproduced its geometry and its hydraulic characteristics. Rock mass is simulated by solid concrete blocks, instrumented with pressure sensors. Using various configurations of these blocks, the effect of different rock mass parameters like joint opening, joint orientation, protrusion, block volume and block shape on the erosion can be studied. Preliminary tests show that the model effectively measures pressure variation on the instrumented block's faces. Moreover, ongoing tests show that some displacement was observed when the first row of blocks protruded. The main effect of joint opening was observed on the pressure sensors located at the top of the block, which showed a higher range of pressure variation. More tests are to be done, where joint

openings will be changed with varying protrusion, joint orientation and block shape and volume. The scaled physical model will be used to calibrate a numerical model simulating conditions hardly manageable in a physical model. Ultimately, it is hoped that this research will develop an erosion evaluation method that can be adapted to erosion of crystalline rock mass in parallel flow spillways.



## **CHAPITRE 5: EFFETS DE L'OUVERTURE DES JOINTS ET DE LA SAILLIE DES BLOCS SUR LES PARAMÈTRES HYDRAULIQUES DANS LE MASSIF ROCHEUX D'UN ÉVACUATEURS DE CRUES À L'AIDE D'UN MODÈLE PHYSIQUE EN LABORATOIRE**

Ce chapitre présente un article dont la première auteure est l'auteure de ce mémoire. Le chapitre présente les résultats obtenus suite aux essais effectués par l'auteur de ce mémoire sur le modèle réduit d'évacuateur de crues.

Cet article est au stade de la révision avant soumission.

# Effects of Joint Opening and Block Protrusion on the Hydraulic Parameters and Uplift Pressure inside rock joints using a reduced-scale model of unlined spillway

Marie-Hélène Wisse<sup>1\*</sup>, Ali Saeidi<sup>1</sup>, Marco Quirion<sup>2</sup>

<sup>1</sup>Applied Sciences, Université du Québec à Chicoutimi, 555 Boul. de l'Université, Chicoutimi, QC, G7H 2B1

<sup>2</sup>Rock Mechanics, Hydro-Québec, 75 Boul. René-Lévesque W, Montréal, QC, H2Z 1A4

\*Corresponding author (e-mail: [marie-helene.wisse1@uqac.ca](mailto:marie-helene.wisse1@uqac.ca))

## ACKNOWLEDGMENTS

The authors would like to thank the research group R<sup>2</sup>Eau for their helpful comments and suggestions.

## AUTHORS CONTRIBUTION

**Marie-Hélène Wisse:** Conceptualization, Validation, Methodology, Visualization, Formal analysis, Investigation, Methodology, Writing – Original Draft, Writing – Review and Editing

**Ali Saeidi:** Conceptualization, Resources, Writing – Review and Editing, Supervision, Project administration, Funding acquisition, Validation

**Marco Quirion:** Writing – Review and Editing, Supervision, Funding acquisition

## ABSTRACT

Dam spillways permit the release of excess water from reservoirs; however, these structures can experience erosion during these releases, causing damage to dam infrastructure. Here we build a scaled physical model of an unlined parallel-flow spillway to study rock mass erodibility in this context. Our setup allows studying multiple parameters influencing rock mass erosion, such as joint orientation, joint opening, block protrusion, joint roughness, and block shape and size. The model also permits varying hydraulic parameters,

including channel roughness, flow velocity, and flow turbulence. Using this model, we evaluate how joint opening and surface protrusion (height and configuration) affect hydraulic parameters both on the block surface and inside rock joints responsible for rock block uplift. Total pressure, including static and dynamic pressure, in the joints varied less than on the block top, with less variability as joint opening size decreased. Dynamic pressure was responsible for the variations in total pressure. The force acting on the block top, i.e., on the channel surface, was the main force influencing block uplift, and its effectiveness was affected by protrusion configuration, protrusion height, and joint opening. The uplift force under the block remained constant regardless of protrusion configuration and joint opening. However, a larger space between the base of the block and the flowing water surface may induce less dynamic pressure under the block. Therefore, block geometry may alter the relative effects of protrusion and joint opening on uplift pressure. Future studies should evaluate how block shape affects the role of both parameters on rock mass erodibility. Finally, the friction force acting on the lateral block surfaces of the block depends highly on the block configuration.

#### KEYWORDS

Erosion, Rock mass, Spillway, Hydraulic, Joint Opening, Protrusion

## 5.1 INTRODUCTION

Dams are equipped with spillways that permit lowering reservoir levels during floods. Nonetheless, major erosion events can occur in dam spillways, e.g., the Oroville dam in the United States and the Paradise dam in Australia. This erosion can affect the stability and security of the spillway structure. With climate change, larger flood events are expected, and these erosional situations must be prevented to avoid similar or worse damage to dam infrastructure.

The most common types of water flow at the exit of spillways are parallel and plunging jet flows. In unlined spillways, the rock mass is exposed directly to the erosive power of the flow. Erosion by rock block plucking can occur in both types of flows, but the hydraulic forces act differently on block uplift, mainly because of the flow direction above the bedrock blocks. Therefore, methods designed to evaluate rock mass erosion in plunge pools are not applicable to parallel-flow channels. Some parallel-flow spillways are lined with concrete to protect the bedrock from damage; however, this lining is expensive and will often only be used on specific sections of the spillway where poor-quality rock is visible.

The erosion of some parallel-flow spillways has led to a number of erosion characterization methods. The most common is the Kirsten index (Kirsten, 1982). Other more recent characterization methods include the erodibility geological strength index (eGSI) (Pells, 2016), the rock mass erodibility index (RMEI) (Pells, 2016), and the comprehensive scour model (CSM) (Bollaert, 2004). The Kirsten index was used by Van Schalkwyk et al. (1994), Annandale (1995), and Kirsten et al. (2000); these studies led to the identification of scour thresholds. In some cases, the observed degree of erosion was contrary to that expected when these scour thresholds were applied (Boumaiza et al., 2021). Pells (2016) developed the eGSI and the RMEI approaches by analysing the damage level of more than a hundred sections of 24 dams in Australia and South Africa having experienced erosion events. This overview was coupled with a physical flow model in which an instrumented block was subjected to flow. Nonetheless, Boumaiza et al. (2021) noted that the damage-level projections of eGSI and RMEI classifications can be inconsistent. All these above-listed methods use selected parameters to evaluate rock mass erodibility. Of these parameters, Boumaiza et al. (2021) identified joint opening and block protrusion as two key rock mass characteristics affecting rock mass erosion.

Reinius (1986) used a physical model to study the effect of block protrusion on the pressure applied to a block. In this model, the blocks were aligned in a horizontal channel. Similarly, George et al. (2015) placed a single tetrahedral block in an inclined open channel, and Pells (2016) placed a cubic block in an inclined open channel for their respective physical models. The George et al. (2015) and Pells (2016) models allowed measuring the effect of protrusion and orientation of a single block; however, their setups could not permit assessing the effect of protrusion for multiple blocks. Moreover, these two studies did not let water flow through the joints around and under the block, an important effect when evaluating block uplift.

In the Reinius (1986) open-channel model, the pressure coefficient of each face of the instrumented block was calculated as the ratio between the dynamic pressure recorded on the block's face and the dynamic pressure of the flow in the channel. The uplift of a rock block becomes possible when the uplift pressure coefficient ( $C_{up}$ ) is positive.  $C_{up}$  is calculated as the difference between the pressure coefficient in a simulated joint under the block ( $C_{joint}$ ) and the pressure coefficient at the block surface ( $C_{surf}$ ).  $C_{joint}$  is obtained using the mean dynamic pressure of two pressure sensors located on opposite lateral faces of the block rather than under the block. The means of obtaining the pressure coefficient at the block surface ( $C_{surf}$ ) remains questionable. According to the definition of a pressure coefficient given by Reinius (1986),  $C_{surf}$  should be close to 1 if the flow is minimally or not disturbed above the blocks, i.e., the dynamic pressure at the top of the block should be approximately equal to the dynamic pressure of the flow in the channel. There is also a problem with the Bollaert (2012) QSI approach when using  $C_{up}$  as the uplift coefficient.  $C_{up}$  is the difference between the dynamic pressure on the block top and the dynamic pressure under the block; however, this approach does not consider the difference in static pressure. A rock block is uplifted when the total pressure under the block exceeds the total pressure at the block top, the friction force, and the weight of the block. Because total pressure is the sum of the dynamic pressure and the static pressure, static pressure must also be considered when calculating the block uplift.

The effects of rock mass joint opening in an open channel were only partly studied by Reinius (1986). Interblock joint openings in the Reinius model varied in width (1, 0.75, and 0.3 mm). However, these joints were maintained sealed such that only water flow along the block top could enter the joint, thereby preventing water circulation around the instrumented block. Moreover, no mention of the results of the joint opening

variation effect on pressure is made in the study. Bollaert (2012) developed a semi-analytical method to predict erosion using the Reinius (1986)  $C_{surf}$  and  $C_{up}$  coefficients. His method, the comprehensive scour model, has three modules to account for the different erosion types in a plunging jet spillway. It was developed partly using a physical model with a falling jet in an open instrumented joint. One of these modules, the quasi-steady impulsion (QSI), is applicable to flow parallel to the surface of the rock mass; thus it is used in the context of parallel-flow spillways. To assess the possibility of block uplift, the QSI module uses the difference between the downward and uplifting forces using the  $C_{surf}$  and  $C_{up}$  coefficients on a rock block.

Pressure fluctuations must also be considered when studying block uplift. In the CSM (comprehensive scour model), Bollaert (2004) pointed out that pressure fluctuations under the block could cause the block to vibrate. A sufficient amplitude of the pressure fluctuations could eventually force the block to be ejected and, therefore, cause erosion. Pan et al. (2014) numerically simulated the separation of a block using the pressure fluctuation theory. The simulation considered the amplitude of the surface fluctuations equal to the amplitude of the water fluctuations in the joint. Uplift occurred only when the phasing between the top and bottom fluctuations was not synchronous.

Mean dynamic pressure (and its variability) over and under the block are therefore important for evaluating block uplift vulnerability. Nonetheless, the effect of joint opening and block protrusion on the hydraulic parameters (including their variability) in the joint and on the rock mass surfaces remains uncertain. Here we aim to determine these parameters for vertical joint sets. For this purpose, we use an open-channel flow physical model with a simulated rock mass that was built in the hydrogeomechanics laboratory of the Université du Québec à Chicoutimi (UQAC). We apply an innovative method and instrumentation setup to measure hydraulic parameters in the joints and at the surface of a simulated block in a flow channel. Our goal is to establish the relationship between the block surface and joint hydraulic parameters according to various joint opening widths and protrusion configurations.

## 5.2 METHODOLOGY

### 5.2.1 PRESENTATION OF THE PHYSICAL MODEL

The physical model of Hydro-Québec's Romaine-4 dam spillway was designed according to Froude's similitude criterion at a 1:40 scale (Table 5.1; Figure 5.1).

Table 5.1 : Scale hydraulic design of the physical model based on the prototype (Koulibaly, 2021)

Prototype dimensions (m)		Ratio factor	Model dimensions (m)	
L	166.4	$Fr = \frac{1}{40}$	L	4.2
W <sub>up</sub>	27.2		W <sub>1</sub>	0.68
W <sub>do</sub>	35		W <sub>2</sub>	0.87
H <sub>Pr</sub>	22.3		H <sub>Mo</sub>	0.56
BH <sub>up</sub>	30		BH <sub>up</sub>	0.75
BH <sub>do</sub>	30		BH <sub>do</sub>	0.75
Q <sub>Pr</sub>	2950 m <sup>3</sup> /s	$Fr^{5/2} = 1/10119.19$	Q <sub>Mo</sub>	0.292 m <sup>3</sup> /s
V <sub>Pr</sub>	20 m/s	$Fr^{1/2} = 1/6.325$	V <sub>Mo</sub>	3.162 m/s
θ <sub>Pr</sub>	9°	-	θ <sub>Mo</sub>	9°

Note: Pr = prototype; Mo = model; L = length of the channel; W<sub>up</sub> = upstream channel width; W<sub>do</sub> = downstream channel width; H = spillway height; BH<sub>up</sub> = channel bank's height upstream; BH<sub>do</sub> = channel bank's height downstream; Q = flow rate; V = flow velocity; and θ = channel inclination.

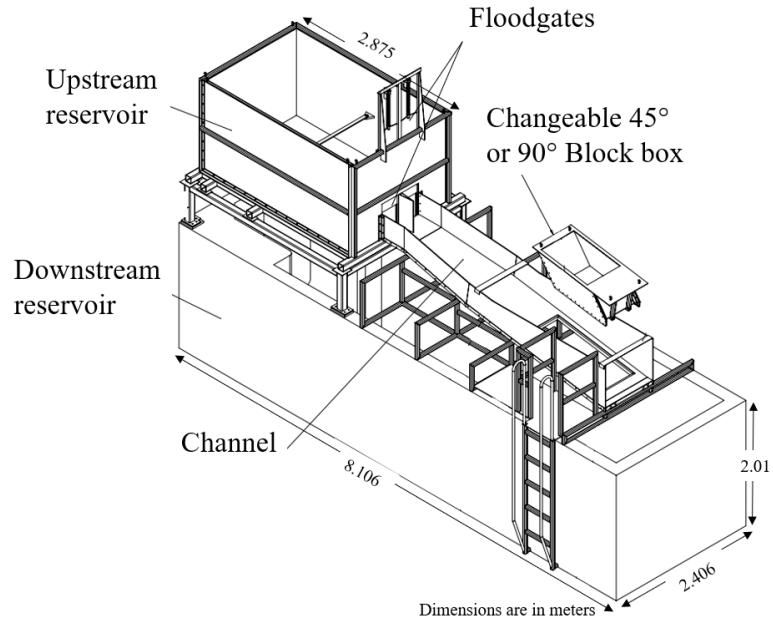


Figure 5.1 : Layout and dimensions of the physical model. Modified from Koulibaly et al. (2022)

The scaled physical model permits studying some of the geomechanical and geometric parameters relevant to rock mass erosion in an unlined spillway. Hydraulic parameters such as velocity and pressure can be measured at each point along the hydraulic channel. To simulate the rock mass, we used nine concrete blocks, including one instrumented block. They were placed at the end of the channel tailrace and inserted inside a support box within the channel. Using this simulated rock mass, we could test the rock mass parameters affecting rock mass erodibility, such as joint orientation, joint opening, joint roughness, block protrusion, and block shape and volume. The instrumented block was placed in the centre of the eight non-instrumented blocks to simulate a block surrounded by flow.

## 5.2.2 GOVERNING EQUATIONS

The uplift of a rock block occurs when the uplift force is greater than the total downward force (Equation 5.1). In the case of the physical model used for this study, the uplift force ( $F_{up}$ ) is the force (N) obtained through the product of the total pressure measured on the bottom face of the block ( $P_B$ ) (m), the area of this face ( $A_B$ ) ( $m^2$ ), and unit weight of water ( $\gamma_w$ ) ( $N/m^3$ ) (Equation 5.2). The total pressure under the block is the sum of the static pressure ( $P_{B,stat}$ ) (m), caused by the height of the water table above the bottom face of the block ( $\gamma+h$ ) (m), and the dynamic pressure ( $P_{B,dyn}$ ) (m), which is calculated using the flow velocity  $v$  (m/s) (Equation 5.3). The total downward force ( $F_{down}$ ) (N) is the sum of the forces acting on the top face of the block



( $F_A$ ) (N) , the weight of the block ( $G_{b,down}$ ) (kg) in the direction of  $F_{down}$  (N), and the friction force ( $F_f$ ) (N). All pressure units are in meters to easily relate the block's height with the static and dynamic pressures. Equation 5.4 describes the total downward force, and Equation 5.5 decomposes the total pressure on top of the block into static pressure ( $P_{A,stat}$ ) (m), which is calculated as the height of the water table above the top of the block, and dynamic pressure ( $P_{A,dyn}$ ) (m). The friction force is presented in Equation 5.6. Figure 5.2 shows the distribution of the forces applied on the block..

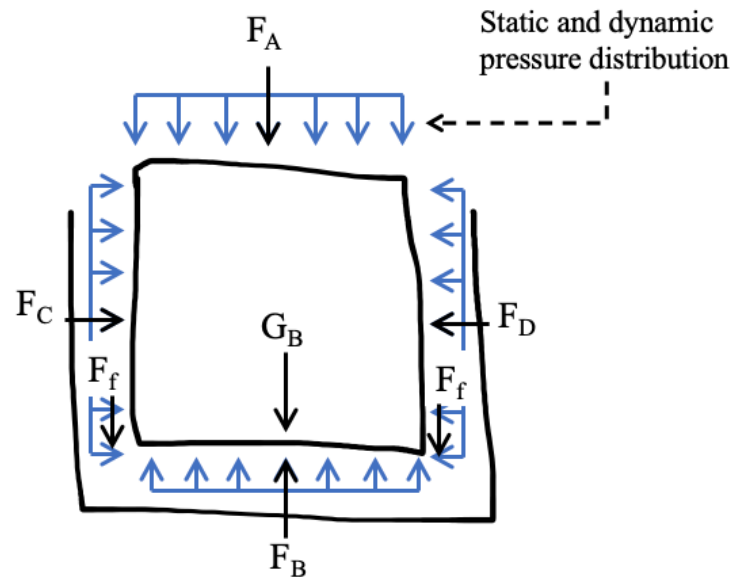


Figure 5.2 : Distribution of forces and water pressure applied around a block (© Marie-Hélène Wisse)

$$F_{up} > F_{down} \tag{5.1}$$

$$F_{up} = F_B = P_B * A_B * \gamma_w \tag{5.2}$$

$$P_B = P_{B,stat} + P_{B,dyn} = y + h + \frac{v_B^2}{2g} \tag{5.3}$$

$$F_{down} = F_A + G_{b,down} + F_f = P_A * A_A * \gamma_w + G_{b,down} + F_f \tag{5.4}$$

$$P_A = P_{A,stat} + P_{A,dyn} = y + \frac{v_A^2}{2g} \tag{5.5}$$

where  $F_B$  is the force acting on the bottom face of the block.  $F_B$  is calculated using  $P_B$  and  $A_B$ , where  $P_B$  is the pressure on face B (m) and  $A_B$  is the area of face B ( $m^2$ ).  $F_A$  is the force acting on the top of the block, calculated with  $P_A$  and  $A_A$ , where  $P_A$  is the pressure on face A (m) and  $A_A$  is the area of face A ( $m^2$ ). Because the block in our physical model is symmetrical,  $A_B = A_A = A_{Base}$ . Finally,  $g$  is the gravitational acceleration,  $y$  is the height of the water table above the top of the block (m),  $h$  is the height of the block (m), and  $\gamma_w$  is the unit weight of water ( $N/m^3$ ).

$$F_f = \frac{|(F_C + G_{b,n} * A_L) - F_D| + |F_E - F_F|}{A_L} * 2A_f * \tan\phi \quad (5.6)$$

where  $F_C$ ,  $F_D$ ,  $F_E$ , and  $F_F$  are, respectively, the forces (N) calculated on faces C, D, E, and F using the pressure measured on these faces (m) multiplied by the lateral area  $A_L$  ( $m^2$ ) and the unit weight of water ( $N/m^3$ ).  $A_f$  is the friction area ( $m^2$ ),  $\phi$  is the used friction angle (approximately  $30^\circ$ ), and  $G_{b,n}$  is the component of the block's weight acting as a normal force on the block's lateral face (N).

### 5.2.3 TESTING PROGRAM

The testing program used for this study is summarized in the Figure 5.3.

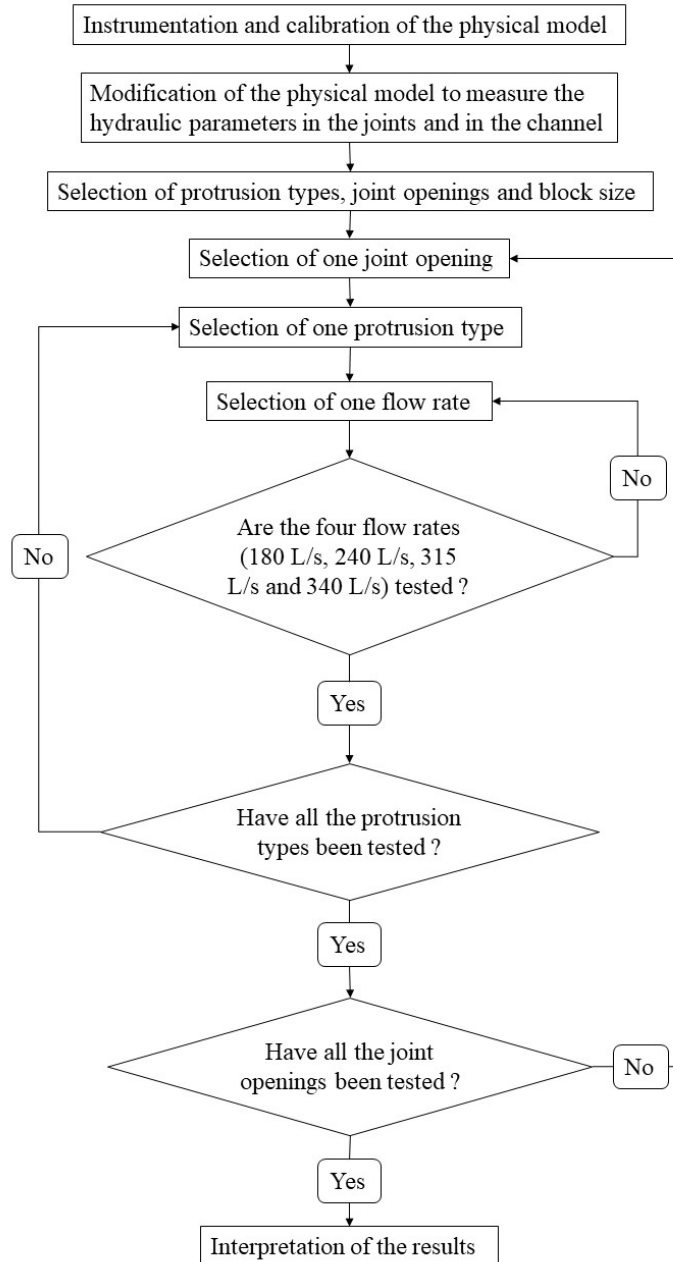


Figure 5.3 : Testing protocol applied to the physical model of Hydro-Québec's Romaine-4 dam spillway

#### 5.2.4 INSTRUMENTATION AND CALIBRATION OF THE PHYSICAL MODEL

Pressure on the block's faces was determined by three pressure sensors, each having a range of 0–103.421 kPa (0–15 psi). The pressure sensors were connected to plastic tubes, which were connected with copper tubes at the top of the block. Each copper tube was linked to a water entry on the block's faces. The copper tubes installed inside the mould were used to build an instrumented block (Figure 5.4a). A total of twelve water entries, two per face, were initially connected with the copper tubes. The water entries were positioned flush to the block's faces (Figure 5.4b).

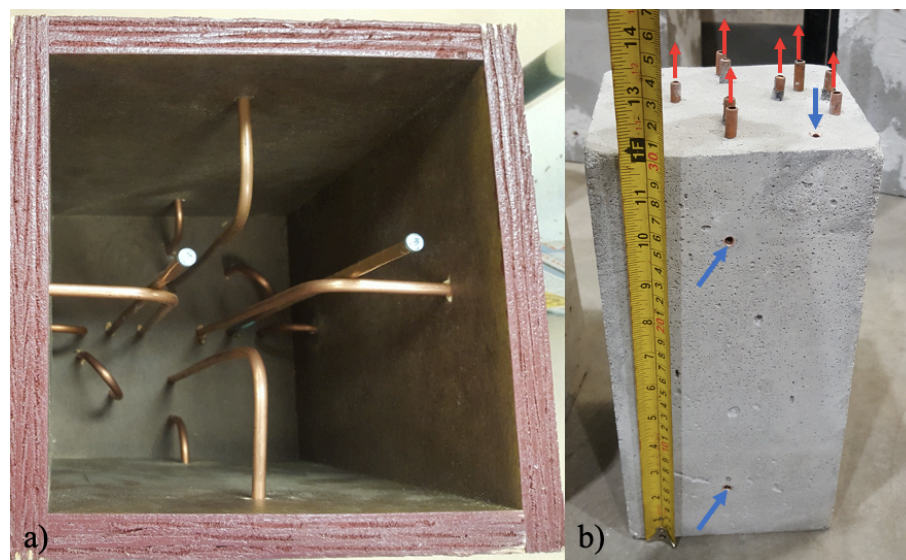


Figure 5.4 : **a**) copper tubes installed inside the mould; **b**) initial water entries (blue arrows) and water exits (red arrows) (© Marie-Hélène Wisse)

Total pressure, recorded by the pressure sensors, was meant to include static pressure, dynamic pressure, and position pressure, the latter related to the height between the pressure sensors and the position of the water entries of the instrumented block. All measurements were adjusted by eliminating the position pressure by placing the pressure sensors at a fixed position during all the tests, which allowed calculating the height difference between the pressure sensor position and the water entry position for each protrusion and joint opening, given the channel inclination of  $9^\circ$ .

### **5.2.5 MODIFICATION OF THE PHYSICAL TO MEASURE HYDRAULIC PARAMETERS IN THE JOINTS AND IN THE CHANNEL**

The first series of tests revealed that dynamic pressure was not recorded when the copper tubes were flush with the water entries. Two reasons could produce this result. First, the water entries were on the block surface. In fluid mechanics, it is commonly assumed that flow velocity is zero at the contact of a surface. Second, the flow direction was always perpendicular to the water entry tubes. The velocity component entering the water entry at the surface of the block was thus close to zero. To measure flow velocity in the joints and total pressure on each face, we modified the water entries by placing elbows on them; the elbows were used as pitot tubes—pitot tubes could not be used in the joints because of the lack of space between the blocks and because a pitot tube only works with laminar flow.

A new instrumented block version was moulded to measure the dynamic pressure in the joints (Figure 5.5a). The elbows placed on the water entries, illustrated with blue arrows in Figure 5.5b, permitted measuring static and dynamic pressures on each block face. To measure static pressure only, we placed an LVDT (linear variable differential transformer) sensor connected to a carbon stick on the top of the channel (Figure 5.5c). The carbon stick floats on the flowing water, and the LVDT sensor records water height variation. By knowing the precise static pressure at each water entry, one can then isolate dynamic pressure from total pressure.

Eleven water entries were used on the new version of the instrumented block: two on the bottom and each lateral face and only one water entry on the top face. The instrumented block was always placed in the centre of the eight non-instrumented blocks (Figure 5.5c) to allow water to circulate in all directions around the instrumented block. The elbows were oriented toward the top and bottom of the block for each lateral face (Figure 5.5b). In preliminary tests, some wool strings were attached to the sides of the block to visualize the flow direction between the blocks. The flow was predominantly upward and downward; thus, we oriented the elbows toward the block top and bottom. The elbow on the block top was oriented upstream because water flowed toward the downstream direction in the channel. Both elbows on the block bottom were oriented upstream and downstream (one of each). All water entries were connected to a water exit on the block top (Figure 5.5c). Water exits are identified with red arrows in Figure 5.5b. A tube was connected to these exits and reached the pressure sensors located outside the channel. Therefore, three simultaneous pressure measurements

could be recorded. Each two water entries on the same face and the top water entry were simultaneously recorded for one minute. An accelerometer is planned to be installed on the instrumented block for future experiments to measure the block's displacement during tests.

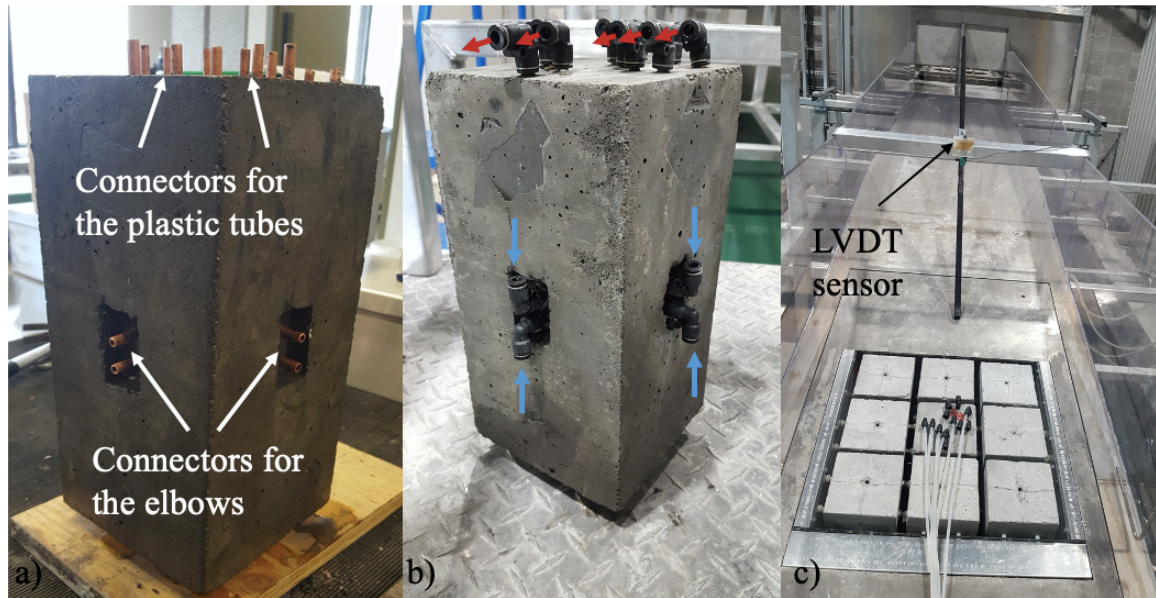


Figure 5.5 : **a)** Instrumented  $15 \times 15 \times 30$  cm block without elbows; **b)** instrumented  $15 \times 15 \times 30$  cm block with connected elbows; **c)** the physical model channel equipped with the LVDT sensor and the tubes connected to the water exits at the top of the instrumented block (© Marie-Hélène Wisse)

### 5.2.6 SELECTION OF JOINT OPENINGS, PROTRUSION TYPES AND BLOCK SIZES

Joint opening is defined as the aperture between the lateral faces of each block. Joint opening values were decided keeping in mind the technical limitations of the physical model. Therefore, they were not meant to fairly represent the joint opening scale of a fractured rock mass. The use of elbows on the block's lateral faces limited the joint opening values to a minimum of 10 mm. To have a range of values and be able to evaluate the effect of joint opening on hydraulic parameters in the joints, we fixed our joint opening values at 10, 20, and 38 mm. We also added a 3 mm opening to test a more common size observed in jointed rock masses. In this latter case, elbows were only used on the top and bottom faces of the instrumented block. The 3 mm joint opening around the block still permitted measuring the pressure variation on top and beneath the block but not on the lateral faces.

The joint openings were maintained during the tests by inserting 38, 20, 10, and 3 mm long bolts on the lateral faces of the non-instrumented blocks (Figure 5.6).

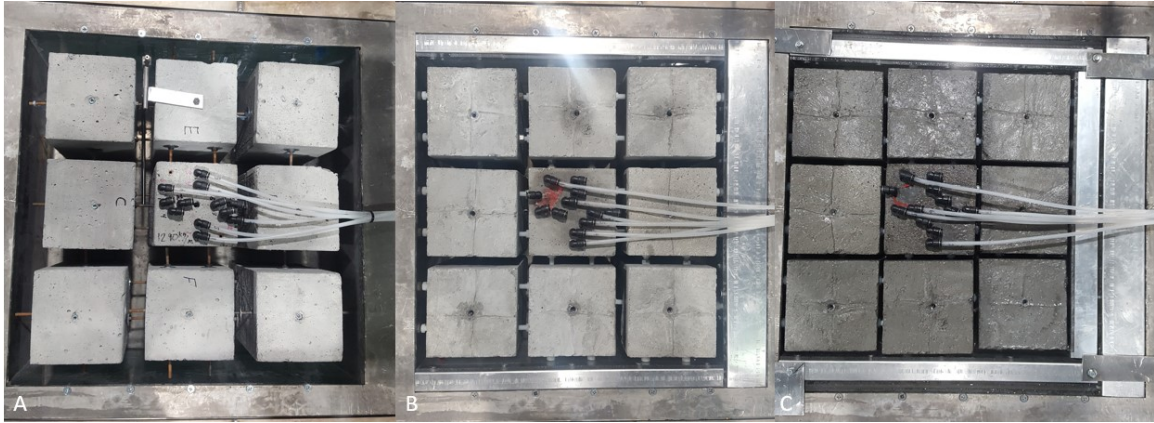


Figure 5.6 : Examples of the joint openings tested on the  $15 \times 15 \times 30$  cm blocks; a) 38 mm; b) 20 mm; and c) 10 mm (© Marie-Hélène Wisse)

Block protrusion was tested in a similar manner as for joint openings by using different spacing bolt sizes under the blocks. The joint opening under the block was 7 mm without protrusion; therefore, a 27 mm gap between the channel floor and the underside of the block represented a 20 mm protrusion (Figure 5.7).

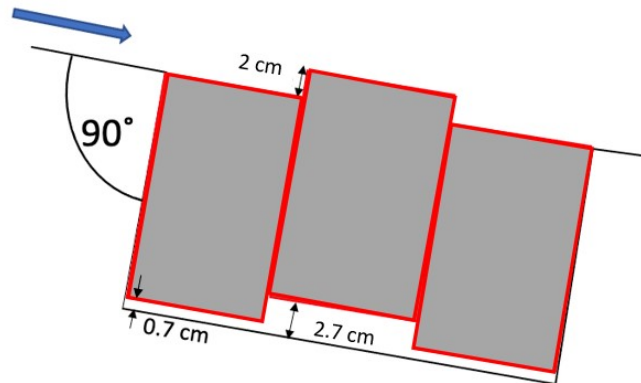
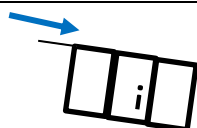
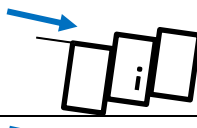
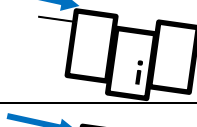
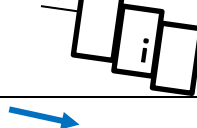
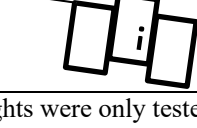


Figure 5.7 : Example of a protrusion setup with the centre block having a 20 mm protrusion. A 7 mm joint opening was used along the bottom of all blocks (© Marie-Hélène Wisse)

Four joint opening patterns were tested (Table 5.2). Protrusion was defined as the height of a block's top face in relation to the channel surface. The protrusion configurations were selected on the basis of spillway profiles, which are excavated by drilling and blasting patterns. Blasting will produce an irregular channel surface, which we aimed to reproduce with our protrusion configuration. The protrusion configuration varied for each row perpendicular to the flow. Protrusion height was based on the joint opening values, as protrusion height produced an equivalent joint opening under the blocks. Configurations 3 and 6 (Table 5.2) were designed to have the same protrusion between each row of blocks. In configuration 3, for example, as the centre row had

a 6 mm protrusion relative to the upstream block, the downstream block had a 6 mm difference with the centre block as well; the downstream block therefore had a total protrusion of 12 mm with the channel. Only two protrusion heights were tested with the joint opening of 3 mm: 6 mm and 20 mm for protrusion configurations 3 and 6.

Table 5.2 : Configuration setup and the variation of protrusion height for each row of blocks with the flow direction (blue arrow).

Configuration # and setup		Protrusion of upstream row (mm)			Protrusion of the middle row (mm)			Protrusion of downstream row (mm)		
0		0			0			0		
3		0			6 <sup>1</sup>	13	20 <sup>1</sup>	12 <sup>1</sup>	26	40 <sup>1</sup>
4		13	20	30	0			13	20	30
6		12 <sup>1</sup>	26	40 <sup>1</sup>	6 <sup>1</sup>	13	20 <sup>1</sup>	0		
8		0			13	20	30	0		

<sup>1</sup> These protrusion heights were only tested with a 3 mm joint opening

There are lots of possibilities of blocks shape and volume, since it is relatively easy to be built different shapes of moulds. For the purpose of this study, only 15 cm x 15 cm x 30 cm blocks were used.

### 5.2.6.1 Selection of one joint opening

The initial joint opening used was 38 mm because it necessitated the least modification of the model. A 38 mm joint opening was the maximum joint opening allowed with our block box and block size. Spacers were used to maintain the opening between the blocks during the tests (see Figure 5.6b,c).

### 5.2.6.2 Selection of One Protrusion Type

One protrusion configuration and height were chosen from table 5.2. No specific order was followed.



### **5.2.6.3 Selection of One Flow Rate**

Four flow rates were used for all tests: 180, 240, 315, and 340 L/s. Each test began with the lowest flow, and the flow increased after a recording time of one minute of the previous flow rate.

### **5.2.6.4 Interpretation of the Results**

A sensibility analysis of the used variables was done using the mean flow velocity recorded over the full 1 min recording period and the flow rate in the channel. The sensibility analysis was performed in relation to protrusion configuration, protrusion height, joint opening, and the various water entries.

## **5.3 RESULTS AND DISCUSSION**

### **5.3.1 ANALYSIS OF THE PHYSICAL MODEL DATA**

The raw data obtained from the physical model were the static pressure above the channel surface upstream of the blocks, obtained with the LVDT sensor, and the total pressure of all the eleven water entries around the block. We converted all pressure values, originally obtained in psi, to meters. Eleven pressure sensors covered the instrumented block's faces; for simplicity, we only present four pressure sensors. Face A is located on the top of the block, B is on the bottom face, C is on the upstream face, and D is on the downstream face. Faces C and D were oriented perpendicular to flow, and faces A and B were oriented parallel to flow. Figures 5.8, 5.9, and 5.10 give an example of the data obtained with a flow velocity in the channel of 3.3 m/s (flow rate of 180 L/s), for configuration 3 with a 13 mm protrusion height and a 10 mm joint opening.

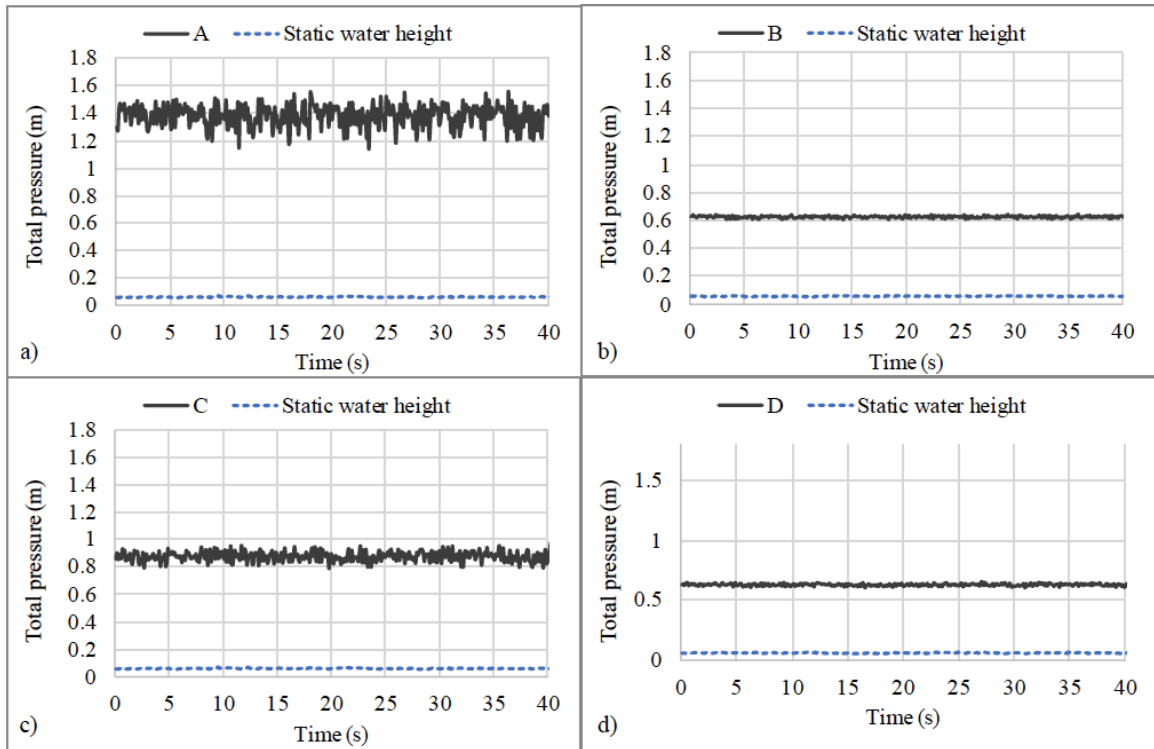


Figure 5.8 : Total pressure and static water height for a) face A; b) face B; c) face C; and d) face D

The total pressure combines static pressure ( $P_{\text{stat}}$ ), dynamic pressure ( $P_{\text{dyn}}$ ), and position pressure ( $z$ ); the latter is calculated by knowing the height difference of each water entry and then subtracted from the total pressure to obtain the sum of the dynamic and static pressure. We calculated static pressure using the LVDT measurements and the height difference between the water entry and the top of the block, given that the top of the block was flush with the channel.

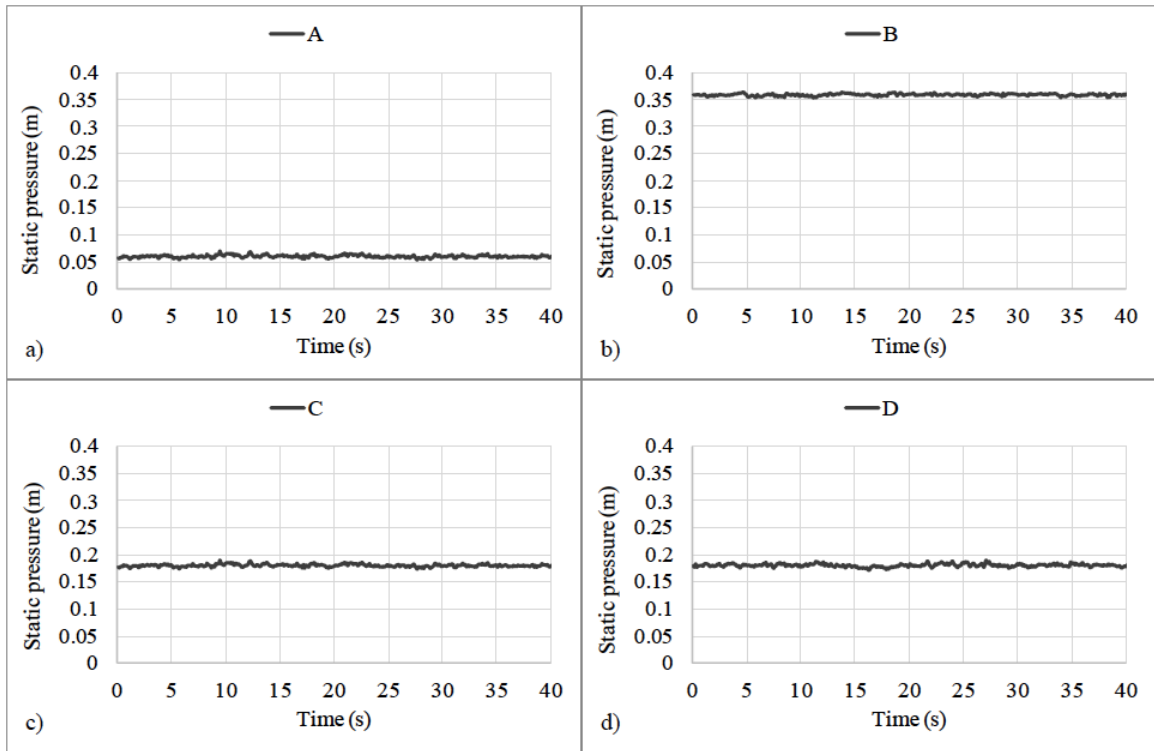


Figure 5.9 : Static pressure on a) face A; b) face B; c) face C; and d) face D

Static pressure remained very constant throughout all the tests and was therefore not responsible for pressure variation (Figures 5.8 and 5.9). The dynamic pressure was then isolated from the total pressure, and

velocity in the joints was calculated via  $P_{dyn} = \frac{v^2}{2g}$ .

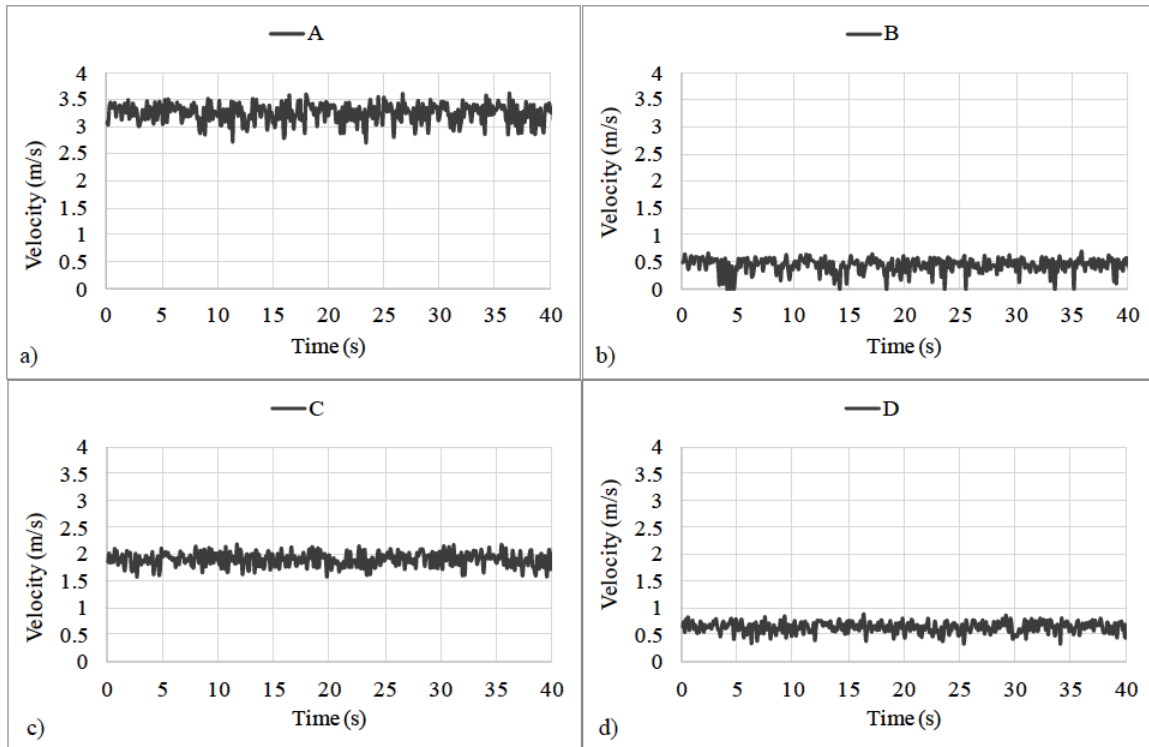


Figure 5.10 : Velocity on a) face A; b) face B; c) face C; and d) face D

The calculated dynamic pressure, the pressure presented as flow velocity, varied most on the block top (Figure 5.10a), and more variation was observed on the upstream block face (Figure 5.10b) than on the downstream face (Figure 5.10c). Pressure variation amplitude on the bottom of the block (Figure 5.10d) was much lower than that on the block top. The ratio of pressure variation amplitude to mean dynamic pressure increased with mean dynamic pressure..

### 5.3.2 EVALUATION OF THE EFFECTS OF JOINT OPENING AND PROTRUSION CONFIGURATION ON SURFACE PRESSURE FLUCTUATIONS

The effects of joint opening and protrusion configuration on surface pressure fluctuations for a 13 mm protrusion were analysed for all flow rates (Figure 5.11). The coefficient of variation (CV) indicated the degree of pressure variation for each tested parameter (Figure 5.11), regardless of the mean pressure value:  $CV = \frac{\sigma}{\mu} * 100$ , where  $\sigma$  is the standard deviation of the data and  $\mu$  is the mean value of the data.

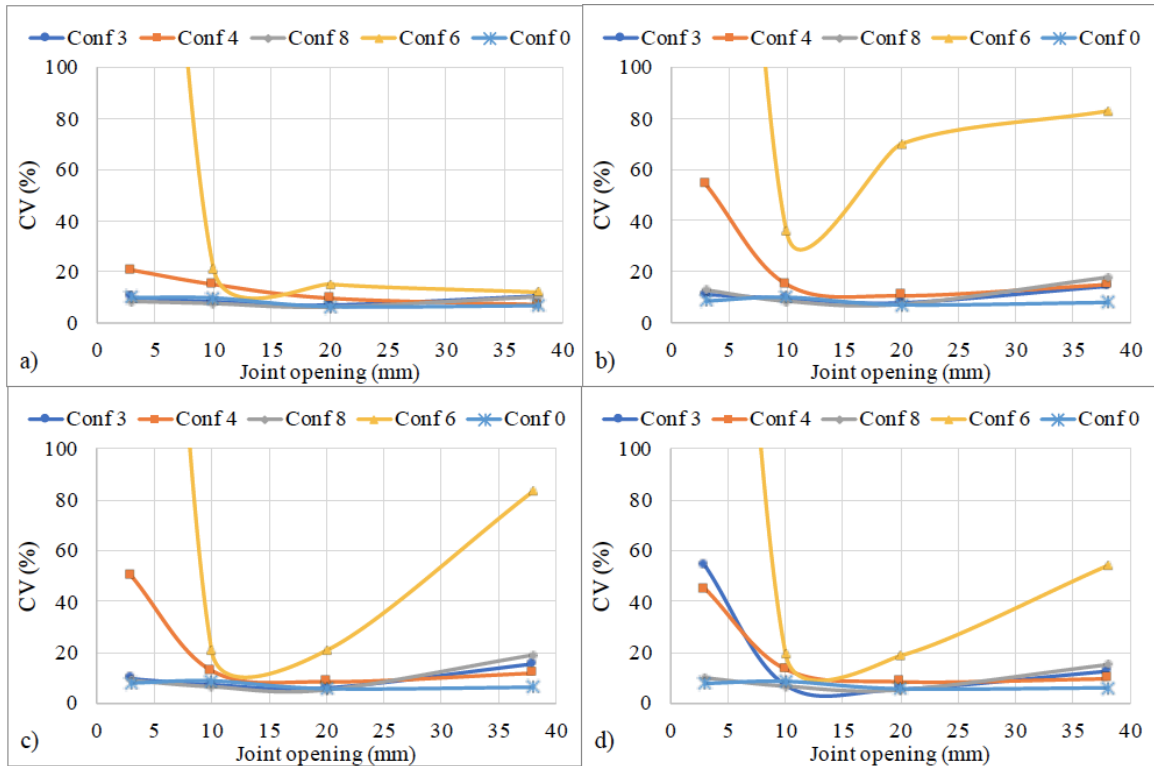


Figure 5.11 : Face A pressure coefficient of variation for flow rates of a) 180 L/s; b) 240 L/s; c) 315 L/s; and d) 340 L/s

Protrusion configurations 4 and 6 induced the greatest pressure fluctuations on the block top (Figure 5.11). Joint opening produced variable effects on pressure fluctuations for both configurations; the flow rate effect was very similar for all tests. In the case of configuration 6, we obtained very high CV values for a 3 mm joint opening because the blocks uplifted very easily. With greater lift, the pressure fluctuations also increased and mean pressure decreased, thereby producing the higher CV values. With greater lift, the pressure fluctuations also increased and mean pressure decreased, thereby producing higher CV values; the obtained CV for configuration 6 is therefore exaggerated. The same phenomenon occurred with configuration 3 (Figure 5.11d), where the blocks were also uplifted with a 3 mm joint opening.

### 5.3.3 MEAN FLOW VELOCITY ON TOP OF THE BLOCKS AND IN THE JOINTS

The elbow on top of the block always produced the total pressure at its position. The size of joint opening did not alter the flow velocity on top of the blocks without protrusion (configuration 0; Figure 5.12).

We could therefore calculate mean flow velocity for each flow rate. The mean flow velocities over the block tops were 3.3, 4.0, 4.7, and 4.9 m/s for flow rates of 180, 240, 315, and 340 L/s, respectively.

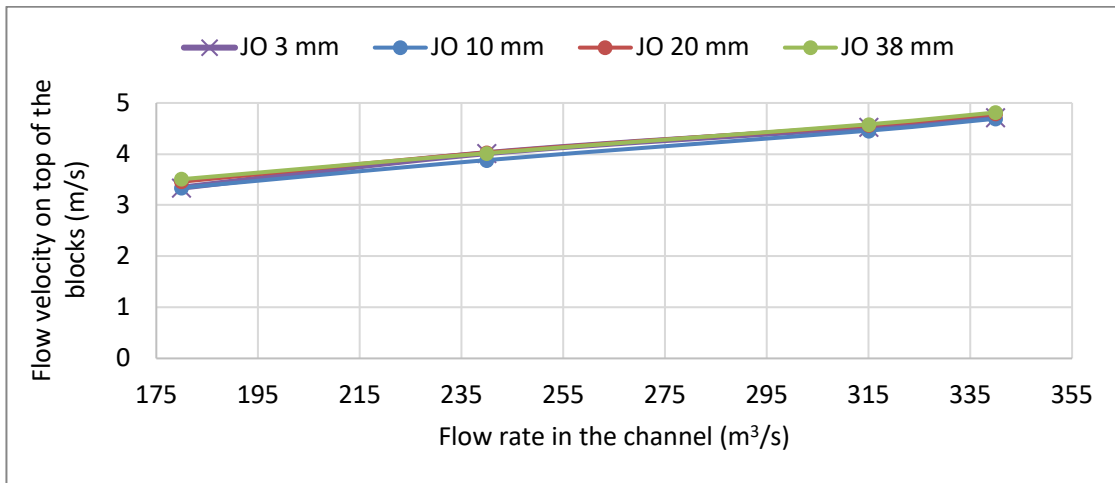


Figure 5.12 : Mean flow velocity on top of the blocks for different joint openings (JO) and flow rate in the channel in the case of no protrusion (configuration 0)

We then compared the relative effects of protrusion configuration, protrusion height, and joint opening using the relation between the flow velocity measured on face A ( $V_A$ ) for varying configurations and the flow velocity on face A for a flat configuration (configuration 0), which corresponds to the flow velocity in the channel ( $V_{ch}$ ) (Figure 5.13).

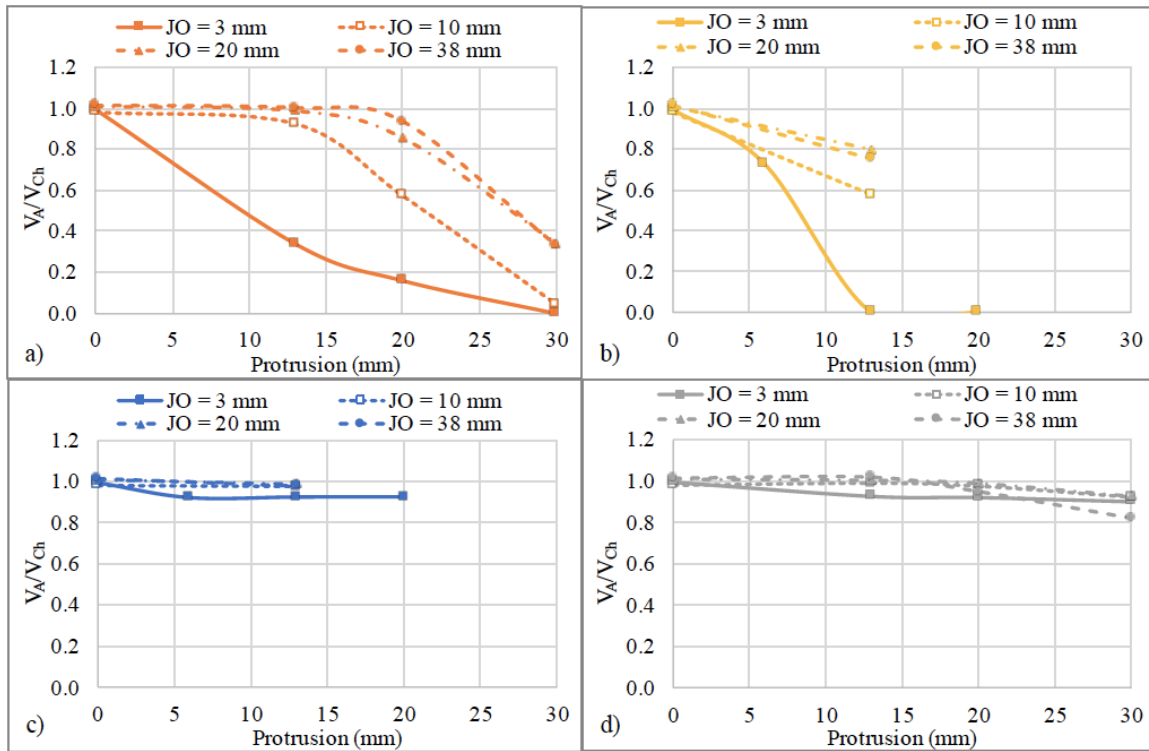


Figure 5.13 : Variation of  $V_A/V_{Ch}$  a) protrusion configuration 4; b) configuration 6; c) configuration 3; and d) configuration 8

We adjusted the data to only consider pressure values before uplift occurred during the test, specifically for configuration 3 and configuration 6, both with a 3 mm joint opening (Figure 5.13). Protrusion height and joint opening had the greatest effect on configurations 4 and 6. Increased protrusion height induced a lower dynamic pressure on the block top, and a narrower joint opening produced a lower dynamic pressure on the block top.  $V_A/V_{Ch}$  coefficients for configurations 3 and 8 were minimally affected by protrusion height and joint opening.

Because the pressure on the block top is a stabilizing force, configurations 4 and 6 were deemed more susceptible to block uplift, especially for smaller joint openings and a greater protrusion height.

Figure 5.14 shows the variation of the flow velocity under the instrumented block ratio with the flow velocity in the channel for all configurations, protrusions heights, and joint openings.

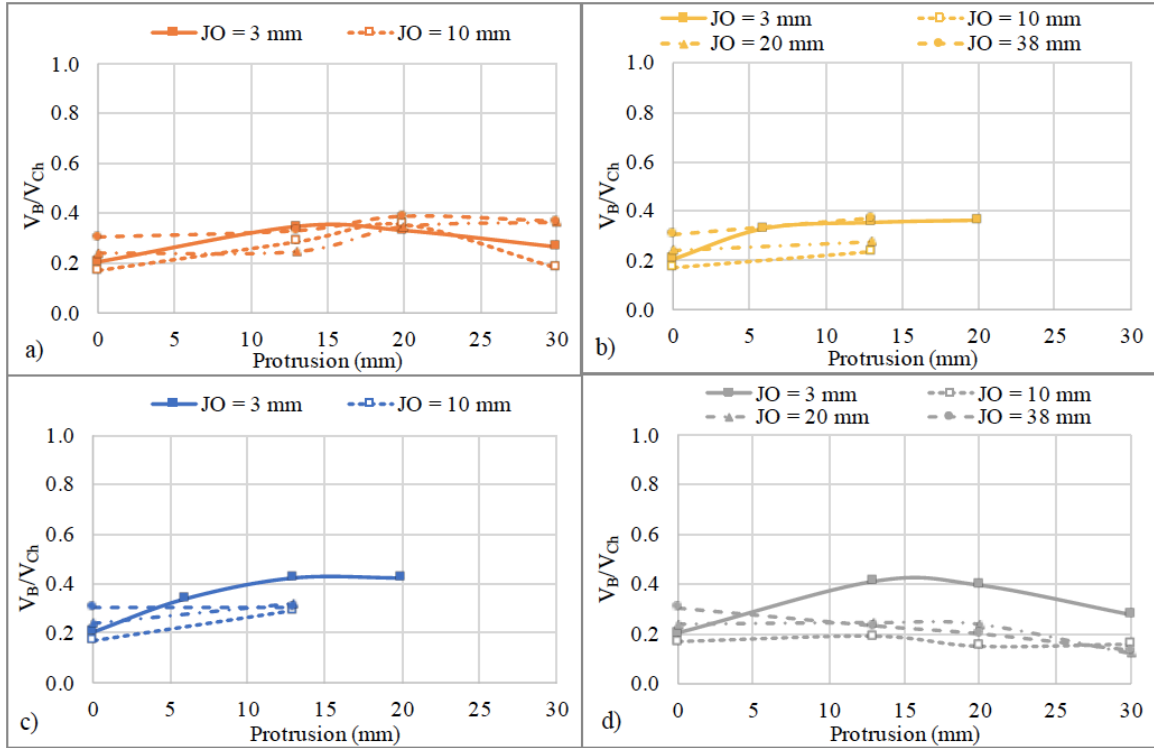


Figure 5.14 : Variation of  $V_B/V_{Ch}$  for a) protrusion configuration 4; b) configuration 6; c) configuration 3; and d) configuration 8

In regard to the dynamic pressure under the block, we observed that flow velocity under the block does not depend on protrusion configuration, protrusion height, or joint opening (Figure 5.14). Nonetheless, configurations 3 and 8 produced a slightly higher dynamic pressure than the other combinations having a joint opening of 3 mm.

The pressure under the block is a mobilizing force; however, the dynamic pressure under the block remained constant despite varying joint openings, protrusion configurations, and protrusion heights. It must be noted, however, that the used block was a high rectangular prism. A block having a more reduced height may show more variation on its bottom face.

The friction force is caused by a difference in flow velocity between opposite lateral faces of the block. A greater difference was observed between the upstream and downstream lateral faces than between the left and right lateral block faces. The difference between upstream and downstream velocities can be calculated by  $|V_C - V_D|/V_{Ch}$  (Figure 5.15), where  $V_C$  is the flow velocity on the upstream lateral block face,  $V_D$  is the flow



velocity on the downstream lateral block face, and  $V_{ch}$  is the flow velocity in the channel. Joint openings of 3 mm could not be tested for lateral flow velocity. Static pressure is assumed to be equal on both faces.

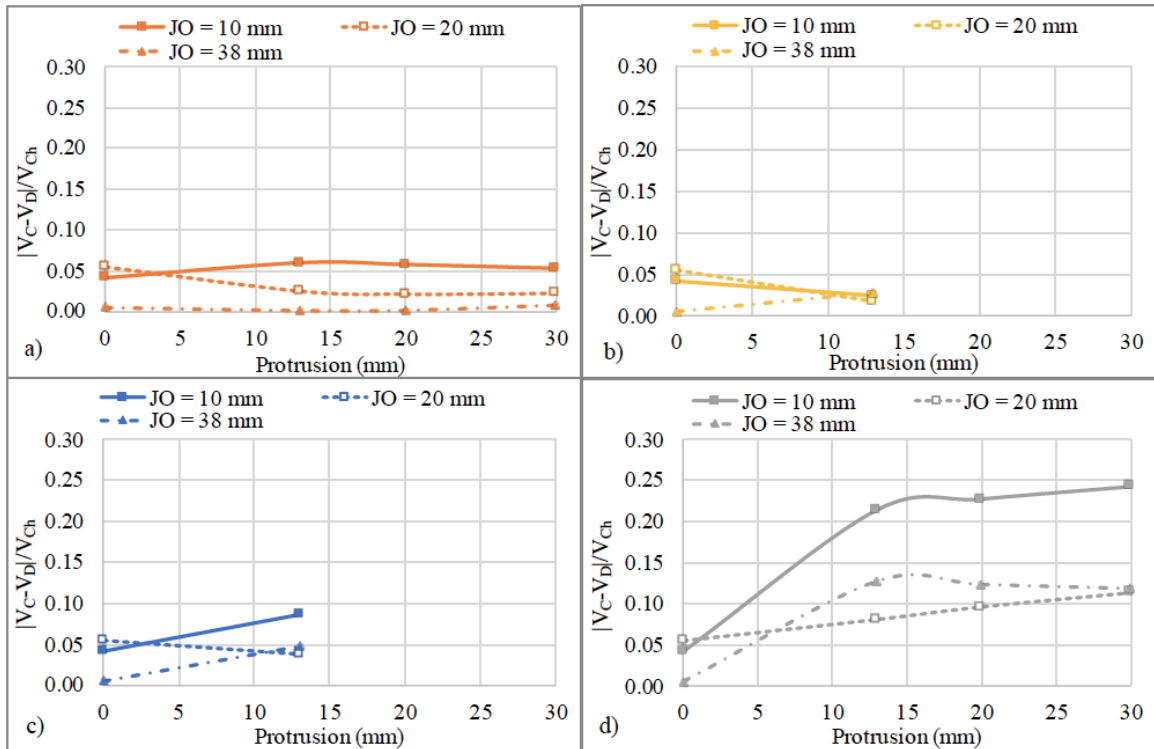


Figure 5.15 : The velocity differential between the upstream and the downstream face of the instrumented block a) configuration 4; b) configuration 6; c) configuration 3; and d) configuration 8

The velocity difference between the upstream and downstream block face was very low and constant among the various protrusion and joint opening combinations, e.g., for configurations 4 and 6 (Figure 5.15a, b). Configuration 3 (Figure 5.15c) showed a slight increase for 10 mm joint openings. Configuration 8 (Figure 5.14d) produced the largest flow velocity difference between the upstream and downstream block faces. Narrower joint openings and greater protrusion heights had a marked effect on differential flow velocity between the joints for configuration 8. We also noted that face C presented mostly higher values for velocity than face D.

The friction force is a stabilizing force. As the  $|V_C - V_D|$  coefficient increased, so did the friction force. Configuration 8 thus appears as a stabilizing configuration because of its higher  $|V_C - V_D|$  coefficient.

From these tests, we found configurations 4 and 6 combined with a high protrusion height and small joint opening as the combination of parameters making the block most vulnerable to uplift; this vulnerability occurs mainly because of the marked decrease in the top dynamic pressure. Configuration 3 and, in particular, configuration 8 were the most stable configurations because of the top dynamic pressure changes in the parameter values and, for configuration 8, because of the increased difference in the lateral pressure.

#### **5.4 CONCLUSION**

A scaled physical model of an unlined spillway was built to study the phenomenon of rock mass erosion in unlined spillways. The physical model was a 1:40 scale of Hydro-Québec's Romaine-4 dam spillway to reproduce realistic flow conditions. The model setup permitted the varying of hydraulic parameters and those rock mass characteristics affecting rock mass erodibility in unlined spillways. We aimed to determine the relationship between surface and joint hydraulic parameters according to joint opening and protrusion configuration and height.

An innovative instrumentation layout recorded flow velocity between the joints of the simulated rock mass, allowing total pressure to be determined for each face of the instrumented block. Total pressure was measured over the course of the complete test to record pressure fluctuations and mean pressure; total pressure was separated into static pressure and dynamic pressure. Static pressure remained constant on all block faces, but dynamic pressure varied to a much greater extent on the block top than on the other faces.

Joint opening and protrusion height increased the possibility of block uplift when the blocks' configuration decreased pressure on the block's top, i.e., a reduced stabilizing force. Block configuration and joint opening combinations that heighten the friction force, a stabilizing force, reduce the possibility of block uplift. Finally, protrusion height, protrusion configuration, and joint opening did not greatly affect the mobilizing force, which depends on the pressure under the block. As block geometry could alter the influence of protrusion and joint opening size, future tests should use blocks of shorter height to study different lateral side ratios, as ours was limited to a 2:1 ratio.

## **CHAPITRE 6: CONCLUSIONS**

### **6.1 CONCLUSIONS SUR LES MODÈLES PHYSIQUES EXISTANTS D'ÉVACUATEURS DE CRUES**

La revue de littérature effectuée sur les modèles physiques existants d'évacuateurs de crues a démontré que principalement deux types de modèles existent : ceux étudiant l'érosion causée par différents aspects hydrauliques de l'écoulement et ceux étudiant les différentes caractéristiques du massif rocheux ayant un impact sur son érodabilité. Deux types de modèles se concentrent sur les effets des caractéristiques du massif rocheux : des modèles physiques reproduisant un évacuateur de crues à jet plongeant et des modèles physiques reproduisant un évacuateur de crues à écoulement parallèle. Parmi les modèles physiques reproduisant un écoulement parallèle, les caractéristiques du massif rocheux étudiées sont limitées. De plus, tous sauf un se limitent à l'étude d'un seul bloc placés dans un canal d'écoulement, plutôt qu'une série de blocs reproduisant un massif rocheux. Cette revue de littérature démontre que la construction d'un nouveau modèle réduit en laboratoire est nécessaire. Ce modèle réduit devra avoir la capacité de permettre la variation des paramètres du massif rocheux ayant un impact sur son érodabilité, tels que l'orientation des joints, l'ouverture des joints, la taille et la forme des blocs, la rugosité des joints et la saillie des blocs. De plus, ce modèle réduit devra permettre l'étude de paramètres hydrauliques ayant une incidence sur l'érodabilité du massif rocheux, comme la rugosité du canal et la vitesse de l'écoulement. Ce modèle réduit devra être construit sur une base réaliste afin d'assurer la reproductibilité des résultats à grande échelle et sur un modèle numérique.

### **6.2 CONCLUSIONS LES PARAMÈTRES D'ORIENTATION DES JOINTS**

L'étude comparative des paramètres d'orientation des joints a permis de dresser un portrait des principaux indices d'orientation des joints et de leur effet comparatif. Cette comparaison a été réalisée à l'aide d'une base de données compilant les données géomécaniques, hydrauliques et de niveau d'érosion atteint dans plus de 100 sections de 24 barrages répartis en Afrique du sud et en Australie. En combinant un indice d'orientation des joints à l'indice de qualité du massif rocheux GSI, une évaluation de l'efficacité de classement de chacun des indices étudiés a été réalisée en se servant de l'érosion réelle rapportée par la base de données. Cette étude révèle qu'aucun paramètre d'orientation des joints existant ne représente correctement le niveau d'érosion pour toutes les classes de qualité du massif rocheux. De plus, l'étude révèle que la combinaison d'un

paramètre d'orientation des joints et d'un indice de qualité du massif rocheux ne prend pas en considération tous les paramètres reconnus comme ayant une influence sur l'érodabilité de la masse rocheuse. L'étude conclut qu'un nouvel indice incluant tous les paramètres du massif rocheux considérés comme ayant un effet sur son érodabilité doit être conçu et que l'étude de l'effet de l'orientation des joints sur l'érosion de la masse rocheuse doit être poursuivie.

### **6.3 CONCLUSIONS SUR LES EFFETS DE LA SAILLIE ET DE L'OUVERTURE DES JOINTS SUR L'ÉROSION**

Un modèle réduit de l'évacuateur de crues Romaine-4 à canal ouvert et écoulement parallèle d'Hydro-Québec a été construit dans un laboratoire de l'UQAC. Ce modèle réduit permet l'étude de paramètres du massif rocheux reconnus comme ayant une influence sur son érodabilité, tels que l'orientation, l'ouverture, la rugosité ainsi que la taille, la forme et la saillie des blocs. Le modèle réduit permet aussi de varier les caractéristiques hydrauliques de l'écoulement en modifiant la rugosité du canal, la vitesse de l'écoulement et sa turbulence. L'objectif de cette étude est d'évaluer l'effet de l'ouverture des joints et de la saillie des blocs sur les paramètres hydrauliques dans les joints du massif rocheux et ainsi de déterminer la possibilité de soulèvement des blocs. Deux aspects des saillies sont distingués, soit leur configuration leur hauteur. En dressant un portrait des forces auxquelles le bloc instrumenté est soumis, il a été possible de tirer des conclusions quant aux effets de ces caractéristiques. La principale force agissant sur le bloc est la force stabilisatrice agissant sur le dessus du bloc. Cette force est principalement affectée par la configuration de saillie. Pour certaines configurations de saillies, cette force varie grandement en fonction à la fois de l'ouverture des joints et de la hauteur de saillie. La force s'appliquant sur le dessus du bloc est aussi grandement variable en fonction du temps. Cette variation s'observe surtout pour les deux mêmes configurations affectant sa valeur moyenne. La deuxième force stabilisatrice rencontrée est la force de friction. Bien qu'elle varie surtout en fonction de la surface de friction, l'angle de friction ainsi que la force normale appliquée à la surface de friction sont également d'importants paramètres. La force normale appliquée à la surface de friction varie en fonction de l'ouverture des joints et de la hauteur de saillie pour une configuration de saillie en particulier. Les autres configurations de saillie n'ont que très peu d'effet sur les pressions mesurées au cours des essais. Le poids du bloc agit aussi comme une force stabilisatrice, mais aucun des paramètres mis à l'essai n'avait une influence sur ses composantes. La vitesse de l'écoulement sous le bloc est peu affectée par la configuration de saillie, la hauteur de saillie et l'ouverture des joints autour

du bloc. Selon la géométrie et le volume de blocs choisis pour la réalisation des essais, la vitesse de l'écoulement sous le bloc est demeurée assez constante pour tous les essais. La pression sous le bloc agissant comme force mobilisatrice, il est possible de dire qu'en considérant la géométrie des blocs utilisée pour les essais, cette force ne varie pas en fonction de la saillie et de l'ouverture des joints.

Parmi les paramètres reconnus comme ayant une importance sur l'érodabilité du massif rocheux, seuls deux ont été mis à l'essai dans le modèle réduit jusqu'à maintenant: l'ouverture des joints et la saillie des blocs. L'effet de la taille et la forme des blocs, même si elle n'a pas été directement mise à l'essai dans le modèle réduit, a un effet sur la pression de soulèvement sous le bloc en influençant la pression statique. Cependant, la question la variation de la pression dynamique sous le bloc en fonction de la variation de la taille et de la forme des blocs n'a pas été abordée. Il serait intéressant de rechercher de quelle façon la pression de soulèvement dynamique est affectée lorsque la base du bloc est plus proche de la base du canal. Est-ce que cette pression dynamique est plus variable en fonction du temps? Est-ce que sa valeur moyenne augmente? Plus la base du bloc est proche de la surface, moins la pression de soulèvement est influencée par la pression statique, donc plus la pression dynamique est importante à considérer. Les autres paramètres reconnus comme ayant un effet sur l'érodabilité du roc sont l'orientation des joints et la résistance au cisaillement. Il serait intéressant d'établir une relation de la vitesse dans les joints par rapport à la vitesse dans le canal selon différentes orientations des joints et de pendage. L'effet de la résistance au cisaillement peut être calculé en considérant la force normale appliquée sur une paroi du bloc comme étant la différence de pression dans les joints amont et aval du bloc. La différence de pression entre les joints de chaque côté latéral (gauche et droite) du bloc est nulle lorsque le bloc se trouve au centre du canal. Cette situation est donc celle où le bloc subit le moins de frottement, donc où son soulèvement est le plus critique. Cependant, en changeant la position du bloc instrumenté de façon à ce qu'il ne soit plus centré, il serait possible de mesurer l'effet de changement de position sur la différence de pression entre les joints de côté du bloc, et ainsi de définir l'effet qu'à l'emplacement du bloc sur la force de frottement. La suite de cette recherche devrait donc comprendre l'étude de l'effet de l'orientation des joints, de la résistance au cisaillement et de l'effet de la taille et de la forme des blocs.

## RÉFÉRENCES

- Annandale, G.W. 1995. Erodibility. *Journal of Hydraulic Research* **33**(4): 471-494. doi: <https://doi.org/10.1080/00221689509498656>.
- Annandale, G.W., Ruff, J.F., Wittler, R.J., et Lewis, T.M. 1998. Prototype Validation of Erodibility Index for Scour in Fractured Rock Media. *International Water Resources Engineer Engineering Conference*, Memphis, Tennessee, American Society of Civil Engineers, pp. 1096-1101.
- Barton, N., Lien, R., et Lunde, J. 1974. Engineering classification of rock masses for the design of tunnel support. *Rock mechanics : Journal of the International Society of Rock Mechanics* **6**(4): 189-236. doi: 10.1007/BF01239496.
- Bienawski, Z. 1976. Rock mass classifications in rock engineering. *Exploration for rock engineering*, Cape Town, Balkema, pp. 97-106.
- Bieniawski, Z.T. 1989. *Engineering rock mass classifications: a complete manual for engineers and geologists in mining, civil, and petroleum engineering*. John Wiley & Sons.
- Bollaert, E. 2004. A comprehensive model to evaluate scour formation in plunge pools. *International Journal on Hydropower and Dams* **11**(1): 94-102.
- Bollaert, E. 2010. The comprehensive scour model: Theory and feedback from practice. *5th International Conference on Scour and Erosion*, San Francisco, pp. 465-480.
- Bollaert, E. 2012. A quasi-3D prediction model of wall jet rock scour in plunge pools. *International Journal on Hydropower and Dams* **19**(4): 70-77.
- Bollaert, E., Annandale, G., et Schleiss, A. 2002. Scour of rock due to high-velocity jet impact: a physically based scour model compared to Annandale's erodibility index method.
- Bollaert, E., et Schleiss, A. 2002. Transient water pressures in joints and formation of rock scour due to high-velocity jet impact. Thesis, EPFL-LCH.
- Bollaert, E., et Schleiss, A. 2003. Scour of rock due to the impact of plunging high velocity jets Part I: A state-of-the-art review. *Journal of Hydraulic Research* **41**(5): 451-464. doi: <https://doi.org/10.1080/00221680309499991>.
- Bollaert, E., et Schleiss, A. 2005. Physically Based Model for Evaluation of Rock Scour due to High-Velocity Jet Impact. *Journal of Hydraulic Engineering* **131**(3): 153-165. doi: [https://doi.org/10.1061/\(ASCE\)0733-9429\(2005\)131:3\(153\)](https://doi.org/10.1061/(ASCE)0733-9429(2005)131:3(153)).
- Boumaiza, L. 2019. Rock mass parameters governing the hydraulic erodibility of rock in unlined spillways. Ph.D Thesis, UQAC.
- Boumaiza, L., Saeidi, A., et Quirion, M. 2019a. Determining relative block structure rating for rock erodibility evaluation in the case of non-orthogonal joint sets. *Journal of Rock Mechanics and Geotechnical Engineering* **11**(1): 72-87. doi: 10.1016/j.jrmge.2018.06.010.
- Boumaiza, L., Saeidi, A., et Quirion, M. 2019b. A method to determine relevant geomechanical parameters for evaluating the hydraulic erodibility of rock. *Journal of Rock Mechanics and Geotechnical Engineering* **11**(5): 1004-1018. doi: <https://dx.doi.org/doi:10.1016/j.jrmge.2019.04.002>.

Boumaiza, L., Saeidi, A., et Quirion, M. 2021. A method to determine the relative importance of geological parameters that control the hydraulic erodibility of rock. *Quarterly Journal of Engineering Geology and Hydrogeology* **54**(4): 2020-2154. doi: <https://doi.org/10.1144/qjegh2020-154>.

Castillo, L.G., et Carrillo, J., M. 2016. Scour, Velocities and Pressures Evaluations Produced by Spillway and Outlets of Dam. *Water* **8**(3). doi: 10.3390/w8030068.

Chamani, M., et Rajaratnam, N. 1999. Characteristics of skimming flow over stepped spillways. *Journal of Hydraulic Engineering* **125**(4): 361-368.

Dargahi, B. 2003. Scour development downstream of a spillway. *Journal of Hydraulic Research* **41**(4): 417-426. doi: <https://doi.org/10.1080/00221680309499986>.

Ervine, D.A., Falvey, H.T., et Withers, W. 1997. Pressure fluctuations on plunge pool floors. *Journal of Hydraulic Research* **35**(2): 257-259. doi: <https://doi.org/10.1080/00221689709498430>.

George, M., Sitar, N., et Sklar, L. 2015. Experimental evaluation of rock erosion in spillway channels. 49th US Rock Mechanics / Geomechanics Symposium 2015, ARMA, San Francisco.

Gu, S., Liqun, R., Xing, W., Hongwei, X., Yuefei, H., Jiahua, W., et Songdong, S. 2017. SPHysics Simulation of Experimental Spillway Hydraulics. *Water* **9**(12): 973. doi: <https://doi.org/10.3390/w9120973>.

Hearden, T. 2018. Lawmaker voices concern over Oroville cost overruns *Western Farm Press* **40**(14). Disponible à <https://www.farmprogress.com/water/lawmaker-voices-concerns-over-oroville-cost-overruns> [cité le November 2020].

Hoek, E., Kaiser, P.K., et Bawden, W.F. 1995. Support of underground excavations in hard rock. 1st éd. Balkema, Rotherdam, Netherlands.

Hydro-Québec. 2019. Voir grand avec notre énergie propre.

Jalili Kashtiban, Y., Saeidi, A., Farinas, M.-I., et Quirion, M. 2021. A Review on Existing Methods to Assess Hydraulic Erodibility Downstream of Dam Spillways. *Water* **13**(22): 3205. doi: <https://doi.org/10.3390/w13223205>.

Kirsten, H. 1982. A classification system for excavation in natural materials. *Civil Engineer in South Africa* **24**(7): 293-308.

Kirsten, H.A., Moore, J.S., Kirsten, L.H., et Temple, D.M. 2000. Erodibility criterion for auxiliary spillways of dams. *International Journal of Sediment Research* **15**(1): 93-107.

Kote, A.S., et Nangare, P.B. 2019. Hydraulic Model Investigation on Stepped Spillway's Plain and Slotted Roller Bucket. *Engineering, Technology & Applied Science Research* **9**(4): 4419-4422. doi: <https://doi.org/10.48084/etasr.2837>.

Koulibaly, A.S. 2021. Conception d'un modèle de laboratoire d'un évacuateur de crues pour étudier l'érosion des masses rocheuses. MSc Thesis, Université du Québec à Chicoutimi.

Koulibaly, A.S., Saeidi, A., Rouleau, A., et Quirion, M. 2022. A Reduced-Scale Physical Model of a Spillway to Evaluate the Hydraulic Erodibility of a Fractured Rock Mass. *Rock Mechanics and Rock Engineering*. doi: 10.1007/s00603-022-03101-5.

Leslighter, E.J., Bollaert, E.F.R., McPherson, B.L., et Scriven, D.C. 2016. Spillway Rock Scour Analysis - Composite of Physical & Numerical Modelling, Paradise Dam, Australia. *Dans* 6th IAHR International Symposium on Hydraulic Structures, Portland. pp. 343-352.

- Liu, P.Q., Dong, J.R., et Yu, C. 1998. Experimental investigation of fluctuation uplift on rock blocks at the bottom of the scour pool downstream of Three-Gorges spillway. *Journal of Hydraulic Research* **36**(1): 55-68. doi: <https://doi.org/10.1080/00221689809498377>.
- Manso, P.F.d.A., et Schleiss, A. 2006. The influence of pool geometry and induced flow patterns in rock scour by high-velocity plunging jets. Dissertation, EPFL, Lausanne.
- Marinos, P., et Hoek, E. 2000. GSI: A Geologically Friendly Tool For Rock Mass Strength Estimation. *Dans ISRM International Symposium*, Melbourne, Australia.
- Montgomery, R.A. 1984. Investigations into rock erosion by high velocity water flows. Dissertation, University of Washington, Stockholm.
- Pan, Y.-W., Li, K.-W., et Liao, J.-J. 2014. Mechanics and response of a surface rock block subjected to pressure fluctuations: A plucking model and its application. *Engineering Geology* **171**: 1-10. doi: 10.1016/j.enggeo.2013.12.008.
- Pells, S. 2016. Erosion of Rocks in Spillways. Thesis, Civil and Environmental Engineering, University of New South Wales.
- Quaresma, A.L., Ferreira, R.M., et Pinheiro, A.N. 2017. Comparative analysis of particle image velocimetry and acoustic Doppler velocimetry in relation to a pool-type fishway flow. *Journal of Hydraulic Research* **55**(4): 582-591. doi: <https://doi.org/10.1080/00221686.2016.1275051>.
- Reinius, E. 1986. Rock erosion. *International Water Power and Dam Construction* **38**(6): 43-48.
- Rinaldo, A., et Fiorotto, V. 1992. Fluctuating Uplift and Lining Design in Spillway Stilling Basins. *Journal of Hydraulic Engineering* **118**(4): 578-596. doi: [https://doi.org/10.1061/\(ASCE\)0733-9429\(1992\)118:4\(578\)](https://doi.org/10.1061/(ASCE)0733-9429(1992)118:4(578)).
- Roberts, D.F. 1943. The dissipating of the energy of a flood passing over a high dam. *Civil Engineering*(1): 48-92.
- Rong, G., Tan, J., Zhan, H., He, R., et Zhang, Z. 2020. Quantitative evaluation of fracture geometry influence on nonlinear flow in a single rock fracture. *Journal of Hydrology* **589**. doi: <https://doi.org/10.1016/j.jhydrol.2020.125162>.
- Sawadogo, O. 2010. Scour of Unlined Dam Spillways. Dissertation, Engineering Sciences (Civil), Stellenbosch University, Stellenbosch University.
- Schimdt, S., Hawkins, D., et Phillips, K. 2017. 188 000 evacuated as California's massive Oroville Dam threatens catastrophic floods. Disponible à <https://www.washingtonpost.com/news/morning-mix/wp/2017/02/13/not-a-drill-thousands-evacuated-in-calif-as-oroville-dam-threatens-to-flood/> [cité le January 2021].
- Tuna, M.C. 2012. Effect of offtake channel base angle of stepped spillway on scour hole. *Iranian Journal of Science and Technology. Transactions of Civil Engineering* **36**(C2): 239-251. doi: <https://10.22099/IJSTC.2012.639>.
- Van Schalkwyk, A., Jordaan, J., et Dooge, N. 1994. Erosion of rock in unlined spillways. *International Commission on Large Dams*, Paris, pp. 555-571.
- Wang, Y.-k., et Jiang, C.-b. 2010. Experimental study of drag reduction in flumes and spillway tunnels. *Water Science and Engineering* **3**(2): 200-207. doi: <https://doi.org/10.3882/j.issn.1674-2370.2010.02.008>.



Wilkinson, C., Harbor, D.J., Helgans, E., et Kuehner, J.P. 2018. Plucking phenomena in nonuniform flow. *Geosphere* **14**(5): 2157-2170. doi: <https://doi.org/10.1130/GES01623.1>.

Withers, W.J. 1991. Pressure fluctuations in the plunge pool of an impinging jet spillway. Dissertation, Civil Engineering, University of Glasgow, Glasgow.

Wu, W. 2001. CCHE2D sediment transport model. National Center for Computational Hydroscience and Engineering. NCCHE-TR-2001-3.